Max-Planck-Institut für Polymerforschung

Max Planck Institute for Polymer Research

Photoresponsive Nanocomposites for Photopatterning: Integration of a Photoresponsive Polymer and Upconverting Nanoparticles

Dissertation

Zur Erlangung des Grades

Doktor der Naturwissenschaften

im Promotionsfach Chemie

Eingereicht am

Fachbereich Chemie, Pharmazie und Geowissenschaften

der Johannes Gutenberg-Universität Mainz

Von

Yazhi Liu

Mainz, 2023

Die vorliegende Arbeit wurde im Zeitraum von Juli 2019 bis September 2023 am Max-Planck-Institut für Polymerforschung in Mainz im Arbeitskreis von Prof. Dr. Hans-Jürgen Butt and Prof. Dr. Si Wu angefertigt.

Dekan: Prof. Dr. Axel Schäfer
Gutachter 1: Prof. Dr. Hans-Jürgen Butt
Gutachter 2: Prof. Dr. Wolfgang Tremel
Date of oral examination: 25.09.2023

Contents

Abstract

Photoresponsive materials play a crucial role in photopatterning, enabling the manipulation of material properties through interactions with light. Photopatterning techniques involve utilizing light to control materials, either through inducing chemical reactions or physical changes. The integration of photoresponsive materials with photopatterning techniques offers researchers a platform to explore innovative avenues in material design and advanced manufacturing. In this thesis, novel photoresponsive nanocomposites were developed for photopatterning purposes. These nanocomposites consist of a photoresponsive azobenzene-containing polymer (azopolymer) and β-phase $NaYF_4$:TmYb@$NaYF_4$ upconverting nanoparticles (UCNPs). These UCNPs have the ability to absorb multiple near-infrared (NIR) photons and emit light of shorter wavelengths such as blue or ultraviolet (UV) light. This phenomenon, known as "upconversion", is typically more efficient than two-photon absorption. With respect to photopatterning, this nanocomposite derived from UCNPs presents two distinct advantages over pure azobenzene polymers: deeper penetration of NIR light into the material and improved resolution by necessitating the absorption of two or more photons. The main goal of this research is to create a versatile material suitable for applications in anticounterfeiting and photo information storage.

As the most investigated photoresponsive material, the azopolymer exhibit reversible *cis-trans* photoisomerization, leading to photochromic, photoswitchable glass transition temperatures (T_g), and photoinduced orientations. These inherent photoresponsive properties enable the creation of various two-dimensional (2D) photopatterns on the nanocomposite, such as structures that change color, photonic structures, and structures dependent on polarization. Moreover, the UCNPs possess the ability to convert near-infrared (NIR) light into visible light, resulting in high-contrast color, structure, and polarization-dependent upconversion luminescence within the nanocomposite. These distinctive security features can be readily perceived by the naked eye and characterized using analytical tools. This nanocomposite demonstrates excellent processability and can be conveniently applied to various items, including banknotes, wines, medicines, and other products. Hence, the synergistic integration of the azopolymer and UCNPs establishes the nanocomposite as an advanced material for anticounterfeiting applications.

Despite the successful fabrication of 2D photopatterns using photomasks, the precise fabrication of three-dimensional (3D) patterns through laser direct writing remains a significant challenge yet remarkably appealing. Hence, an innovative three-dimensional (3D) photon upconversion direct lithography (PUDL) system was developed. The system incorporates an

objective lens to focus the beam emitted by a cost-effective continuous wave NIR laser. The focal position remains fixed while the 3D motorized sample stage is manipulated, generating 3D patterns on the optical recording layers. Azobenzene exhibits a remarkable phenomenon known as photoinduced orientation. It occurs when azobenzene chromophores in an azopolymer film align perpendicular to the polarization direction of the incident linearly polarized light irradiation. Hence, before exposure, the nanocomposite film underwent pretreatment to establish alignment under ultraviolet (UV) and polarized blue light. When exposed to NIR light, the upconverted UV and blue light induced a continuous trans-cis-trans isomerization of the azobenzene molecules. This persistent isomerization disrupted the initial molecular alignment, resulting in the adoption of random orientations by the azobenzene molecules. Consequently, a diverse array of patterns with varying orientations was generated, which could be observed using a polarized optical microscope and the reflection mode of a confocal microscope. Our research introduces a promising approach to optical recording and represents a significant advancement in 3D photolithography.

Zusammenfassung

Die Eigenschaften photoresponsiver Materialien lassen sich durch Licht verändern. Die Herausforderung ist, Materialien herzustellen, bei denen sich relevante Eigenschaften reversibel ändern. In dieser Arbeit wurden neuartige photoresponsive Nanokomposite zur Photostrukturierung entwickelt. Diese Nanokomposite bestehen aus einem azobenzolhaltigen Polymer (Azopolymer), und aufkonvertierender Nanopartikel (UCNPs). Azopolymere zeigen eine reversible *cis-trans* Photoisomerisierung, die zu Photochromie, photoschaltbaren Glasübergangstemperaturen (T_g) und photoinduzierten Orientierungen führt. UCNPs absorbieren zwei oder mehr Photonen im nahen Infrarot (NIR) und emittieren Licht kürzerer Wellenlänge (blau, UV). Diese Aufkonversion ist bei anorganischen Nanopartikeln oft effizienter als bei organischen Molekülen. Das Komposit hat im Vergleich zum reinen Azobenzol-Polymer zwei potentielle Vorteile: NIR-Licht dringt tiefer ins Material ein und die Auflösung wird durch die Notwendigkeit von zwei oder mehr Photonen besser. Ziel der Arbeit ist, ein Material zum fälschungssicheren Beschriften zu designen.

Die photoresponsiven Komposite ermöglichen die Erzeugung verschiedener fälschungssicherer Merkmale. Dazu gehören Farbwechsel-Strukturen, photonische Strukturen und Strukturen, die von der Polarisation abhängig sind. Die Fähigkeit der UCNPs, NIR-Licht in sichtbares Licht umzuwandeln, führt zu kontrastreicher Farbe, Struktur und polarisationsabhängiger Aufkonversions-Lumineszenz innerhalb des Nanokomposits. Darüber hinaus lässt sich dieses Nanokomposit gut verarbeiten und kann bequem auf verschiedene Gegenstände aufgetragen werden, wie Banknoten, Wein-Etiketten und Medikamentverpackungen. Die Kombination des Azopolymers mit den UCNPs ist damit interessant als photoresponsives, fälschungssicheres Material.

Obwohl es bereits erfolgreich möglich ist, 2D-Fotomuster mithilfe von Fotomasken herzustellen, stellt die präzise Herstellung dreidimensionaler (3D) Muster durch Laserdirektschreiben nach wie vor eine große Herausforderung dar und bleibt dennoch äußerst attraktiv. Dazu habe ich ein dreidimensionales (3D) Photonen-Upconversion-Direktlithographiesystem (PUDL) entwickelt. Das System umfasst eine Objektivlinse, um den von einem kostengünstigen Dauerstrich-NIR-Laser emittierten Strahl zu fokussieren. Die Fokusposition bleibt fixiert, während der motorisierte 3D-Probentisch manipuliert wird. Dadurch lassen sich 3D-Mustern in einem Nanokompositfilm erzeugen. Azobenzol zeigt ein bemerkenswertes Phänomen, das als photoinduzierte Orientierung bekannt ist. Dieses Phänomen tritt auf, da sich die Chromophore in einem Azopolymerfilm sich in einer

Ausrichtung senkrecht zur Polarisationsrichtung des einfallenden linear polarisierten Lichts organisieren. Vor der Belichtung wurden die Azobenzol-Gruppen im Nanokompositfilm durch polarisiertes UV und blaues Licht orientiert. Bei Einwirkung von NIR-Licht induzierte das aufkonvertierte UV- und blaue Licht eine kontinuierliche trans-cis-trans-Isomerisierung der Azobenzolmoleküle. Diese anhaltende Isomerisierung störte die anfängliche molekulare Ausrichtung, was dazu führte, dass die Azobenzole zufällige Orientierungen annehmen. Dadurch konnten Muster mit unterschiedlichen Ausrichtungen erzeugt werden, die mit einem polarisierten optischen Mikroskop und im Reflexionsmodus eines konfokalen Mikroskops beobachtet werden konnten. Unsere Forschung führt einen vielversprechenden Ansatz zur optischen Aufzeichnung ein und stellt einen bedeutenden Fortschritt in der 3D-Fotolithographie dar.

Motivation

Photoresponsive materials have emerged as precious tools in a wide range of applications, especially in photopatterning, due to their unique properties. These materials have found extensive use in domains such as anticounterfeiting, encryption, and information storage, offering great potential for enhanced security measures. However, traditional photoresponsive anticounterfeiting materials typically possess only one anticounterfeiting function, limiting their effectiveness in providing robust security.

Addressing this limitation, this thesis presents a nanocomposite that shows multiple security features, aiming to overcome the existing bottleneck and provide a solution for improved security applications. The nanocomposite is fabricated by doping UCNPs in a photoresponsive azopolymer. Because of the *cis–trans* photoisomerization of the azopolymer, the nanocomposite exhibits photoinduced reversible color changes suitable for anticounterfeiting applications. Additionally, the hard nanocomposite can be converted to a rubber-like soft solid by light irradiation. Imprinted microstructures are fabricated on the photo-softened nanocomposite, which results in vivid colors. Moreover, polarization-dependent structures that can be used for encryption are fabricated on the nanocomposite via photoinduced orientation. UCNPs in the nanocomposite emit visible light upon excitation by near-infrared light (NIR), enabling the observation of various anticounterfeiting structures with high contrast. An advantage of the anticounterfeiting nanocomposite is that the security features can be observed by the naked eye for quick discrimination and can be analyzed using laboratory equipment for higher accuracy. The anticounterfeiting nanocomposite is easily processed on paper, glass, and plastic, demonstrating its potential anticounterfeiting functions for banknotes, wines, and medicines.

Despite our success in fabricating high-quality 2D photopatterns on this nanocomposite using photomasks, there is an increasing interest in the development of a laser-based method for directly writing 3D patterns. This approach offers unique advantages that are driving the exploration of this field. Currently, the prevailing method for fabricating 3D patterns involves two-photon absorption, which aims to increase information density. However, this approach suffers from inefficiency and requires expensive femtosecond lasers. This thesis presents a novel approach to overcome these bottlenecks: developing a 3D photon upconversion direct lithography system using the previously mentioned photoresponsive nanocomposite as the optical material. In contrast to two-photon absorption, the photon upconversion process exhibits significantly higher efficiency and eliminates the need for costly ultrafast lasers. In the focal

region of the laser, UCNPs can convert NIR light into UV and visible light, which serves as a stimulus for continuous *trans-cis-trans* photoisomerization of the azopolymer. This continuous isomerization disrupts the initial molecular alignment, leading to the adoption of random orientations by the azobenzene molecules. Consequently, the focused NIR laser can inscribe unaligned patterns onto pre-aligned optical recording layers. Due to the good penetration depth of NIR light, the successful generation of 3D photopatterns was achieved. The application scope of this system extends to photopatterning, encryption, and data storage.

Chapter 1: Introduction

1.1 Photopatterning

Photopatterning, a cutting-edge technique bridging the realms of science and art, has emerged as a captivating method to create intricate patterns and designs with remarkable precision. [1-3] Leveraging the principles of photochemistry and materials science, this process has gathered attention in various fields, from information storage, [4, 5] anticounterfeiting, [6, 7] and microelectronics [8] to visual arts [9]. At its core, photopatterning involves selectively illuminating photosensitive materials to induce desired chemical or physical transformations. Photoresponsive materials encompass a broad range of substances that undergo reversible changes in their physical or chemical properties upon exposure to light. These materials include polymers, [10] liquid crystals, [11] nanoparticles, [12] and molecular switches. [13] Their response to light can manifest as changes in shape, color, refractive index, conductivity, or fluorescence.

Photopatterning techniques have become integral to the field of anticounterfeiting. By enabling the precise fabrication of complex patterns, [14] holography, [15] microprinting, [16] security inks and tags, [7, 17, 18] and nanopatterning [6] can be incorporated into various products and documents, enhancing their security and making them significantly more resistant to counterfeiting. In the context of information storage, photopatterning also plays a crucial role in producing various storage media, including optical discs, [19] hard disk drives, [20] and solid-state drives. [21] In optical disc manufacturing, photolithography is used to create microscopic pits on the surface of the disc, which represent digital data in the form of binary code. The patterned disc is coated with reflective layers and protective coatings to ensure data integrity and longevity. Additionally, photopatterning finds extensive applications in micro-electronics, enabling the fabrication of intricate circuits [22] and electronic components [23] with exceptional precision. Using photolithography techniques, scientists and engineers can create intricate patterns on semiconductor substrates, facilitating the development of smaller, faster, and more efficient electronic devices. [24] Furthermore, photopatterning has found applications in developing advanced materials, such as nanocomposites and functional coatings. [25-27] By precisely controlling the arrangement

of nanoparticles or polymers, researchers can engineer materials with tailored properties, including enhanced mechanical strength, electrical conductivity, or optical characteristics.

Overall, the development of photopatterning has significantly advanced the field of materials engineering, enabling the creation of intricate patterns and structures with high precision and versatility. As the technique continues to evolve and new materials and processes are developed, it holds great promise for driving further innovation in various scientific and technological domains.

1.2 Photoresponsive materials

Photoresponsive materials are substances that change their physical or chemical properties in response to light. [28] They are part of the broader class of stimuli-responsive materials, including materials that respond to changes in temperature, [29, 30] pH, [31, 32] magnetic fields, [33, 34], and other environmental stimuli. One of the main advantages of photoresponsive materials is their ability to control light in a precise manner, leading to improved performance in various applications. For example, in photonics, photo-responsive materials can be used to develop optical switches and modulators, enabling the manipulation of light signals in real time. [35] In biomedicine, photoresponsive materials can be used to develop new therapies, such as photodynamic therapy, [36] which uses light to activate drugs and destroy diseased cells. Additionally, photoresponsive materials can be used to develop new imaging techniques, allowing for more precise imaging of biological tissues and cells. [37] Despite the promising potential of photoresponsive materials, some challenges are associated with their development and use. For example, ensuring the stability and reproducibility of the materials over time can be challenging, and the need for precise control of light intensity and duration can be difficult to achieve. Overall, photoresponsive materials have the potential to impact a wide range of industries and have already shown promising results in various applications. Further research and development in this field is likely to lead to even more exciting breakthroughs in the future.

1.2.1 Photoresponsive molecules

Photoresponsive molecules, also known as photoswitchable or photosensitive molecules, are chemical compounds that can undergo reversible structural changes in response to light stimulation. The photoresponsive behavior of these molecules is often attributed to a specific molecular motif called a chromophore, which absorbs light energy and undergoes an intramolecular transformation. Depending on the particular design and chemical structure, photoresponsive molecules can exhibit different photoreactions, including photoisomerization, photodimerization, photocleavage, or controlled release of other molecules.

One prominent class of photoresponsive molecules is azobenzene, which contains an azo group (-N=N-) as the chromophore (**Figure 1.1a**). Azobenzene can exist in two isomeric forms, the *trans* and *cis* isomers, which have different molecular arrangements due to the rotation around the azo bond. [38] These isomers can interconvert by absorbing light within specific wavelength ranges, typically in the ultraviolet or visible spectrum. [39] This reversible photoisomerization makes azobenzene widely used as molecular switches in nanotechnology, materials science, and biophysics.

Another example of photoresponsive molecules is spiropyran-based compounds. Spiropyrans possess a spiropyran core structure that can undergo ring-opening to form a merocyanine compound upon absorption of light (**Figure 1.1b**). [40] The ring-opening process is reversible, and the spiropyran can be regenerated by exposure to a different wavelength of light. Recently, spiropyran-based hydrogel showed the abilities of phase transitions [41] and macroscopic actuation such as bending [42] and walking [43].

Dithienylethene also undergoes a reversible phototriggered ring-opening and ring-closing reaction. Irradiating the molecule with UV light converts the opened form to the closed form. The closed-form can be reversibly formed with the use of visible light (**Figure 1.1c**). [44, 45] The conjugation and electronic properties of two isomers exhibit significant disparities due to the restricted rotation and the conjugation of thienyl units in the closed-form configuration. Additionally, the reversible process involved in interconverting between the two isomers demonstrates remarkable recyclability, as it can be repeated multiple times without experiencing any noticeable alterations. This phenomenon highlights the stability and robustness of the isomerization process, further emphasizing its potential for various applications in functional materials and devices.

Photodimerization is the reaction that occurs between two of the same molecules and forms covalent bonds between each other upon light irradiation. This reaction is reversible when a different wavelength of light or heating is applied. Representative photodimerization reactions are [2+2] cycloaddition of coumarins and [4+4] cycloaddition anthracenes (**Figure 1.1d and e**). [46] Both cycloadditions can be reversed with light irradiation or heating.

Photocleavage is a significant irreversible photoreaction wherein chemical bonds can be permanently severed. This reaction extensively applies to controlled drug release systems and dynamic microenvironments within cells. [47] Among the various photolabile groups, o-nitrobenzyl compounds are widely employed as photocages or photolabile linkers in hydrogel chemistry. [48, 49] Upon exposure to UV light, the o-nitrobenzyl group undergoes cleavage, resulting in the permanent formation of o-nitrosobenzyl aldehyde and carboxylic acid species (**Figure 1.1f**). This photorelease mechanism provides precise spatiotemporal control over the release of bioactive molecules and enables the manipulation of complex cellular processes.

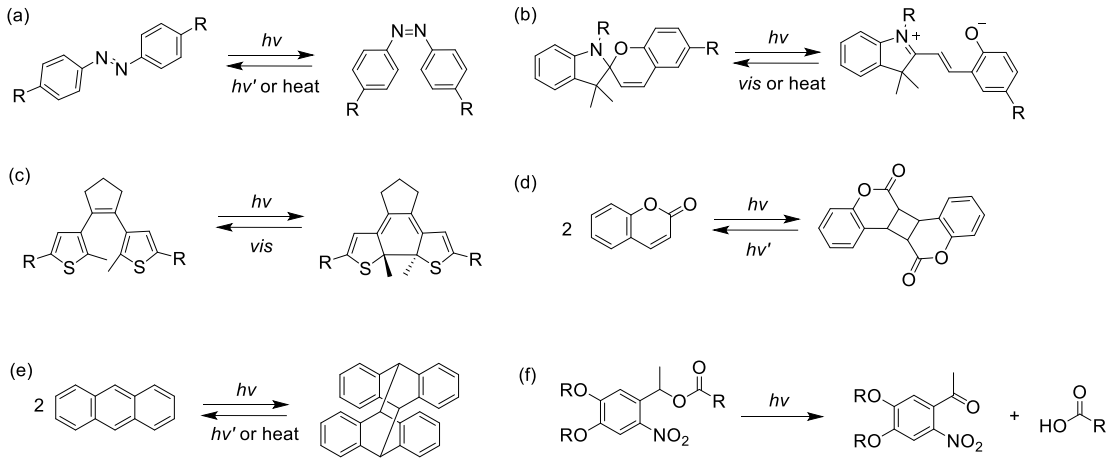

Figure 1.1 Representative reversible photoisomerization (a, b, and c), photo-dimerization (d and e), and photocleavage (f).

Overall, continuously exploring and designing novel photoresponsive molecules with tailored properties are promising for advancing technologies and scientific understanding. The ability to control and manipulate molecules with light provides a powerful tool for developing innovative applications across various disciplines, making photoresponsive molecules an exciting and rapidly evolving field of research.

1.2.2 Photoresponsive materials for photopatterning

Photoresponsive materials refer to a class of materials that exhibit changes in their properties or behavior when exposed to light. One significant application of photoresponsive materials is photopatterning, which allows for precise spatial control over material properties or composition using light. Photopatterning involves selectively modifying a material's properties or structure in specific areas by exposing it to light patterns. This technique enables the creation of complex patterns and structures with high precision and control, making it invaluable in many applications.

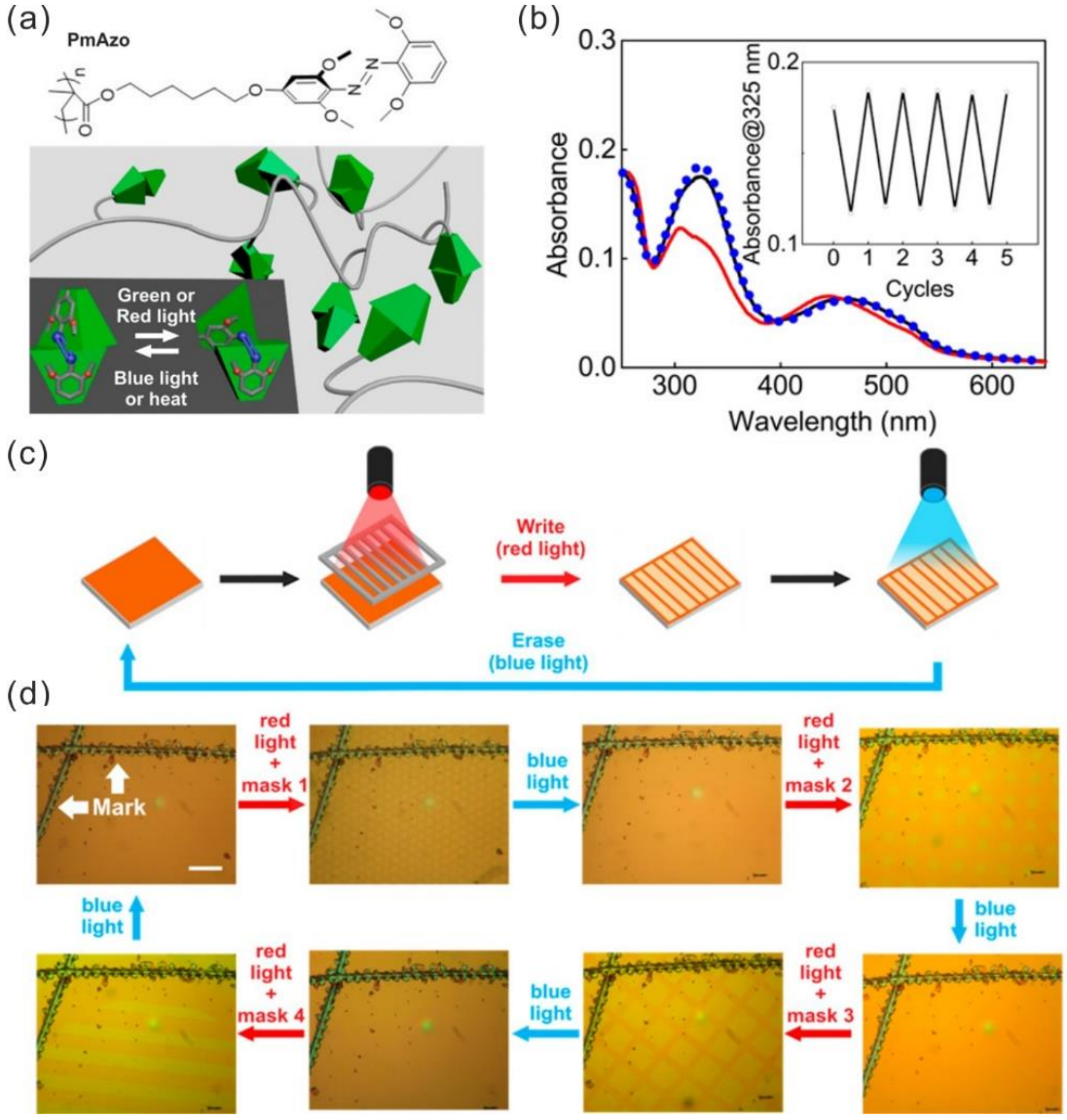

Figure 1.2 (a) Chemical Structures of Visible-Light-Responsive Azopolymer PmAzo. (b) UV–vis absorption spectra of a PmAzo film. Inset shows absorbance at 325 nm for five irradiation cycles. (c) Schematic illustration of reversible photopatterning of

PmAzo. (d) Photopatterning PmAzo imaged by optical microscopy. Reproduced by permission of ref. 50. Copyright 2016 American Chemical Society.

Photoresponsive materials are promising candidates for information storage. However, two general problems for photoresponsive materials used in rewritable optical storage are photobleaching and inefficient switching processes in solid state. To overcome both of these obstacles, our group demonstrate the synthesis of a new visible-light-switchable azopolymer with nonstackable azo chromophores for reversible and stable information storage (**Figure 1.2**). [50] The new azopolymer (PmAzo) contains ortho-methoxy-substituted azobenzene (mAzo) groups on the polymer side chains and shows reversible trans-to-cis or cis-to-trans isomerization by using distinct wavelengths of visible light. Moreover, photoinduced patterns on PmAzo can be stored for more than half a year. These properties distinguish PmAzo as a promising candidate for rewritable and stable information storage.

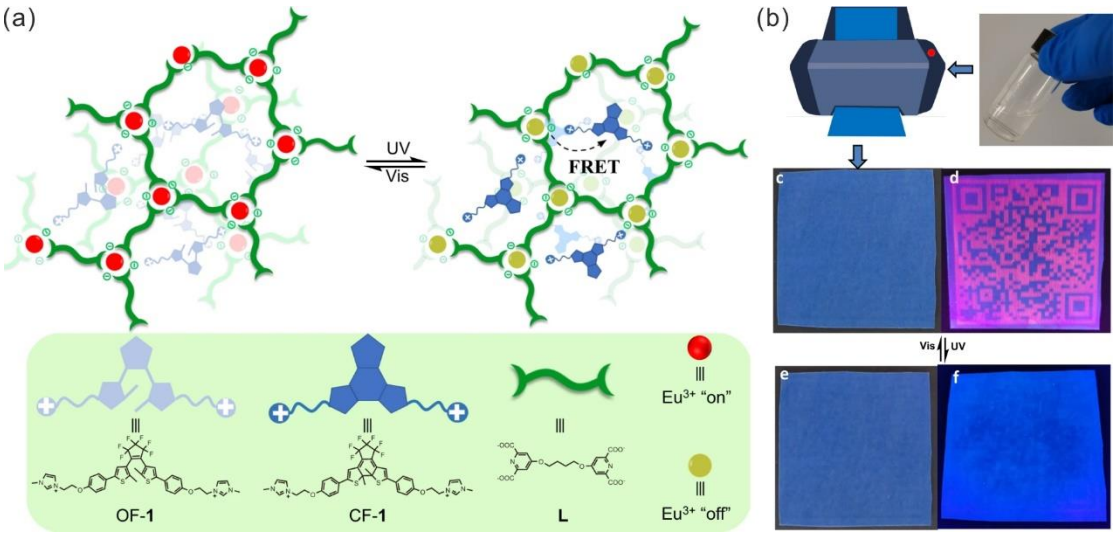

Figure 1.3 (a) The construction of the photochromic supramolecular coordination polyelectrolyte, and the chemical structures of corresponding components. (b) Light triggered quick response (QR) code with visible/invisible transformation behavior was achieved by using supramolecular coordination polyelectrolyte (SCP) as the smart ink. Reproduced by permission of ref. 7. Copyright 2021 Nature.

For developing new generation anticounterfeiting materials with high security, Zhao and coworkers reported the construction of a photoresponsive supramolecular

coordination polyelectrolyte (SCP) through hierarchical self-assembly of lanthanide ion, bis-ligand and diarylethene unit, driven by metal-ligand coordination and ionic interaction (**Figure 1.3**). [7] Owing to the conformation-dependent photochromic fluorescence resonance energy transfer between the lanthanide donor and diarylethene acceptor, the ring-closure/ring-opening isomerization of the diarylethene unit leads to a photoreversible luminescence on/off switch in the SCP. The SCP is then utilized as security ink to print various patterns, through which photoreversible multiple information patterns with visible/invisible transformations are realized by simply alternating the irradiation with UV and visible light.

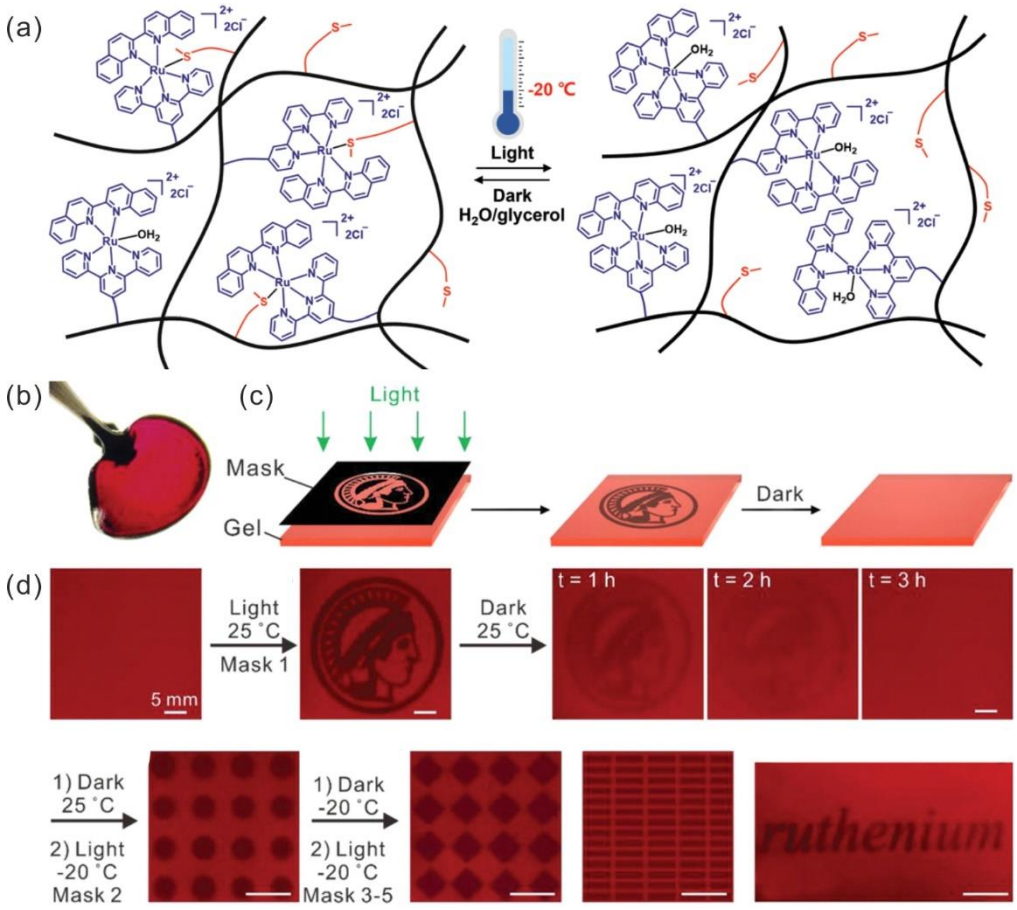

Figure 1.4 (a) Schematic illustration of a metallopolymer organohydrogel with photo-controlled Ru–thioether coordination crosslinks. (b) Photograph of freestanding organohydrogel. (c) Schematic illustration of writing patterns on the organohydrogel and the self-erasing process in the dark. (d) Self-erasable and rewritable patterns fabricated on an organohydrogel using different photomasks and different temperatures.

Reproduced by permission of ref. 63. Copyright 2020 WILEY-VCH Verlag GmbH & Co. KGaA.

By using Ru–thioether coordination bonds as photoresponsive crosslinks, our group reported metallopolymer organohydrogels that are photoresponsive even at −20 °C (**Figure 1.4a**). [51] The photoresponsiveness is attributed to ligand photo substitution of the Ru complex moieties. Ligand photo-substitution means that a coordinated ligand in a metal complex is replaced by another ligand upon light irradiation. The reversible coordination of Ruthenium–thioether not only results in changes in the crosslinking density but also results in color changes. Therefore, the organohydrogel is a suitable material for reversible photopatterning. A piece of free-standing organohydrogel (**Figure 1.4b**). The organohydrogel was irradiated with green light through a mask (**Figure 1.4c**). The color of the exposed areas changed, and a pattern was generated (**Figure 1.4d**). The Ru moieties and thioether moieties coordinated spontaneously when the irradiated organohydrogel was kept in the dark. The color of the irradiated areas changed back, and the pattern was self-erased in the dark at room temperature. Self-erasable gels were proposed for storing sensitive or temporary information, anticounterfeiting, and encryption.

Overall, the ability to create intricate patterns and structures using photoresponsive materials for photopatterning has numerous applications. These include information storage, anticounterfeiting, encryption, and the development of responsive surfaces or coatings. Researchers continue to explore and develop new photoresponsive materials and techniques to expand the capabilities of photopatterning, enabling advancements in various scientific and technological domains.

1.3 NIR-Light-responsive materials

Photoresponsive materials commonly exhibit sensitivity towards UV light. However, the utilization of UV light poses challenges in certain applications. In contrast, near-infrared (NIR) light has garnered interest due to its favorable characteristics for biomedical applications, [52, 53] 3D photopatterning, [54, 55] and information storage. [4, 56] NIR light offers advantages such as reduced photodamage and enhanced tissue penetration, enabling its effective interaction with biological systems, extracellular

matrices, and information storage media. By harnessing the benefits of NIR light, researchers aim to address limitations associated with UV light and unlock new possibilities in diverse fields.

1.3.1 Two-photon absorption

Two-photon absorption is a quantum mechanical process in which the simultaneous absorption of two photons leads to the excitation of an atom, molecule, or solid-state material. [57-59] This phenomenon occurs when the combined energy of two lower-energy photons is sufficient to promote an electron to a higher energy state, which would not be possible with the absorption of a single photon. In traditional one-photon absorption, the energy of a single photon is absorbed by an electron, causing it to transition from a lower energy level to a higher energy level (**Figure 1.5a**). The energy of the absorbed photon must match the energy difference between the two levels involved in the transition. However, in two-photon absorption, the total energy of the two photons is the sum of their individual energies, allowing for the absorption of higher-energy photons than would be possible through one-photon absorption alone (**Figure 1.5b**).

Two-photon absorption is a nonlinear optical process that occurs when a material is exposed to an intense laser beam. The probability of this process increases with the square of the laser intensity, making it particularly useful in applications involving high-power lasers. One of the key advantages of two-photon absorption is that it enables the excitation of molecules or materials to higher energy states while using longer wavelength photons, which are less prone to scattering and absorption by other materials. This phenomenon has found various applications in fields such as microscopy, [60] photodynamic therapy, [61] 3D optical data storage, [62] and quantum computing. [63] In microscopy, two-photon absorption allows for deeper tissue penetration compared to traditional microscopy techniques, enabling imaging of thicker samples with reduced photodamage. Photodynamic therapy utilizes two-photon absorption to selectively target and destroy cancer cells while minimizing damage to healthy tissues. In 3D optical data storage, two-photon absorption enables the recording of information in a 3D volume of a material. This allows for increased data storage density and capacity compared to traditional 2D storage methods. Additionally, in the

field of quantum computing, two-photon absorption plays a crucial role in manipulating and controlling quantum states of individual particles, such as ions or quantum dots, for the development of quantum information processing systems.

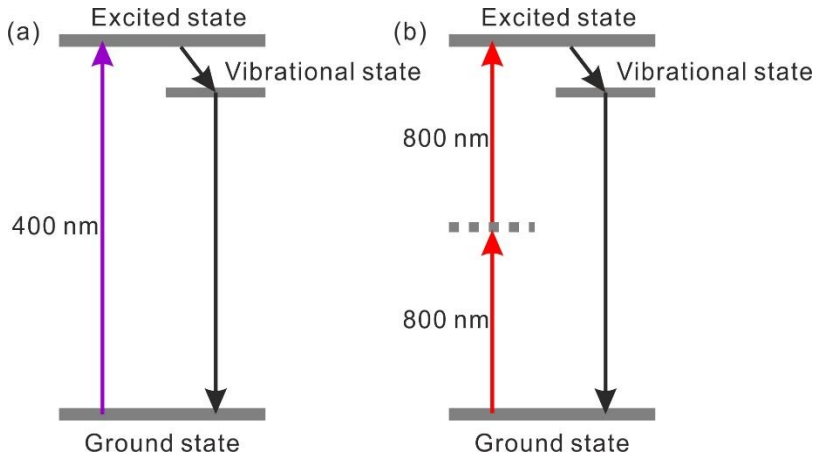

Figure 1.5 Schematic illustration of one-photon absorption (a) and two-photon absorption (b).

Overall, two-photon absorption is a fascinating phenomenon that has opened up new possibilities in various scientific and technological fields, providing unique advantages and applications that are not achievable with conventional one-photon absorption processes. However, the probability of two-photon absorption occurrence is inherently low. Consequently, molecules exhibit an ultra-low two-photon absorption cross section. Furthermore, the utilization of two-photon absorption requires specialized expensive femtosecond lasers with extremely high power to achieve the desired excitation conditions. Hence, the field of two-photon excitation in applications still faces challenges that require further improvement.

1.3.2 Upconversion process

Upconversion is also a nonlinear optical process that involves the absorption of multiple low-energy photons followed by the emission of a higher-energy photon. Unlike two-photon absorption, the upconversion process involves three steps (**Figure 1.6**). The first step is the absorption of multiple lower-energy photons. Each photon excites an electron within the material from its ground state to an intermediate energy level. Once

the electrons are excited to the intermediate energy level, energy transfer processes take place. These processes involve interactions between the excited electrons and neighboring ions within the material. Through various mechanisms such as cross-relaxation or energy migration, the energy is transferred to specific excited ions in higher energy levels. As the energy accumulates in the excited ions, the ions transition to higher energy levels. Upon reaching a sufficiently high energy level, the excited ions undergo a radiative transition, emitting a single, higher-energy photon. This emitted photon carries the combined energy of the absorbed photons, resulting in upconversion.

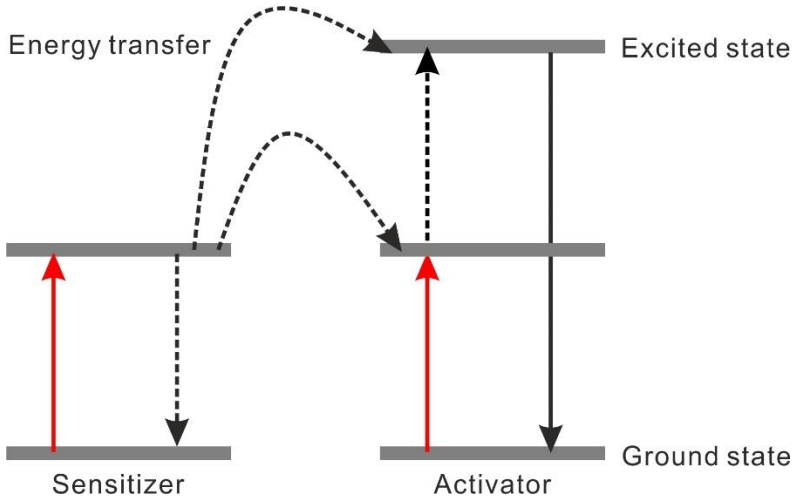

Figure 1.6 Schematic illustration of energy transfer upconversion process.

The upconversion process is primarily employed in two systems: lanthanide-doped UCNPs and triplet-triplet annihilation upconversion systems (TTA). The former system, UCNPs, has gained wide usage in different applications due to its stability and ease of operation. By combining UCNPs with photoresponsive materials, NIR-light-triggered photoreactions can be achieved. NIR irradiation induces the UV to visible emission of UCNPs, subsequently activating the photoreaction. In contrast to two-photon absorption, UCNP-involved photoreactions does not require high-intensity pulsed lasers. A cheap continuous wavelength (CW) laser diode can efficiently trigger upconversion. UCNP-assisted photochemistry is also a general approach for conventional photosensitive compounds. UCNP-assisted photochemistry of various photosensitive compounds, such as photochromic compounds, photocurable resins, and photodegradable polymers, have been reported. Upconversion processes have several

applications, including bioimaging, solar energy harvesting, 3D displays, and optical data storage. By converting infrared light to visible light, upconversion allows for imaging or detection in spectral regions where traditional detectors may be less sensitive. In summary, the upconversion process convert lower-energy photons into higher-energy photons. This process offers several advantages, making it a valuable tool in numerous applications.

1.3.3 NIR-Light-responsive materials for photopatterning

NIR-light-responsive materials incorporating two-photon absorption and UCNPs have gained significant attention in the field of photopatterning due to their unique advantages. [64, 65] NIR light has a longer wavelength compared to UV or visible light, allowing it to penetrate deeper into materials. This property enables efficient photopatterning in thicker samples or substrates that may hinder the penetration of shorter-wavelength light. [53] Consequently, more uniform and controlled patterning can be achieved throughout the material. Furthermore, NIR-light-responsive materials also offer precise spatial and temporal control over photopatterning processes. [66] By carefully designing the composition and properties of these materials, researchers can develop systems that exhibit specific responses, such as photochemical reactions or changes in physical properties, upon NIR light exposure. Additionally, NIR light experiences reduced scattering and absorption in various materials compared to shorter-wavelength light, resulting in diminished background interference. Moreover, NIR-light-responsive materials can exhibit excellent stability under prolonged exposure to NIR light. They can retain their responsiveness over extended periods, ensuring reliable and consistent performance for long-term photopatterning applications. [67]

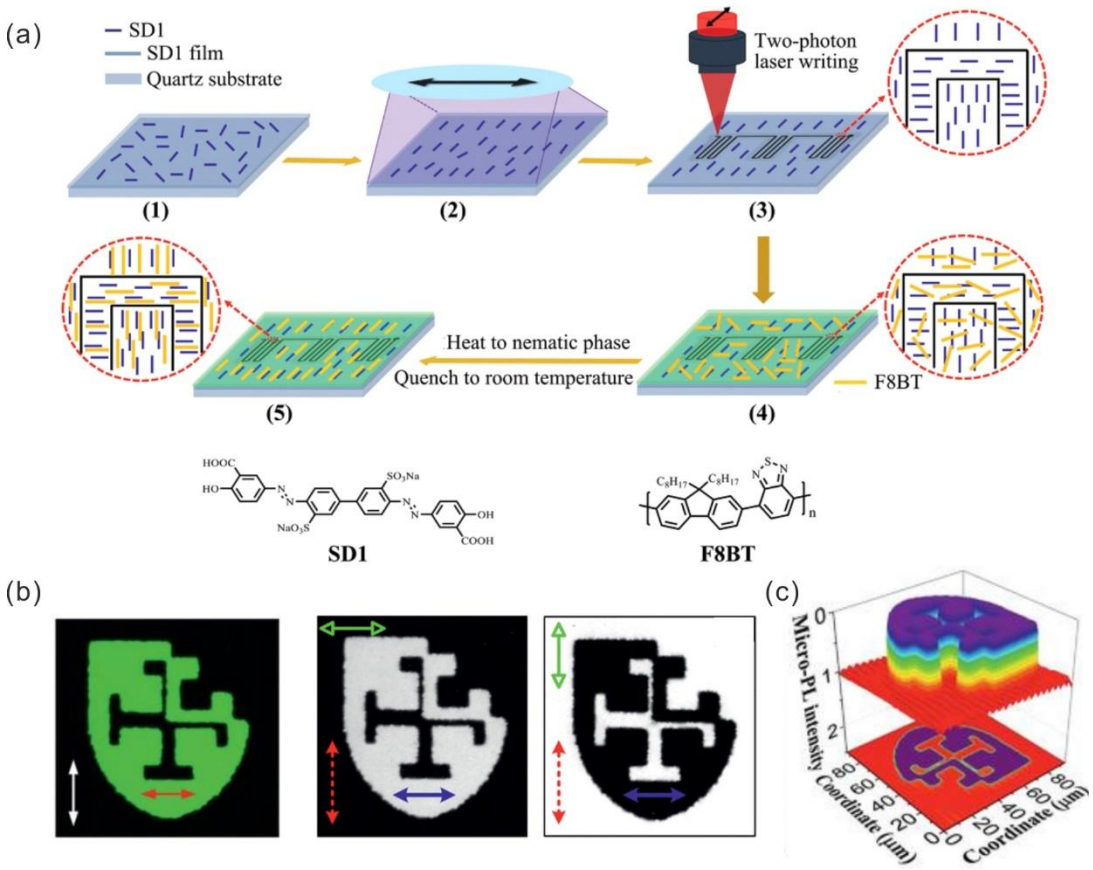

Figure 1.7 (a) Schematic illustration of two-photon laser writing. (b) the two-photon laser written pattern. (c) Spectrally integrated μ-PL intensity maps. Reproduced by permission of ref. 66. Copyright 2020 WILEY-VCH Verlag GmbH & Co. KGaA.

Utilizing the principles of two-photon absorption, Bradley and colleagues conducted a study wherein they demonstrated the laser writing and rewriting of n azobenzene sulphonic dye (SD1) alignment layers (**Figure 1.7a**). This technique enabled the generation of orientation patterns with superior quality in light-emitting liquid crystalline conjugated polymer (F8BT) films. The achieved spatial resolution was approximately 1μm, highlighting the high precision and fine detail achievable through this approach. [66] Noticeably higher anisotropies in optical absorption and PL emission are observed for films oriented on laser-patterned than on UV (LED) patterned SD1. The F8BT films oriented on laser written alignment layers also show a different microstructure (**Figure 1.7b and c**). The combination of photoalignment layers with laser writing/rewriting creates an exciting new platform for the fabrication of a range of photonic structures.

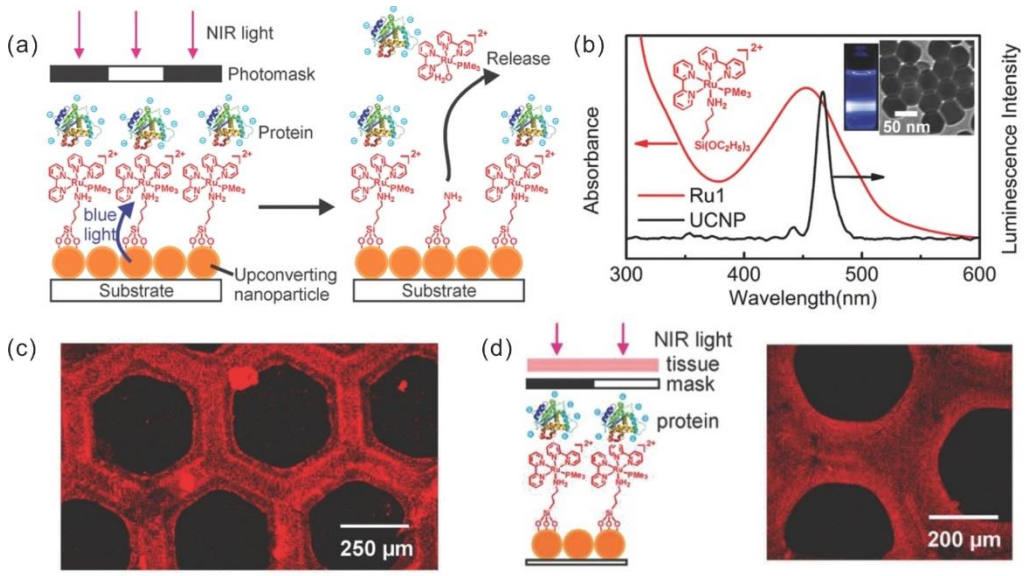

Figure 1.8 (a) Schematic of photon upconversion lithography (PUCL) for the patterning of proteins. (b) Absorption spectrum of Ru1 and emission spectrum of UCNPs. (c) Confocal laser scanning microscopy image of a protein pattern fabricated using PUCL. (d) Fabrication of a protein pattern using 974 nm light passed through 0.5 mm-thick tissue. Reproduced by permission of ref. 53. Copyright 2015 WILEY-VCH Verlag GmbH & Co. KGaA.

With the assisted of UCNPs, our group first presented a novel technique called Photon Upconversion Lithography (PUCL), which utilizes NIR light in conjunction with UCNPs for photo-lithography. [53] **Figure 1.8** demonstrates the successful patterning of proteins using PUCL. To achieve this, a blue-light-cleavable Ru complex (Ru1) and polyethylene glycol (PEG) were co-grafted onto the surface of the UCNP-decorated substrate. Through electrostatic interactions between the negatively charged proteins and the positively charged Ru complexes, the proteins were adsorbed onto the surface. For protein patterning, a photomask was placed between the NIR light source and the protein-coated surface. In the regions exposed to NIR light, the UCNPs convert the NIR light into blue light, triggering the cleavage of the Ru complexes and localized release of the proteins. This method enables the fabrication of precise protein patterns.

Overall, NIR-light-responsive materials based on two-photon and upconversion hold tremendous potential for advancing various technological applications. Continued research in this field is expected to lead to the development of novel materials and

strategies that further enhance their performance, enabling exciting advancements in areas such as information storage, encryption, biomedicine, and nanotechnology.

1.4 NIR-Light-responsive azobenzene-containing polymers

The development of photoresponsive materials relies on the presence of chromophores that exhibit a response to external light irradiation. Among the different types of chromophores, azobenzene is a remarkable chemical compound that has garnered significant attention in various scientific fields due to its unique properties and versatile applications. [13, 68]

1.4.1 Azobenzene

Azobenzene, with the chemical formula $C_{12}H_{10}N_2$, belongs to the class of organic compounds known as azo compounds. It consists of a central azo (-N=N-) group, which connects two aromatic benzene rings. [68-70] The presence of this azo group gives azobenzene its distinct characteristics, including its ability to undergo photoisomerization (**Figure 1.9**).

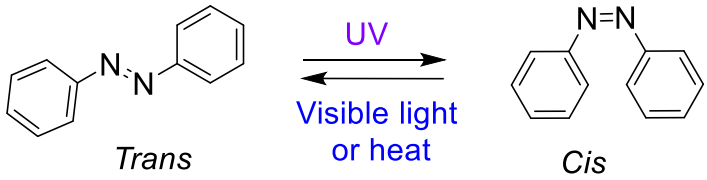

Figure 1.9 Molecular structure and photoisomerization of azobenzene.

One of the most intriguing features of azobenzene is its photoisomerization behavior. The *trans* isomer of azobenzene exhibits a linear conformation, while the *cis* isomer adopts a bent shape due to steric interactions between the phenyl rings. The photoisomerization process involves the conversion of *trans* azobenzene to *cis* azobenzene upon absorption of UV light, followed by the reverse isomerization back to the *trans* state under visible light or heat. In the trans configuration, the azobenzene molecule exhibits a nearly planar structure, with a dihedral angle of approximately 0° between the two benzene rings. As a result, the dipole moment of the trans isomer is measured to be 0 D. Upon exposure to UV light, the azobenzene molecule undergoes isomerization to the cis configuration. In the cis isomer, the molecule adopts a non-

planar structure, with a dihedral angle of approximately 60° between the two benzene rings. This structural change leads to an increase in the dipole moment, which is measured to be 3 D. Comparing the molecular dimensions of the trans and cis isomers, the trans configuration has a length and width of approximately 9.0 Å and 4.5 Å, respectively. In contrast, the cis isomer exhibits a more compact 2D arrangement, with a length and width of approximately 7.1 Å and 4.0 Å, respectively. However, the cis isomer extends in the third dimension due to the ~60° dihedral angle between the two benzene rings. When viewed from the side, the cis isomer resembles a closed equilateral triangle formed by the interlaced benzene rings. The thickness of the cis isomer is calculated to be 4.6 Å (**Figure 1.10**).

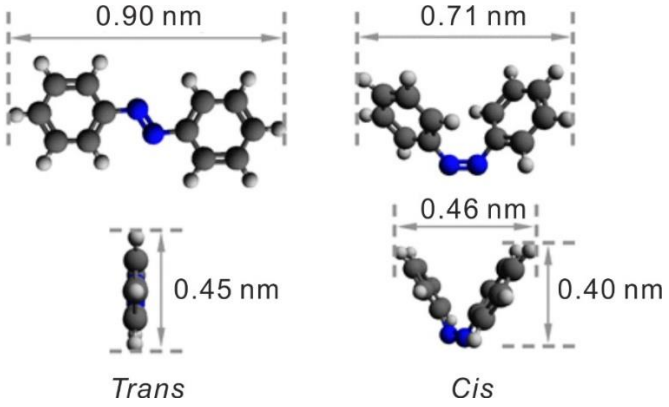

Figure 1.10 DFT calculated model of *trans* and *cis* azobenzene.

There are four mechanisms have been supposed as possible pathways for Azo photoisomerization, including rotation, inversion, concerted inversion, and inversion-assisted rotation (**Figure 1.11**). The rotation mechanism involves the cleavage of the N=N double bond, enabling unrestricted rotation of the N-N bond. [71] While the N-N-C angle remains approximately 120°, the C-N-N-C dihedral angle undergoes changes through rotation. In the inversion mechanism, the N=N double bond remains intact. One of the N=N-C angles increases from around 120° to 180°, while the other N=N-C angle retains its value at approximately 120°. Throughout this process, the C-N=N-C dihedral angle remains fixed at 0°. In the concerted inversion mechanism, both N=N-C bonds reach an angle of 180°, resulting in a linear transition state. The C-N=N-C dihedral angle remains constant at 0° throughout the entire process. The inversion-assisted rotation mechanism involves simultaneous changes in the C-N=N-C dihedral

angle and the N=N-C angles. In order to account for experimental observations, it is common to consider multiple isomerization pathways, as relaxation from any of the four transition states mentioned above can result in the formation of either the *trans* or *cis* isomer. [72]

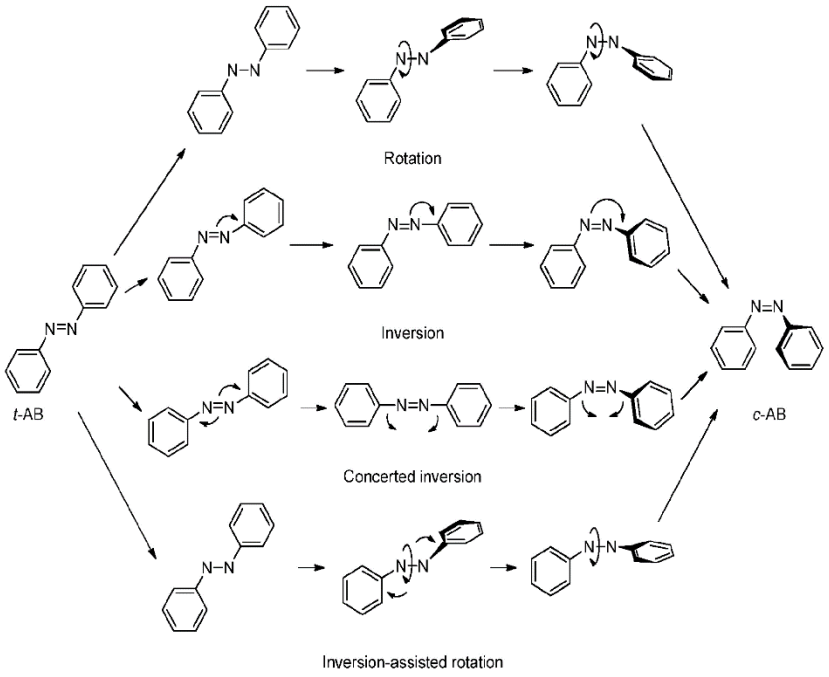

Figure 1.10 The supposed rotation, inversion, concerted inversion and inversion-assisted rotation pathways. Reproduced by permission of ref. 68. Copyright 2011 Royal Society of Chemistry.

1.4.2 Azobenzene-containing polymer

Polymers, with their unique and versatile characteristics, have revolutionized the field of material science. These large, chain-like molecules composed of repeating units offer a myriad of advantages over small molecules. [73] Hence, the transition from azobenzene small molecules to azopolymers has garnered significant attention among researchers. The aim is to retain the key characteristics of azobenzene small molecules to their fullest extent within the polymer matrix. Leveraging the exceptional mechanical properties and processability offered by polymers can be effectively applied in diverse material applications. This transition holds promise for advancing the capabilities of

materials in various fields, including data storage, optical data processing, and photovoltaics.

The most intriguing property of azobenzene compounds is the reversible photoisomerization of azo bond, which can be fast acquired between the thermally stable *trans* form and the meta-stable *cis* form. Thermally stable trans form can be converted to the cis form by illumination with UV light, and the cis form can be converted back to the trans form upon irradiation photochemically at visible light or thermally by heating. [13, 68, 74, 75] Photoisomerization of azo compounds can be used to switch many properties of photoresponsive polymers, such as glass transition temperature, shape, orientation, and polarity. [76]

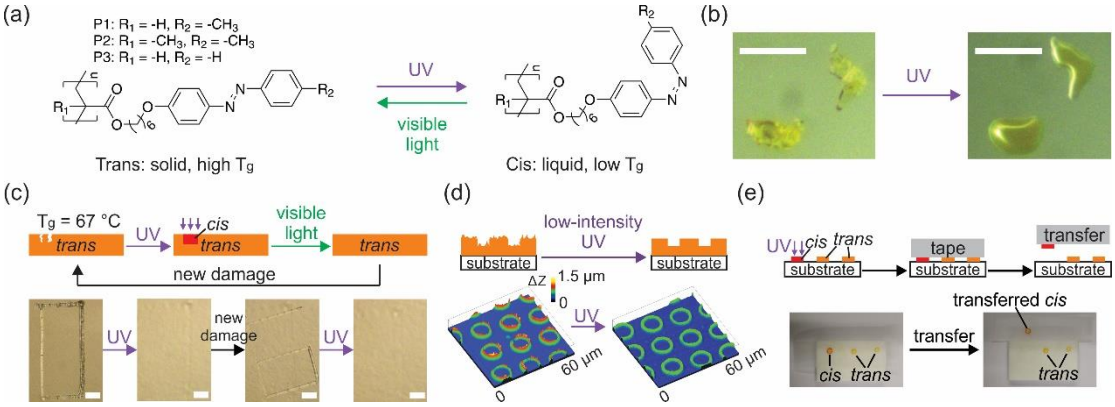

Figure 1.11 (a) Chemical structures and photoisomerization of azopolymers. (b), Optical microscopy images of azopolymer powders before and after UV irradiation (c) Photoinduced healing of scratches on a film based on high molecular weight azopolymers. (d) Photoinduced reduction of the surface roughness. (e) Transfer printing based on photoinduced solid-to-liquid transitions. Reproduced by permission of ref. 13. Copyright 2017, Springer Nature.

Recently, our group developed new azopolymers which show photo-induced moving behaviors. [13] Our group demonstrated that light can switch the T_g of azopolymers and induce reversible solid-to-liquid transitions of the polymers (**Figure 1.11**). The azobenzene groups in the polymers exhibit reversible *cis–trans* photoisomerization abilities. *Trans* azopolymers are solids with T_g above room temperature, whereas *cis* azopolymers are liquids with T_g below room temperature. Because of the photoinduced solid-to-liquid transitions of these polymers, light can reduce the surface roughness of azopolymer films by almost 600%, repeatedly heal cracks in azopolymers,

and control the adhesion of azopolymers for transfer printing. The photoswitching of T_g provides a new strategy for designing healable polymers with high T_g and allows for control over the mechanical properties of polymers with high spatiotemporal resolution.

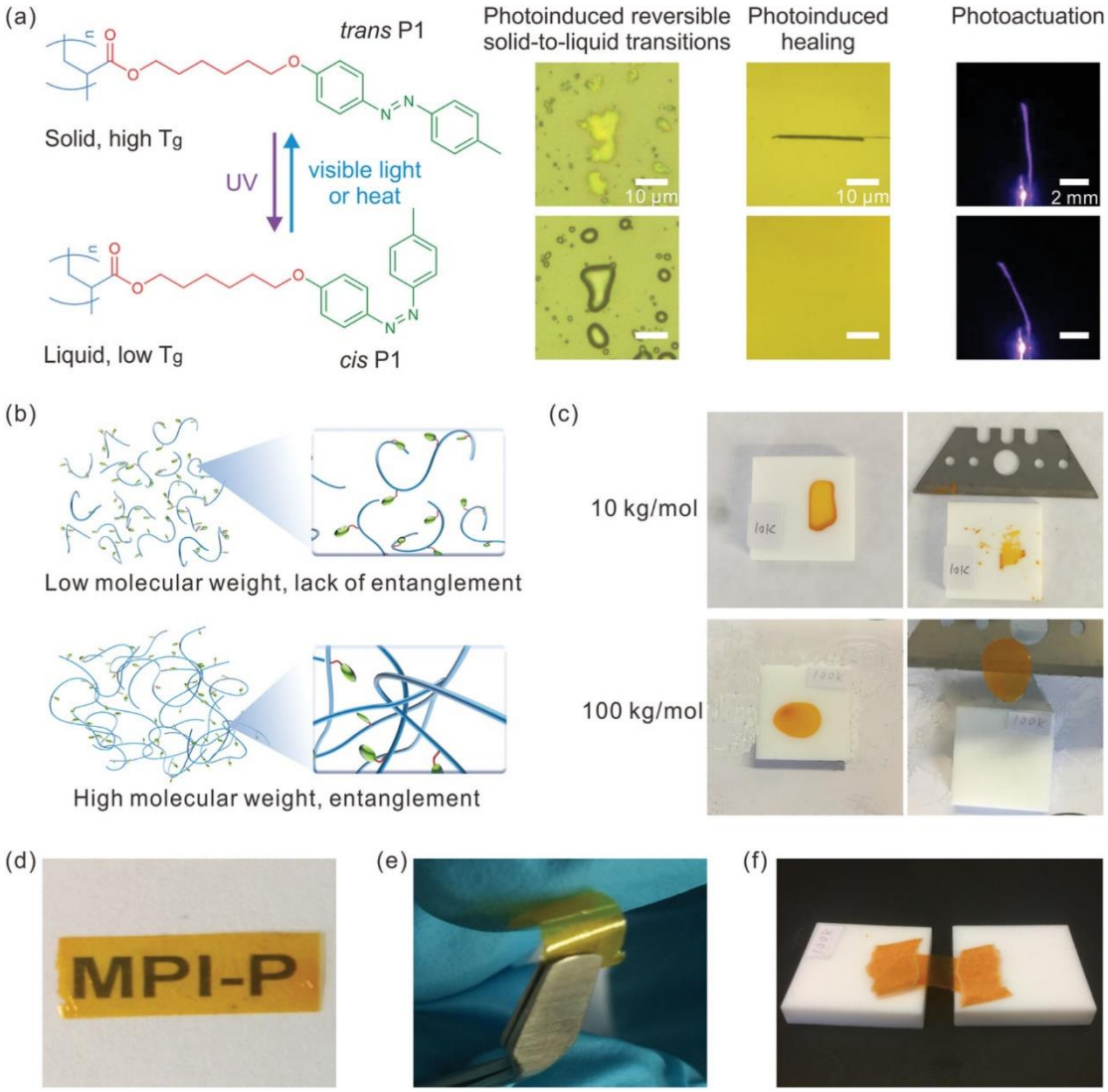

Figure 1.12 Chemical structure, photoresponsive properties, entanglement models, and mechanical properties of the azopolymer P1. Reproduced by permission of ref. 75. Copyright 2019 WILEY-VCH Verlag GmbH & Co. KGaA.

Photoactuators based on liquid crystal elastomers or networks are smart materials that show photoinduced motions. However, their crosslinked networks make their repair or reprocessing difficult. To address this limitation, a healable and reprocessable photoactuator is fabricated using entangled high-molecular-weight azobenzene-

containing polymers (azopolymers) that are non-crosslinked (**Figure 1.12**). [75] The azopolymer photoactuators show photoinduced bending based on photoinduced *trans–cis* isomerization of the azopolymers on the irradiated side. The experiments show not only photoinduced phase transitions or changes in the order parameters but also photoinduced solid-to-liquid transition of the azopolymers resulting in shape changes and mechanical responses. Thus, photoinduced solid-to-liquid transition is a new mechanism for the design of photoactuators. Moreover, the azopolymer photoactuators are healable and reprocessable via solution processing or light irradiation. Healability and reprocessability prolong lifetimes of photoactuators are important for materials reusage and recycling, and represent a new strategy for the preparation of smart materials.

Overall, azobenzene-containing polymers present a promising class of materials that exhibit unique optoelectronic properties and responsiveness to external stimuli. Their ability to undergo reversible photoisomerization makes them highly desirable for different applications. Further advancements in their synthesis, stability, and photoconversion efficiency will undoubtedly expand their applications and unlock new opportunities in various scientific and technological domains. With ongoing research and development efforts, azobenzene-containing polymers hold immense potential to shape the future of materials science and engineering.

1.4.3 Upconverting nanoparticles-assisted photoisomerization of Azopolymers

Most photo sensitive materials are sensitive to UV light. However, UV light is problematic for some applications. Compared with UV light, NIR light is better suited to biomedical applications, 3D photopatterning and information storage. [77] Recently, UCNPs were used to construct NIR-sensitive materials. UCNPs convert NIR light to UV or visible light, which can trigger photoreactions of photosensitive materials. [78, 79]

UCNP-assisted photoisomerization is the process of using NIR light to induce photoisomerization with the assistance of UCNPs (**Figure 1.13**). Azobenzene derivatives show reversible *trans* to *cis* isomerization under the irradiation by UV and visible light, respectively. Wu et al. demonstrated that azotolane showed *trans* to *cis* isomerization by 980 nm light irradiation with the assistance of $NaYF_4$:Yb/Tm UCNPs. [80]

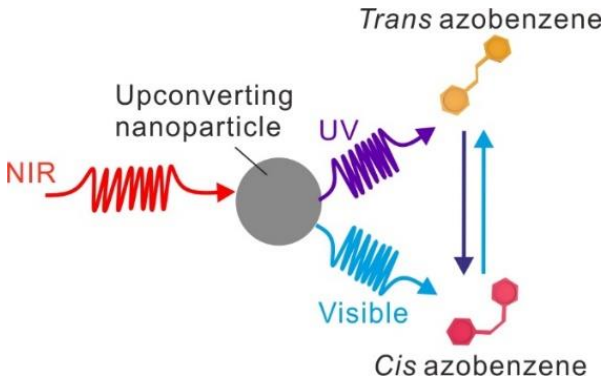

Figure 1.13 Schematic illustration of UCNP-assisted photoisomerization. UCNPs convert NIR light to UV or visible light, which induces photoisomerization of azobenzene.

The combination of UCNPs with drug carriers has been explored. Yao et al. developed a novel liposome drug delivery system (DDS) for NIR light-triggered, repeated, and titratable anticancer drug release based on upconversion nanoparticles (UCNPs) encapsulated azobenzene liposome nanostructure, designated as UCNP@Azo-Lipo (**Figure 1.14**).[81] Upon NIR irradiation, the loaded UCNPs can convert NIR light into the UV/vis region emissions, which can be absorbed immediately by the photoresponsive azobenzene amphiphilic molecules in the liposome frameworks. The reversible isomerization of the azo-groups caused by simultaneous UV and visible light emitted from the UCNPs creates continuous rotation-inversion movement for the liposome membrane, therefore realize the controlled drug release. The NIR light-triggered drug release ability makes this novel DDS an effective chemotherapy to overcome multidrug resistant in cancer therapy by spatiotemporal control. This DDS provides great values in the advancement of clinical NIR light-regulated precise drug release and drug-resistant tumor treatment applications.

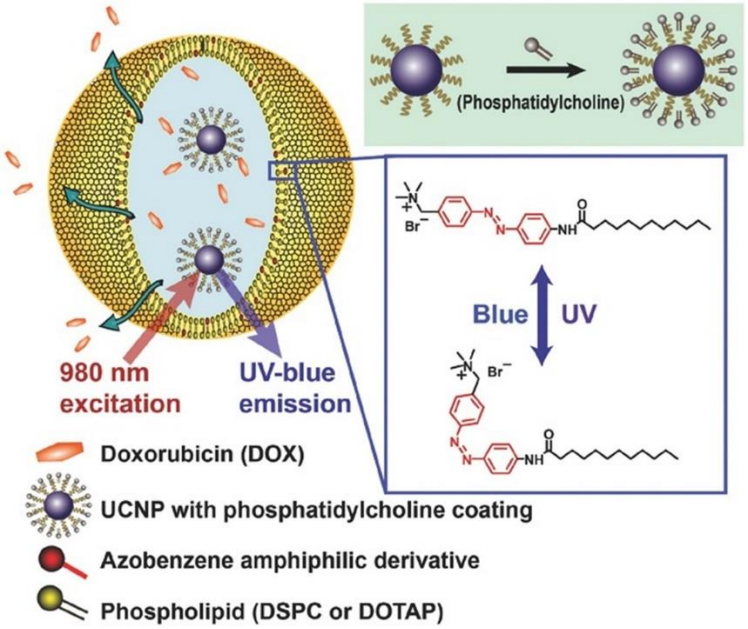

Figure 1.14 Schematic illustration of the NIR-triggered azobenzene-liposome/upconversion nanoparticle hybrid vesicles for controlled drug delivery, depicting the phosphatidylcholine coated UCNPs and anticancer drug DOX can be loaded together within the hydrophilic compartment of the liposome, as well as the azobenzene amphiphilic derivatives are embedded in the liposome bilayers consisting of phospholipid (DSPC and/or DOTAP). Reproduced by permission of ref. 81. Copyright 2019 WILEY-VCH Verlag GmbH & Co. KGaA.

Azobenzene-containing liquid-crystal elastomers have been widely recognized as UV-driven actuators. [82] However, for biomedical applications, there is a need to expand the responsive wavelength of these actuators to the NIR region. To address this, Wu et al. developed a composite film by coating UCNPs onto a cross-linked liquid-crystal polymer containing azotolane units. [80] Azotolane, compared to normal azobenzene, exhibits a longer absorption wavelength that conveniently overlaps with the upconverted blue light emitted by Tm^{3+}-containing UCNPs. Upon exposure to 980 nm light, the upconverted blue light triggers the photoisomerization of the azotolane units within the composite film. This isomerization alters the alignment of the mesogens, leading to bending behavior. Subsequently, when the NIR light is turned off, the bent film returns to its initial flat state.

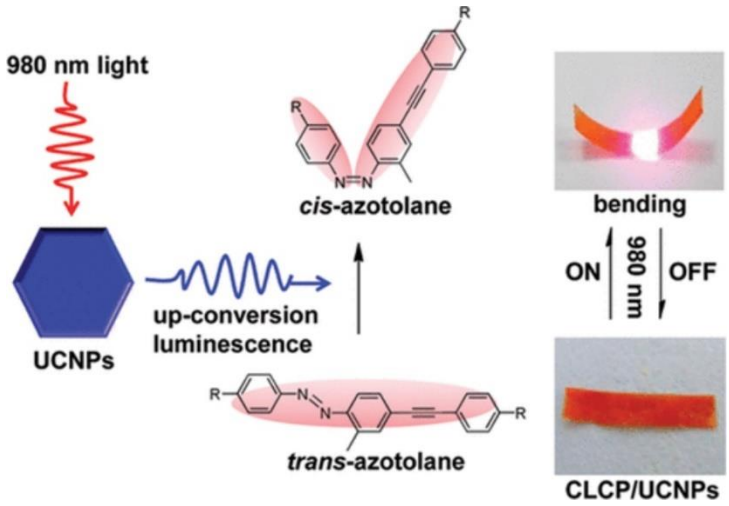

Figure 1.15 Schematic illustration of the UCNP-incorporated azotolane-containing liquid-crystal polymer film. Bending of the film was induced by NIR light at 980 nm. The upconversion luminescence of the UCNPs leads to *trans–cis* isomerization of the azotolane units and an alignment change of the mesogens. The bent film completely returned to the initial flat state after NIR light was turned off. Reproduced by permission of ref. 80. Copyright 2011, American Chemical Society.

UCNP-assisted photoisomerization has emerged as a promising approach for the production of NIR responsive azopolymers. With the utilization of UCNPs, NIR light can effectively initiate photoisomerization. Exploring novel UCNP-assisted materials represents a significant avenue for future research, as it holds the potential to generate NIR responsive materials with innovative functionalities and diverse applications. By uncovering and advancing new photoreactions in the presence of UCNPs, the development of advanced materials that respond to NIR radiation can be greatly enhanced, paving the way for numerous technological advancements in various fields.

1.5 Outline of this thesis

This thesis focuses on the utilization of nanocomposites comprising UCNPs and azopolymer for the fabrication of photopatterns. In the introductory chapter, an overview of the upconversion process and photoresponsive materials is provided.

Chapter 2 presents the fabrication of a photoresponsive nanocomposite composed of UCNPs and azopolymer, exhibiting distinctive security features that can be easily detected with the naked eye and characterized using analytical tools. This

nanocomposite possesses excellent processability and can be conveniently applied to a variety of items, such as banknotes, wines, medicines, and other products. The integration of azopolymer and UCNPs establishes this nanocomposite as an advanced material for anticounterfeiting applications.

In Chapter 3, building upon the demonstrated fabrication of 2D photopatterns using the photoresponsive nanocomposite with photomasks, an innovative 3D PUDL system is developed for the creation of 3D photopatterns without the need for photomasks. This work introduces a promising approach to optical recording and represents a significant advancement in 3D photolithography.

Finally, Chapter 4 summarizes the main achievements and conclusions of this research. It also provides suggestions for future work, highlighting potential ideas and investigations in the field of photoresponsive materials for photopatterning

Chapter 2: Experiments and Methods

2.1 Materials

11-[4-(4-Butylphenylazo)-phenoxy]undecyl methacrylate (>97%), anisole (>99%), and cyclopentanone (>99%) were purchased from TCI. Cyanoisopropyl dithiobenzoate (RAFT agent, CPDB), ytterbium(III) acetate hydrate (99.9%), thulium(III) acetate hydrate (99.9%), yttrium(III) acetate hydrate (99.9%), 1-octadecene (90%), oleic acid (90%), ammonium fluoride (≥99.99%), hydrochloride (≥37%) and 2,2′-azobisisobutyronitrile (AIBN, 98%) were purchased from Sigma-Aldrich. AIBN was recrystallized twice from methanol before use. All other solvents (HPLC grade) were purchased from Sigma-Aldrich or Fisher Scientific and used without further purification.

2.2 Instruments and characterization

UV/Vis/NIR absorption spectra were collected using a Lambda 900 spectrometer (Perkin Elmer).

Transmission electron microscopy (TEM) images were recorded using a JEOL JEM1400.

Scanning electron microscopy (SEM) images were collected using a LEO Gemini 1530 system. Dynamic light scattering (DLS) measurements were performed on a commercially available instrument from ALV GmbH consisting of a goniometer and an ALV-5000 multiple-tau full-digital correlator. The DLS measurements were performed at the scattering angle of 90º with a 532 nm laser.

Upconversion photoluminescence measurements were performed on a Spex Fluorolog II (212) spectrometer.

The molecular weight and polydispersity index of the azopolymer were determined by gel permeation chromatography (GPC) (Waters Alliance 2000).

Differential scanning calorimetry (DSC) curves were measured on a Mettler Toledo DSC 822 system. DSC measurements were conducted under a N_2 atmosphere from -50 °C to 150 °C with heating and cooling rates of 10 °C/min.

Thermogravimetric analysis (TGA) measurements were conducted on a Mettler Toledo TGA/SDTA 851 system with a heating rate of 10 °C/min under a N_2 atmosphere.

Dynamic mechanical analysis (DMA) was conducted on an Advanced Rheometric Expansion System (ARES, Rheometric Scientific Company).

^{1}H nuclear magnetic resonance (^{1}H NMR) spectra were measured using a Bruker Spectrospin spectrometer (250 MHz) at 25 ℃.

Upconversion photoluminescence measurements were performed on an Avaspec-3648-USB2 (Avantes) spectrometer.

FT-IR measurements were conducted with a Varian 1000 FT-IR spectrometer.

Trans-to-*cis* photoisomerization of azopolymer was induced by LED at λ= 365 nm (LCS-0365-07-22, Mightex Systems) and *cis*-*trans* photoisomerization was induced by LEDs at λ= 470 or 530 nm (LCS-0470-03-22 or LCS-0530-15-22, Mightex Systems). The output power of the LEDs was controlled by a LED controller (device type SLC-MA04-MU, Mightex Systems).

Polarized optical microscopy (POM) images were captured under crossed polarizers (90°) on a Zeiss III microscope equipped with a PixeLINK PL-A662 camera.

Optical microscopy images were captured on an optical microscope (Zeiss) equipped with a CCD camera.

Three-dimensional confocal microscopy images were captured by a white-light confocal microscope μsurf explorer (NanoFocus AG) or confocal microscope (Leica SP8).

A diode laser with a wavelength of 979 nm (FC-W-979-25W-Laser, Changchun New Industries Optoelectronics Technology) coupled with a 400-μm (core) fiber was used as the excitation laser source. The diode laser was equipped with an adjustable fiber collimator (Changchun New Industries Optoelectronics Technology). The output

power density of the diode laser was measured using an optical power meter (model 407A, Spectra-Physics Corp.) and an NIR indicator (Newport, model F-IRC1).

Raman spectra were collected using a WITec alpha 300 Raman microscope coupled with a UHTS 300 spectrometer.

Atomic force microscopy (AFM) measurements were performed on a Multi-Mode atomic force microscope (Bruker) in tapping mode. AFM silicon cantilevers (Olympus) with a nominal spring constant of ≈ 70 N m^{-1} and a nominal tip radius of 7 nm were used.

2.3 Design and build of Direct writing system

The laser direct writing system utilized in this study is illustrated in **Figure 2.1**. A homemade setup was employed, utilizing a single-mode continuous-wave diode laser operating at a wavelength of 979±5 nm (TEM-W-980-200mW-Laser, Changchun New Industries Optoelectronics Technology), which was coupled with a 400-μm (core) fiber to serve as the excitation laser source. The diode laser controller was connected to a frequency generator capable of adjusting the pulse repetition rate within the range of 1-30 kHz. The output power density of the diode laser was measured using an optical power meter (model 407A, Spectra-Physics Corp.) and an NIR indicator (Newport, model F-IRC1) (**Figure 2.2**). An adjustable fiber collimator (Changchun New Industries Optoelectronics Technology) was incorporated into the diode laser setup. The laser beam possessed a Gaussian-shaped intensity profile and was focused using a high-power infrared objective (Thorlab, LMH-50x-1064, NA = 0.65), resulting in an estimated focal size of 1.4 μm. The sample was positioned on a computer-controlled 25 mm motorized translation stage (Thorlab, PT3-Z8), enabling 3D movement with a calculated spatial resolution of 29 nm. Direct laser writing was performed by translating the nanocomposite films along a predetermined path.

Figure 2.1 Illustration of the setup of 3D Photon Upconversion Direct Lithography (PUDL) process.

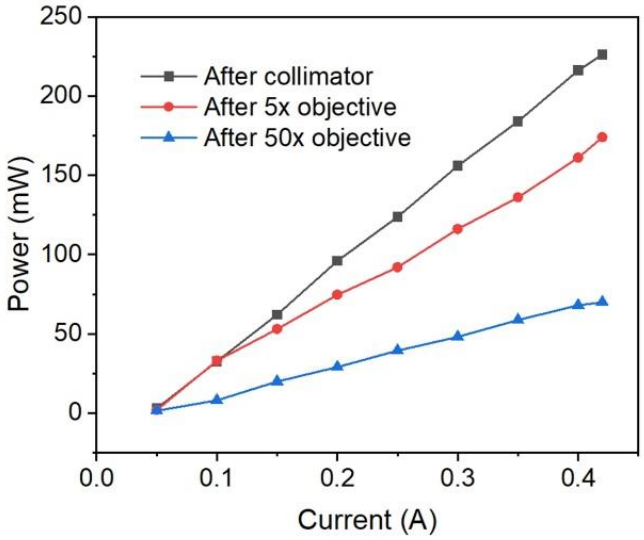

Figure 2.2 The power of NIR laser as function of current after collimator, 5x objective and 50x objective.

2.4 Synthesis and characterization

Azopolymer (PAzo): PAzo was syntheisized by reversible addition-fragmentation chain-transfer polymerisation (RAFT). The azobenzene-containing monomer (11-[4-

(4-butylphenylazo)phenoxy]undecyl methacrylate) (2 g, 4.06 mmol), CPDB (8.69 mg, 0.04 mmol), and AIBN (1.35 mg, 0.006 mmol) were dissolved in anisole (4 mL). The solution was then treated with four freeze-pump-thaw cycles and sealed under Ar gas. The system was placed in an oil bath at 70 °C for 24 h. After polymerisation, the polymer solution was added dropwise to methanol (100 mL). The precipitate was dissolved in THF and precipitated from methanol three times to remove the unreacted monomers. The resulting polymer (PAzo) was collected and dried in a vacuum oven at 40 °C for 24 h. PAzo was in a stable *trans* state. It was dried again in an oven at 120 °C for 6 h and at 40 °C for two days under vacuum for DSC measurements. Yield: 47%. M_n (GPC) = 30 kg/mol and M_w/M_n = 1.12 (**Figure 2.3**). ^{1}H NMR (CD_3Cl): δ (ppm) = 7.85–7.77, 7.27, 6.94 (protons on the azobenzene group), 3.94 (Ar-O-CH_2, -O-CH_2), 2.66 (Ar-CH_2), 1.75–0.91 (protons on the polymer backbone and -CH_2-CH_2-CH_2-CH_2-CH_2-CH_2-CH_2-CH_2-, -CH_2-CH_2-) (**Figure 2.4**).

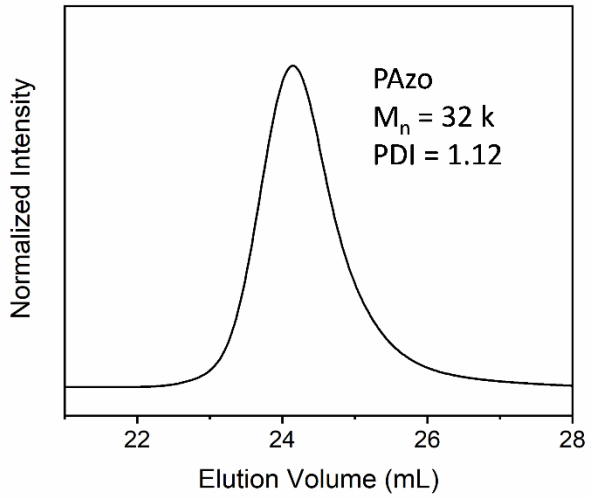

Figure 2.3 GPC trace of PAzo.

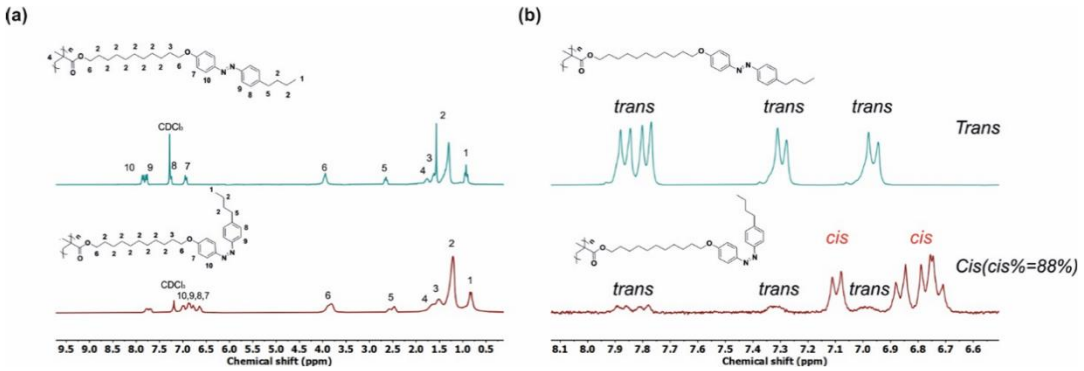

Figure 2.4 ^{1}H NMR spectra of PAzo in CD_3Cl (a) and CD_2Cl_2 (b) before and after 365 nm light irradiation (15 min, 42 mW cm^{-2}). The integration from the spectrum showed that approximately 88% of the *trans* isomers were converted into *cis* isomers.

Synthesis of β-$NaYF_4$: 0.5 mol% Tm^{3+}, 30 mol% Yb^{3+} core nanoparticles: $Y(CH_3COO)_3 \bullet xH_2O$ (372 mg, 1.4 mmol), $Yb(CH_3COO)_3 \bullet xH_2O$ (210 mg, 0.6 mmol) and $Tm(CH_3COO)_3 \bullet xH_2O$ (3.5 mg, 0.01 mmol) were added to a 100 mL threeneck round-bottom flask containing octadecene (30 mL) and oleic acid (12 mL). The solution was stirred magnetically and heated to 120 °C under vacuum (heating rate: 3 °C/min) to form the lanthanide oleate complexes. The solution was degased at 120 °C for 15 min to remove residual water, acetic acid and oxygen. The temperature of the solution was then lowered to 50 °C and the reaction flask was placed under a gentle flow of Ar. During this time, a solution of ammonium fluoride (296 mg, 8.0 mmol) and sodium hydroxide (200 mg, 5.0 mmol) dissolved in methanol (20 mL) was prepared via sonication. Once the reaction mixture reached 50 °C, the methanol solution was added to the reaction flask and the resulting cloudy mixture was stirred for 30 min at 50 °C. The reaction temperature was then increased to ~70 °C and degased for 15 min to remove methanol in the reaction flask. Then, the reaction flask was placed under a gentle flow of Ar. Subsequently, the reaction temperature was increased to 300 °C (heating rate: 20 °C/min) under the Ar flow and kept at this temperature of 90 min. During this time the reaction mixture became progressively clearer until a completely

clear, slightly yellowish solution was obtained. The mixture was allowed to cool to room temperature naturally. The nanoparticles were precipitated by the addition of ethanol (~80 mL) and isolated via centrifugation at 5000 rpm. The resulting pellet was dispersed in a minimal amount of hexane (5-10 mL) and precipitated with excess ethanol (~60 mL). The nanoparticles were isolated via centrifugation at 5000 rpm and then dispersed in hexane (10–15 mL) for the subsequent shell growth procedure.

Synthesis of β-$NaYF_4$: 0.5 mol% Tm^{3+}, 30 mol% Yb^{3+}/β-$NaYF_4$ core/shell nanoparticles: The $NaYF_4$:TmYb@$NaYF_4$ upconverting nanoparticles (UCNPs) were synthesized according to a literature method. $Y(CH_3COO)_3$•xH2O (479 mg, 1.8 mmol) was added to a 100 mL threeneck round-bottom flask containing octadecene (30 mL) and oleic acid (12 mL). The solution was stirred magnetically and heated to 120 °C under vacuum (heating rate: 3 °C/min) and maintain at 120 °C for 15 min. The temperature of the reaction flask was lowered to 80 °C and the reaction flask was placed under a gentle flow of Ar. Then, the dispersion of $NaYF_4$: 0.5 mol% Tm^{3+}, 30 mol% Yb^{3+} core nanoparticles in hexane, which was synthesized by the procedure shown above, was added to the flask. The resulting solution was heated to 110 °C (heating rate: 5 °C/min) and degased for 15 min to remove hexane in the reaction flask. The reaction mixture was cooled to 50 °C and the flask was place under a gentle flow of Ar. Then, a solution of ammonium fluoride (259 mg, 7.0 mmol) and sodium hydroxide (175 mg, 4.4 mmol) in methanol (20 mL) was added. The resulting cloudy mixture was stirred at 50 °C for 30 min. The reaction temperature was then increased to ~70 °C and degased for 15 min to remove methanol in the reaction flask. Then, the reaction flask was placed under a gentle flow of Ar. Subsequently, the reaction temperature was increased to 300 °C (heating rate: 20 °C/min) and kept at this temperature for 90 min under the Ar flow. The mixture was allowed to cool to room temperature naturally. The nanoparticles were precipitated by the addition of ethanol (~80 mL) and isolated via centrifugation at 5000 rpm. The resulting pellet was dispersed in a minimal amount of hexane (5-10 mL) and precipitated with excess ethanol (~60 mL). The nanoparticles were isolated via centrifugation at 5000 rpm and then stored in cyclohexane (15 mL). TEM and DLS studies of these UCNPs showed average particle diameters of 53 nm and 57 nm, respectively (**Figure 2.5**).

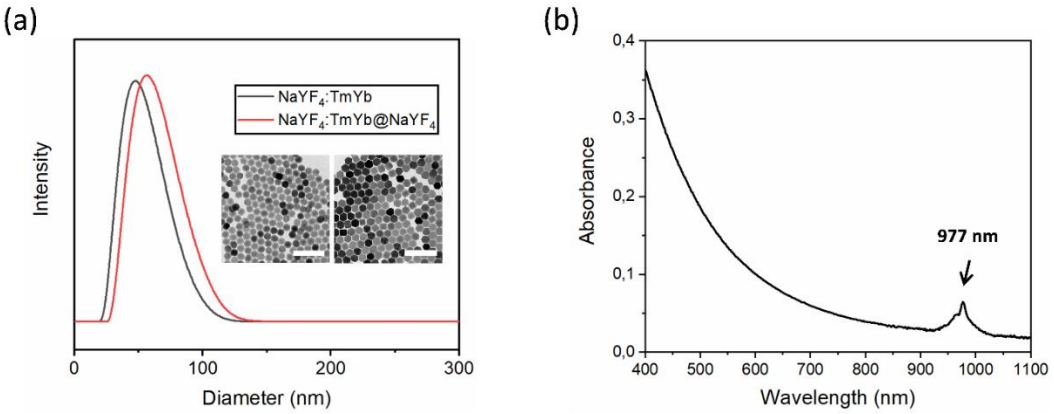

Figure 2.5 (a) $NaYF_4$:TmYb and $NaYF_4$:TmYb@$NaYF_4$ UCNPs studied by dynamic light scattering (DLS). The average diameters for $NaYF_4$:TmYb and $NaYF_4$:TmYb@$NaYF_4$ UCNPs were 50 and 57 nm, respectively. Insets: TEM images of $NaYF_4$:TmYb (left) and $NaYF_4$:TmYb@$NaYF_4$ (right). (b) UV/Vis/NIR absorption spectrum of $NaYF_4$:TmYb@$NaYF_4$ UCNPs in cyclohexane. The absorption maximum is at 977 nm.

Ligand-Free UCNPs: Oleic acid removal was performed by an acid-base reaction. Briefly, 50 mg of UCNPs were dispersed in 5 mL of hexane and added to a 10 mL 0.1 M HCl aqueous solution. This mixture was allowed to stir at room temperature for 4 hours, or until all nanoparticles migrated to the aqueous layer, as viewed under 980 nm excitation. The aqueous layer was isolated and centrifuged at 10000 rpm for 30 minutes to collect the ligand free nanoparticles. The nanoparticles were washed twice with deionized water, twice with THF and redispersed in 1 mL of THF.

Azopolymer capped UCNPs (UCNPs@PAzo): 200 mg PAzo was first dissolved in 9 mL THF. Then, 1 mL of ligand-free nanoparticles was added drop by drop, followed by stirring at room temperature overnight. The obtained yellow nanoparticles were collected via centrifugation at 10000 rpm for 30 min, washed several times with THF, redispersed in 2 mL of THF, and stored in a fridge at 4 °C. TEM images of UCNPs and UCNP@PAzo were shown in **Figure 2.6**. The successful coating of PAzo was confirmed using Fourier transform infrared (FTIR) spectroscopy (**Figure 2.7**)

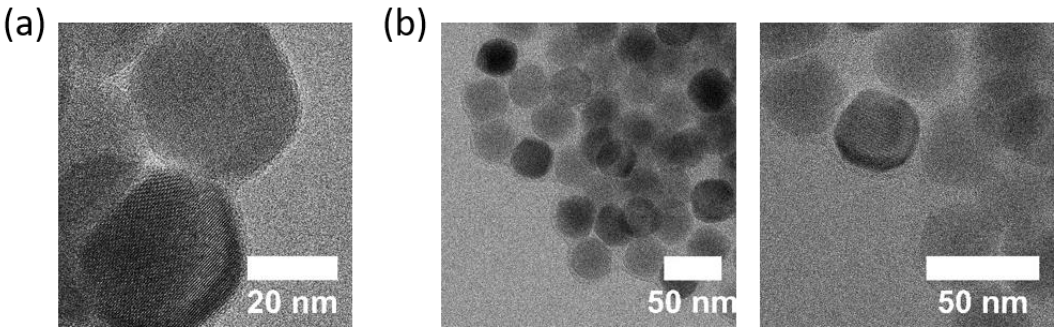

Figure 2.6 High resolution TEM images of UCNPs (a) and UCNP@PAzo (b).

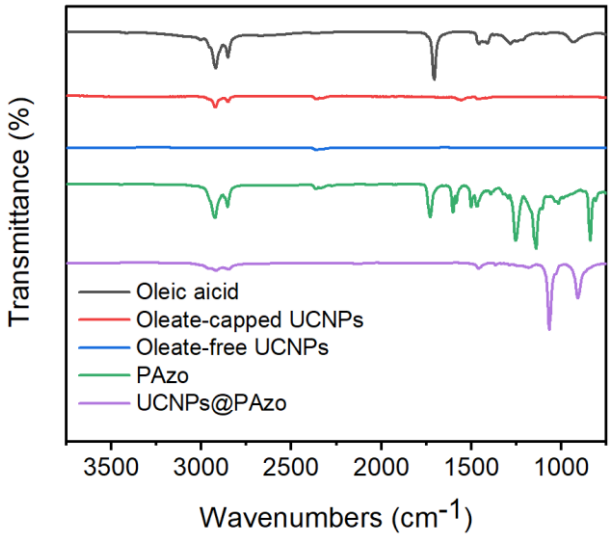

Figure 2.7 Infrared absorption spectra of oleic acid, oleate-capped UCNPs, ligand free UCNPs, PAzo and UCNP@PAzo.

Preparation of the PAzo/UCNP nanocomposite films

Typically, a colloidal dispersion of the $NaYF_4$:YbTm@$NaYF_4$ UCNPs (2 mL, 1 wt% in THF) was added to a vial containing a PAzo solution (2 mL, 20 wt% in cyclopentanone). The dispersion was sonicated for 20 min to yield a homogeneous

PAzo /UCNPs dispersion. Thin films were prepared by spin coating. The THF/cyclopentanone dispersion of UCNPs (0.5% wt) and PAzo (10 wt%) were spin-coated onto glass/wafer/PET (polyethylene terephthalate) substrates. The film thickness was controlled by adjusting the spin rate. The resulting PAzo/UCNPs films were dried in a vacuum oven at 40 °C for 24 h. Thicker films were prepared by drop-casting. The THF/cyclopentanone dispersion of UCNPs (0.5% wt) and PAzo (10 wt%) were drop-casted on glass substrates. The films were then dried overnight under vacuum at 40 °C. **Figure 2.8** showed that a homogeneous material was obtained.

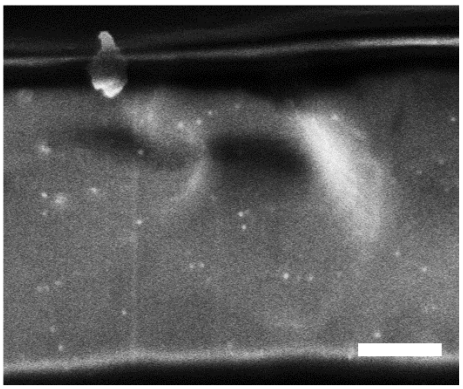

Figure 2.8 Cross-sectional SEM image of a PAzo/UCNP nanocomposite film. The bright spots are UCNPs that are doped in the PAzo matrix. Scale bar, 1 μm.

Preparation of the PAzo/UCNP@PAzo nanocomposite films

50 mg PAzo was dissolved in UCNP@PAzo dispersion (2 mL, 2.5 wt% in THF). The dispersion was sonicated for 1h to yield a homogeneous PAzo/UCNP@PAzo dispersion. Thin films were prepared by spin coating onto silicon wafer substrates (1000 rpm, 60s). The resulting PAzo/UCNP@PAzo films were dried in a vacuum oven at 40 °C for 12 h. The thickness of this layer was around 600 nm. The approximate nanoparticle concentration in the film was ~26 nM (~100 nanoparticles in the focal volume of the 0.65 NA objective lens). TGA indicated that the purified UCNP@PAzo and PAzo/UCNP@PAzo contained 30 wt% and 20 wt% of PAzo, respectively (**Figure 2.9**).

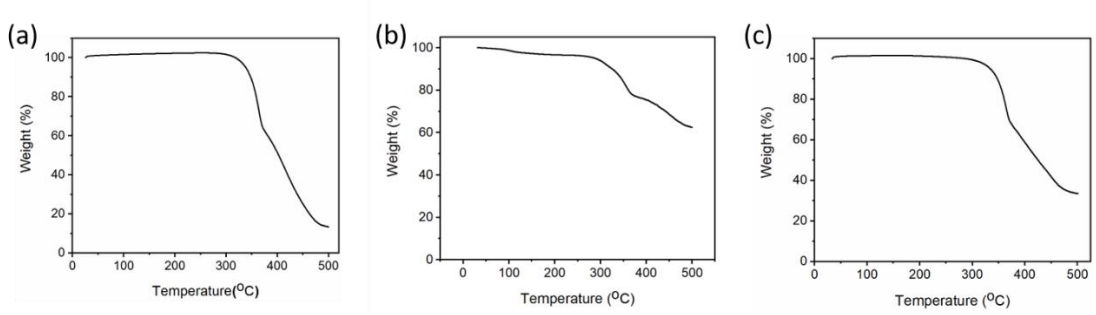

Figure 2.9 TGA curves of pure PAzo (a), UCNPs@PAzo (Grafting rate: 30 wt%, 0.2 nm^2) (b) and PAzo/UCNPs@PAzo (20 wt% UCNPs@PAzo) (c).

Preparation of the three different layers nanocomposite film

50 mg PAzo was dissolved in UCNP@PAzo dispersion (2 mL, 2.5 wt% in THF). The dispersion was sonicated for 1h to yield a homogeneous PAzo/UCNP@PAzo dispersion. Thin films were prepared by spin coating onto silicon wafer substrates (1000 rpm, 60s). The resulting PAzo/UCNP@PAzo films were dried in a vacuum oven at 40 °C for 12 h. Initially, the film was exposed to UV light (365 nm, 67 mW cm^{-2}, 5 min). Subsequently, the cis nanocomposite film was subjected to polarized blue light irradiation (470 nm, 29 mW cm^{-2}, 15 min) to induce chromophore alignment. Following this step, a 100 μm thick cover glass (MENZEL-GLASER) was affixed onto the spin-coated layer. Subsequently, double-layer films were prepared by spin coating onto the cover glass at 1000 rpm for 60 seconds. This process was repeated iteratively until the desired number of layers was achieved.

2.6 Preparation of the Polarization-dependent patterns

UV (365 nm, 67 mW cm^{-2}, 5 min) irradiation induced *trans*-to-*cis* isomerization. Then, irradiation of the *cis* nanocomposite film with polarized blue light (470 nm, 29 mW cm^{-2}, 15 min) induced the alignment of the azobenzene chromophores. Following this, the film underwent dual irradiation of UV light and polarized blue light, facilitated by a photomask. Notably, the polarization direction employed was perpendicular to the previously polarized blue light, resulting in the orientation of the exposed area's

azobenzene chromophores being perpendicular to those in the unexposed regions. Importantly, the pattern could be erased utilizing UV light and was rewritable using a distinct photomask, thereby demonstrating the potential for dynamic control over the pattern formation process (**Figure 2.10**).

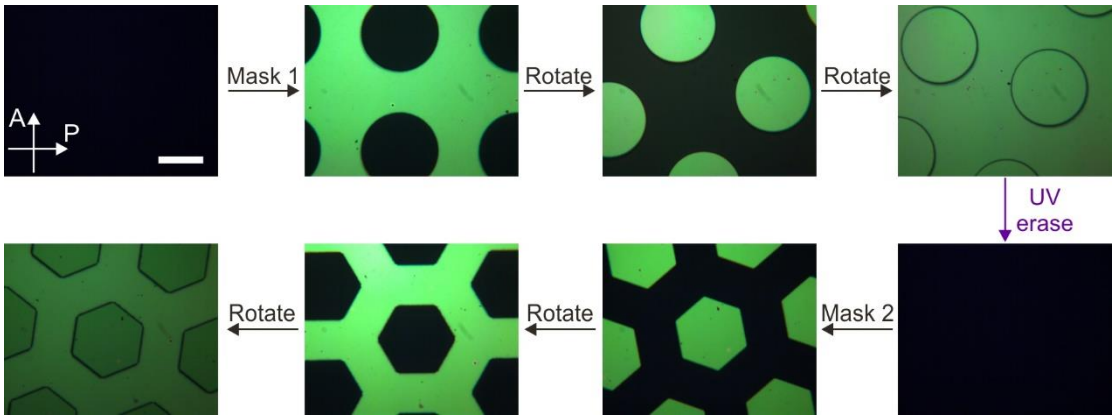

Figure 2.10 Photomask-fabricated films featuring erasable and rewritable polarization-dependent patterns serve as a background for the PUDL process. Scale bar: 200 μm.

Chapter 3: Fabrication of two-dimensional photopatterns for anticounterfeiting applications

Prof. Dr. Si Wu and Yazhi Liu convinced the idea. Prof. Dr. Si Wu and Prof. Dr. Hans-Jürgen Butt led the project. Yazhi Liu synthesized the materials and did the experiments. Shuofeng Liang and Chenrui Yuan revised the manuscript. Dr. Kaloian Koynov and Andreas Best contributed to the optical setup. Dr. Michael Kappl did the nanoindentation measurement.

3.1 Introduction

Counterfeiting is a growing issue worldwide. To combat it, anti-counterfeiting materials, such as digital water marks,[83, 84] diffraction gratings,[85, 86] photonic structures,[87-90] stimuli-responsive materials[90-96], and luminescent materials,[97, 98] have been developed for distinguishing banknotes, valuable products, important documents, etc. These anti-counterfeiting materials alter their appearance, color, optical signal, or other properties in response to external stimuli,[82, 99] and their responses can be observed by the naked eye or validated using analytical tools, thereby helping distinguish counterfeits from real ones. An issue with traditional anti-counterfeiting materials is that they usually have a single security feature, such as a unimodal emission or a color change. Such materials provide a low level of security because the replication of a single security feature is relatively easy. In addition, high-end applications require that anti-counterfeiting materials are discerned quickly (by the naked eye) and accurately (by analytical tools). It is possible to label a product with several anti-counterfeiting materials that impart numerous security features to it; however, processing several anti-counterfeiting materials on a product is complicated, and step-by-step labelling of different counterfeiting materials has low detection efficiency.[18] To solve the above-mentioned problems, it is necessary to integrate multiple security

features, different read-out methods, and easy processing into a single anti-counterfeiting material.

In this study, we introduced a novel nanocomposite, which has several prominent security features that can be discerned with the naked eye and using analytical tools. The nanocomposite has good processability and can be easily applied to banknotes, wines, medicines, and other products (**Figure 3.1a**). It is composed of a photoresponsive azopolymer and UCNPs. Because of reversible *cis-trans* photoisomerization,[101-103] azopolymers show photochromism,[104] photoswitchable glass transition temperatures (T_g),[105] and photoinduced orientations.[106, 107] These photoresponsive properties enable the development of various anti-counterfeiting features, such as color-changing structures, photonic structures, and polarization-dependent structures, on the nanocomposite. UCNPs, which convert NIR light to visible light,[108] impart high-contrast color-, structure-, and polarization-dependent upconversion luminescence to the nanocomposite. The synergistic combination of the azopolymer and UCNPs make the nanocomposite an advanced anti-counterfeiting material.

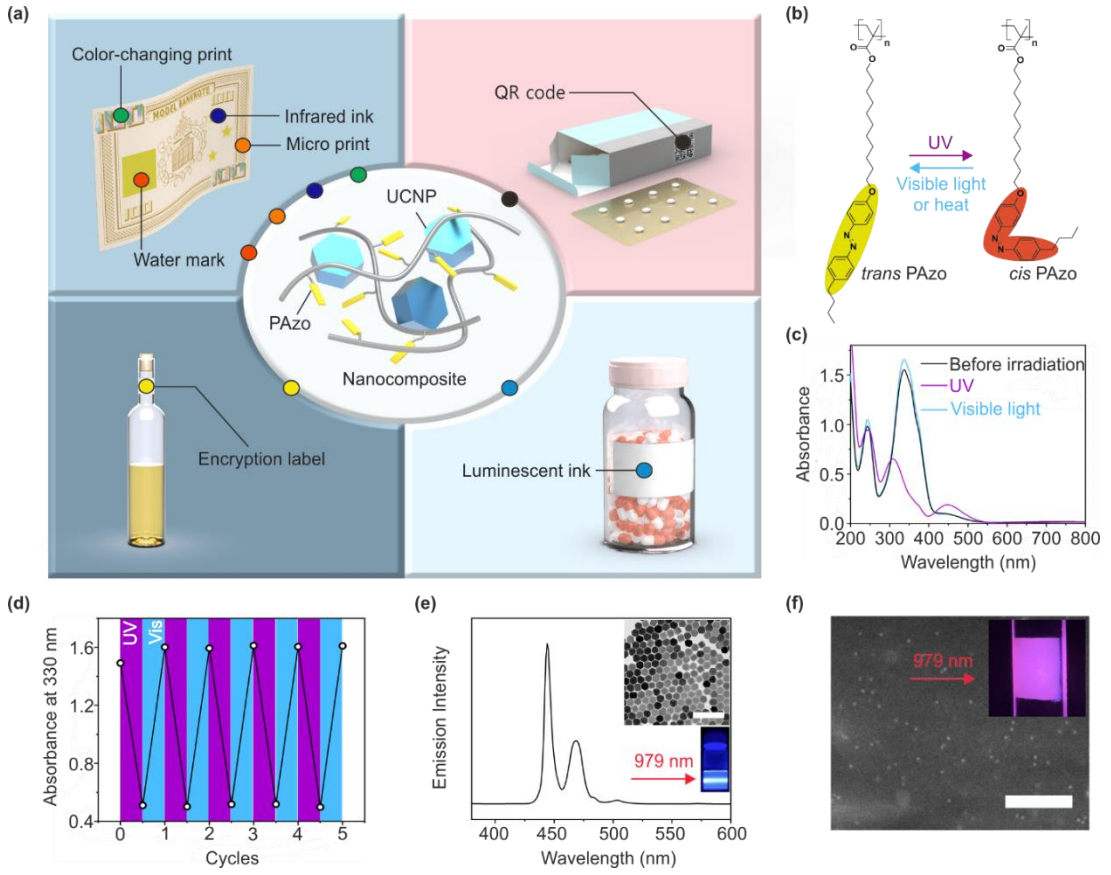

Figure 3.1 (a) Schematic of the anti-counterfeiting nanocomposite comprising of the azopolymer (PAzo) and UCNPs for different applications. (b) Chemical structure and photoisomerization of PAzo. (c) UV–vis absorption spectra of a spin-cast film of PAzo before irradiation, after UV irradiation (365 nm, 67 mW cm^{-2}, 1 min), and subsequent visible light irradiation (530 nm, 42 mW cm^{-2}, 1 min). (d) The absorption changes under alternating UV and visible light irradiation. (e) Upconversion luminescence spectrum (λ_{ex} = 979 nm) of β-phase $NaYF_4$:TmYb@$NaYF_4$ (core = $NaYF_4$: 0.5 mol% Tm^{3+}: 30 mol% Yb^{3+}; shell = $NaYF_4$) UCNPs excited with NIR light (10.8 W cm^{-2}). Insets: a TEM image of UCNPs and a photograph of a dispersion of UCNPs upon a 979-nm-laser exposure. Scale bar: 200 nm. (f) SEM image of PAzo/UCNP nanocomposite. Scale bar: 1 μm. Inset: a photograph of the nanocomposite on a quartz substrate upon a 979-nm-laser exposure. Copyright 2021 WILEY-VCH Verlag GmbH & Co. KGaA.

3.2 Results and disscusion

3.2.1 Characterization of nanocomposite

We synthesized the azopolymer PAzo matrix of the nanocomposite (**Figures 3.1b**). The number-average molecular weight (M_n) and PDI of PAzo measured by GPC were 3.2 × 10^4 g mol^{-1} and 1.12, respectively. PAzo exhibited reversible *cis-trans* photoisomerization (**Figures 3.1b, c**). The spin-cast film of PAzo exhibited a strong π–π* absorption band at 337 nm and a weak n–π* band at 448 nm. UV irradiation decreased the π–π* band intensity and increased the n–π* band intensity, demonstrating that *cis-trans* isomerization had occurred. Subsequent visible-light irradiation transformed the *cis* PAzo back to its *trans* state. Reversible photoisomerization was also induced for multiple cycles (**Figure 3.1d**).

In addition, β-phase $NaYF_4$:TmYb@$NaYF_4$ UCNPs (core = $NaYF_4$: 0.5 mol% Tm^{3+}: 30 mol% Yb^{3+}; shell = $NaYF_4$) were synthesized. TEM and DLS studies of these UCNPs showed average particle diameters of 53 nm and 57 nm, respectively. The UCNPs emitted blue light upon excitation with NIR light at 979 nm (**Figure 3.1e**). To prepare the target nanocomposite, PAzo and UCNPs were mixed in an organic solvent and thin films were prepared by spin-coating or drop-casting. The UCNP content in the nanocomposite was 10 wt%. SEM images of the nanocomposite film showed that a homogeneous material was obtained (**Figures 3.1f**).

3.2.2 Color-changing patterns and photonic structure

To demonstrate the anti-counterfeiting function of the nanocomposite, reversible color-changing patterns were fabricated on a nanocomposite film based on *cis-trans* photoisomerization (**Figure 3.2a**). Initially, a drop-cast film of the PAzo/UCNP nanocomposite was in a stable *trans* state (**Figure 3.2a(i)**). After the film was irradiated with UV light through a photomask, the irradiated areas changed from yellow to orange due to *cis-trans* isomerization (**Figure 3.2a(ii)**), and a pattern was formed. The pattern was then erased via heating, which induced *cis*-to-*trans* reverse isomerization (**Figure 3.2a(iii)**). Another pattern was fabricated on the film using a different photomask (**Figure 3.2a(iv)**). Reversible color changes can be easily observed with the naked eye for anti-counterfeiting.

We observed that the *trans* PAzo/UCNP nanocomposite was a hard solid, while the *cis* PAzo/UCNP nanocomposite was a soft rubber-like material (**Figure 3.2b**). We recently demonstrated that azopolymers exhibit photoswitchable T_g values.[105] Therefore, we inferred that the PAzo/UCNP nanocomposite also exhibits a photoswitchable T_g, which results in reversible photo-softening. Hence, we examined *trans* and *cis* PAzo/UCNP nanocomposites by DMA. *Trans* PAzo/UCNP had a T_g of 71 °C (**Figure 3.2c, Figure 3.6**). Its storage modulus (G) and loss modulus at temperatures (G″) below T_g were similar to those of plastic; thus, it was a hard solid at room temperature. In contrast, the *cis* PAzo/UCNP nanocomposite was a rubber-like material at room temperature because of its T_g of −11 °C (**Figures 3.2d**).

Photonic structures were imprinted on the photo-softened areas of the PAzo/UCNP nanocomposite (**Figure 3.2e**). A spin-cast film of the nanocomposite was irradiated with UV light through a photomask. Then, a pre-designed SU-8 mold was pressed on the film (63.7 kPa) (**Figure 3.7**). After that, the mold was removed and the film was irradiated with green light (530 nm, 58 mW cm^{-2}, 10 min) to transform it back to its hard solid state. Periodic microstructures of the negative mold were replicated in the irradiated areas (**Figure 3.2f(ii)**). The microstructures had a depth of 300 nm (**Figures 3.2g, Figure 3.8**) and showed vivid structural colors (**Figure 3.2f**), which could be used for anti-counterfeiting.

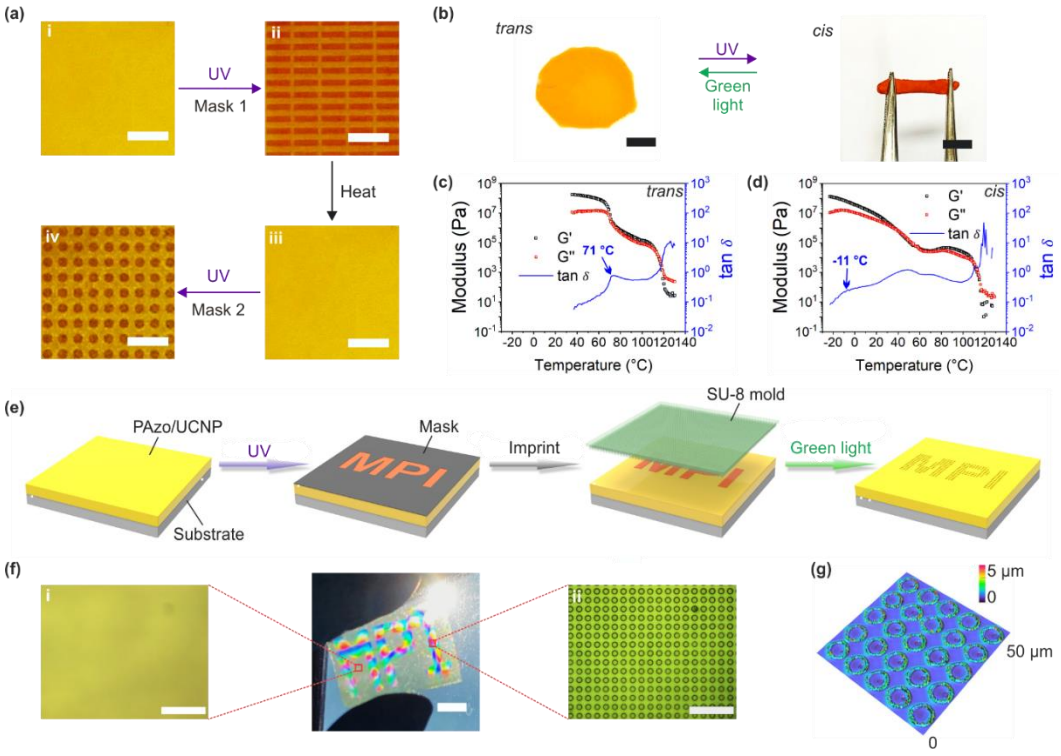

Figure 3.2 (a) Reversible writing and erasure of color-changing patterns on a PAzo/UCNP nanocomposite film. The patterns were fabricated via UV irradiation (365 nm, 67 mW cm^{-2}, 5 min) through a photomask; patterns were erased via heating (130 °C, 10 min). Scale bars: 5 mm. (b) Photographs of *trans* and *cis* PAzo/UCNP nanocomposites. Scale bars: 5 mm. (c, d) Dynamic mechanical analysis (DMA) data of (c) *trans* and (d) *cis* PAzo/UCNP nanocomposites. G′: storage modulus; G″: loss modulus; tan δ: loss tangent. (e) Schematic of the fabrication of imprinted microstructures with structural colors. (f) Photograph of a PAzo/UCNP nanocomposite film with imprinted microstructures on a PET substrate. Scale bar: 1 cm. Optical microscopy images of (i) an unimprinted area and (ii) an imprinted area. Scale bars: 50 μm. (g) Confocal microscopy image of imprinted microstructures on a PAzo/UCNP nanocomposite film. Copyright 2021 WILEY-VCH Verlag GmbH & Co. KGaA.

3.2.3 Polarization-dependent structures

Polarization-dependent structures were fabricated on a PAzo/UCNP nanocomposite film for encryption (**Figure 3.3a**) via *cis-trans* photoisomerization (**Figure 3.3a(i) and (ii)**). Then, irradiation of the *cis* nanocomposite film with polarized blue light induced

the alignment of the azobenzene chromophores (**Figure 3.3a(iii)**), which was confirmed by polarized absorption spectroscopy (**Figure 3.3b**). This phenomenon is called photoinduced orientation, which occurs when azobenzene chromophores in an azopolymer film align perpendicular to the polarization direction of the incident linearly polarized light irradiation.[106, 109, 110] After that, the film was irradiated with UV light and polarized blue light through a photomask (**Figures 3.3a(iv) and (v)**). The polarization direction was perpendicular to the previously polarized blue light; therefore, the azobenzene chromophores in the exposed areas were oriented perpendicular to those in the unexposed areas (**Figure 3.3a(vi)**). The pattern was erasable using UV light (**Figure 3.3a(vii)**) and rewritable using a different photomask (**Figure 3.3a(viii)**).

A polarization-dependent pattern was observed using polarized light from a monitor (**Figure 3.3c**). The light/dark contrast of the pattern was reverted by rotating it by 90° (**Figures 3.3c(ii) and (iii)**) because the transmittance of the polarized monitor light changed. The pattern was erasable and rewritable (**Figures 3.3c(iv)–(vi)**). Moreover, the pattern was hidden under unpolarized light from a desk lamp (**Figure 3.3d**), while it was visible under polarized light from a monitor (**Figure 3.3e**). Thus, the polarization-dependent pattern allows encryption, which secures it against counterfeiting.

Next, we investigated the resolution of our patterning technique using different photomasks (**Figures 3.3f**). The fabrication of patterns with a pixel size smaller than 10 μm is feasible (**Figure 3.9**). Such high-resolution structures make it difficult to replicate anti-counterfeiting patterns. Thus, they meet the standard for high-security applications. To demonstrate the applications of such patterns, we fabricated high-resolution “positive” and “negative” quick response (QR) codes (**Figures 3.3g, h**), which stayed intact for more than 180 days in an office with natural light at room temperature (**Figure 3.10**).

The polarization-dependent patterns (**Figures 3.3f–h**) have uniformly aligned structures. We imparted an additional security feature to the structures using mesophase textures as fingerprint-like structures (**Figure 3.3i**). A pattern with both uniform and textured parts was fabricated by irradiating a nanocomposite film with UV light and polarized blue light through a photomask (**Figure 3.3i**). The texture of the unexposed

areas was attributed to the mesophases of PAzo. Relatively large crystalline grains were formed in the pure PAzo region, while smaller crystalline grains were formed by the introduction of UCNPs into PAzo, which increased the defects in the mesophase structures (**Figure 3.13**). Thus, the textures of the PAzo/UCNP nanocomposites can be tuned by adjusting the UCNP content.

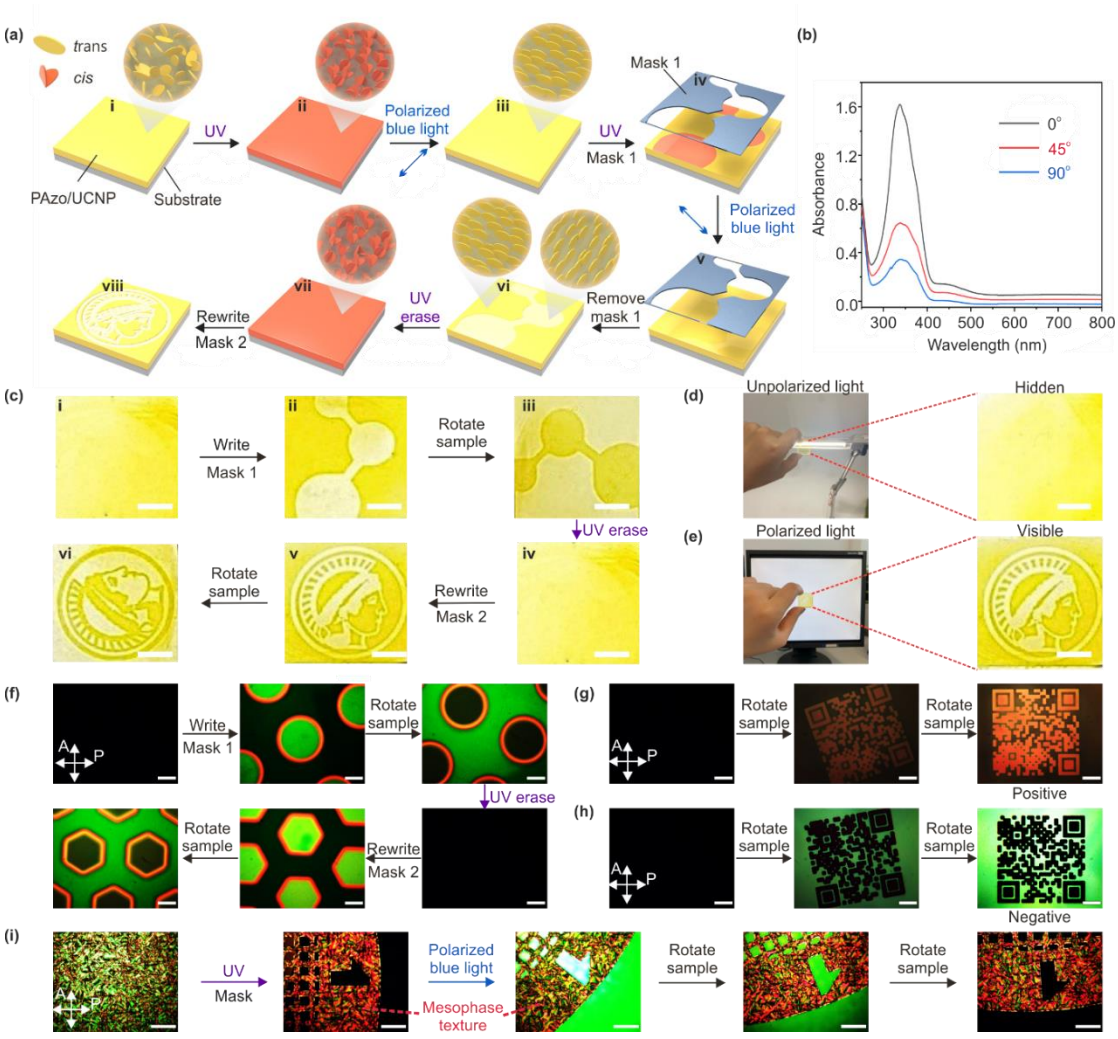

Figure 3.3 (a) Fabrication of rewritable polarization-dependent patterns on a PAzo/UCNP nanocomposite film. (b) Polarized absorption spectra of a nanocomposite film after UV (365 nm, 67 mW cm^{-2}, 10 min) and linearly polarized blue light (470 nm, 29 mW cm^{-2}, 30 min) irradiations. (c) Photographs of a nanocomposite film with rewritable polarization-dependent patterns under polarized light from a monitor. Scale bars: 0.5 mm. (d, e) The polarization-dependent pattern was (d) invisible under unpolarized light from a desk lamp and (e) visible under polarized light from a monitor.

Scale bars: 0.5 mm. (f) The erasure and rewriting of polarization-dependent patterns on a nanocomposite film observed using polarized optical microscopy (POM). A: analyser; P: polariser. Scale bars: 200 μm. (g and h) POM images of the positive and negative QR codes on nanocomposite films. Scale bars: 200 μm. (i) POM images of a nanocomposite film before irradiation and after UV (365 nm, 67 mW cm^{-2}, 10 min) and subsequent linearly polarized blue light irradiations (470 nm, 29 mW cm^{-2}, 30 min) through a photomask. Copyright 2021 WILEY-VCH Verlag GmbH & Co. KGaA.

3.2.4 Upconversion luminescent structures

UCNPs emit visible light upon excitation with NIR light, which provides the nanocomposite with a new security feature (**Figure 3.4.a**). A star-shaped structure made of PAzo/UCNP nanocomposite was stamped on a glass substrate, which exhibited upconversion luminescence (**Figure 3.4b**). Upconversion luminescence was combined with rewritable photochromic patterns. When the photochromic pattern was excited with NIR light, the *trans* PAzo/UCNP part (yellow) emitted stronger upconversion luminescence, while the *cis* PAzo/UCNP part (orange) emitted weaker upconversion luminescence (**Figure 3.4c**), because *cis* PAzo absorbed upconversion luminescence (**Figure 3.14**). Therefore, the synergy of UCNPs and PAzo can be used for anti-counterfeiting applications.

The PAzo/UCNP nanocomposites showed polarization-dependent upconversion luminescence, which represents a high-end technique for anti-counterfeiting (**Figure 3.4d**). We fabricated a polarization-dependent pattern on a nanocomposite film via a photoinduced orientation (**Figure 3.3**). Polarization-dependent patterns were invisible under natural light, but were legible using polarized upconversion luminescence (**Figure 3.4e, Figure 3.15**). The brightness of the polarized upconversion luminescence patterns changed with the rotation of the polariser. Polarized upconversion luminescence patterns are also erasable and rewritable. Moreover, because excitation by NIR light avoids fluorescence and light from the background, a weak polarization-dependent pattern was observed using polarized upconversion luminescence (**Figure 3.4e**). Thus, these properties can be used for high-contrast patterns and high-quality encryption, which provide a high level of security.

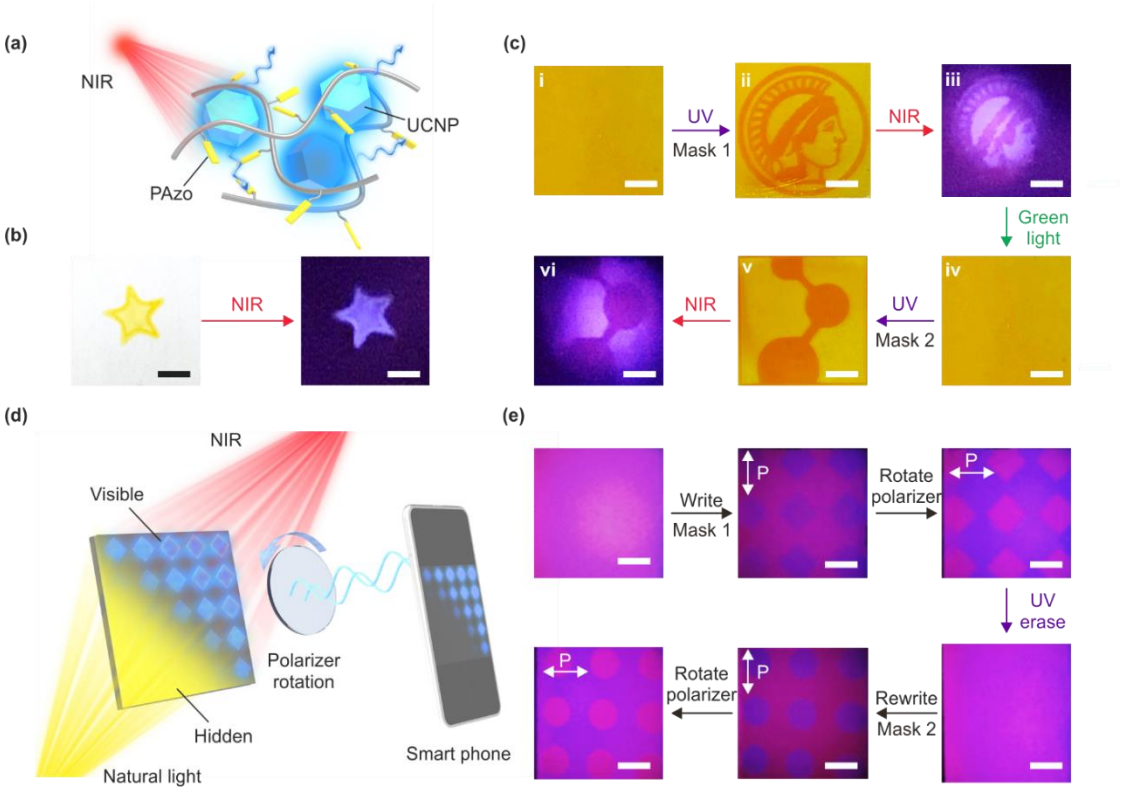

Figure 3.4 (a) Schematic of upconversion luminescence of PAzo/UCNP nanocomposite excited with NIR light. (b) Photographs of a star-shaped PAzo/UCNP nanocomposite stamped on a substrate excited with NIR light (10.8 W cm^{-2}). Scale bars: 5 mm. (c) Photographs of rewritable photochromic patterns of PAzo/UCNP nanocomposite unravelled using upconversion luminescence. Scale bars: 5 mm. (d) Schematic of accessing encrypted information on a polarization-dependent display using upconversion luminescence. (e) Photographs of rewritable patterns with polarization-dependent upconversion luminescence. P indicates the polarization direction. Scale bars: 5 mm. Copyright 2021 WILEY-VCH Verlag GmbH & Co. KGaA.

3.3 Applications

To demonstrate multiple security features, we integrated four anti-counterfeiting functions of the PAzo/UCNP nanocomposite on a model banknote (**Figure 3.5a**). Structural colors, upconversion luminescence, polarization-dependent patterns, and high-resolution microprints with mesophase textures provide numerous prominent features for anti-counterfeiting applications. Furthermore, PAzo/UCNP nanocomposites are also suitable for anti-counterfeiting applications for a variety of

products. For example, we fabricated a QR code on a medicine box using PAzo/UCNP composites (**Figure 3.5b**). In addition, because of their good mechanical properties and processability, PAzo/UCNP composites can be applied to the curved surfaces of wine and capsule bottles (**Figures 3.5c, d**).

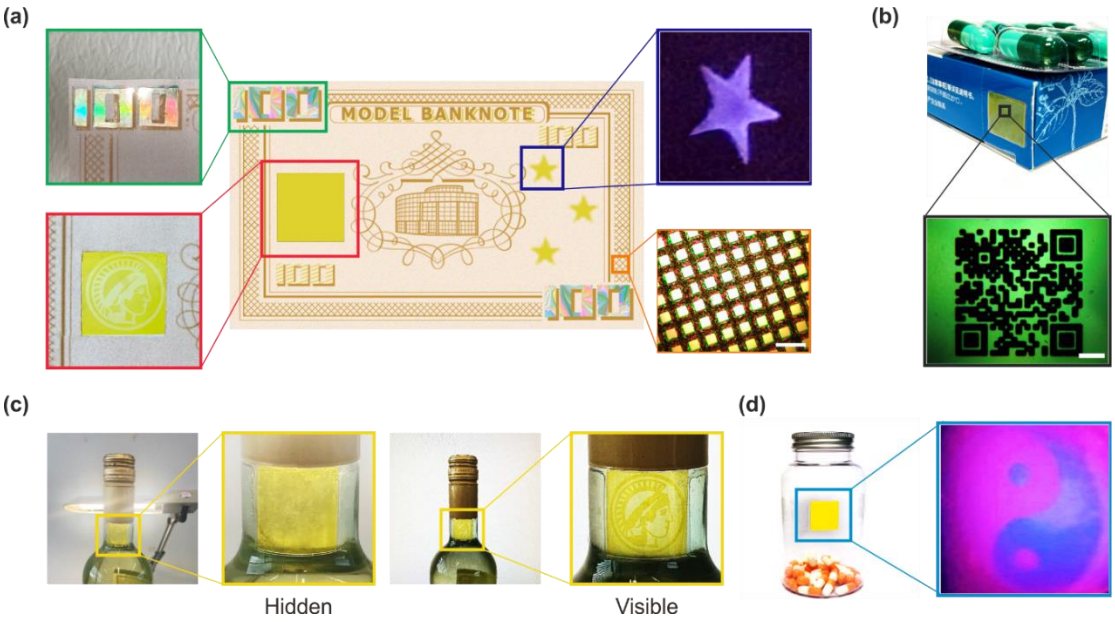

Figure 3.5 (a) The integration of multiple anti-counterfeiting functions of PAzo/UCNP nanocomposites in a model banknote. Upper left: structural color; Upper right: upconversion luminescence; Down left: polarization-dependent pattern; Down right: patterned structures with mesophase textures. Scale bar: 100 μm. (b) POM image of a QR code on a medicine box. Scale bar: 200 μm. (c) A label on the curved surface of a wine bottle observed under a desk lamp (left) and monitor light (right). (d) A label with polarized upconversion luminescence on a curved surface of a bottle under NIR light.

3.4 Conclusion

In conclusion, we developed an anti-counterfeiting nanocomposite with multiple security features, different read-out methods, and easy processing. These properties are based on the integration of a photoresponsive azopolymer and UCNPs into the nanocomposite. These nanocomposites can be conveniently processed and applied to banknotes, medicines, wines, and other products. The anti-counterfeiting structures in the nanocomposite have high resolution, are durable, and can be discerned with the naked eye for quick discrimination and with analytical tools for high accuracy. The results of this study open a new avenue for the development of high-end anti-counterfeiting materials.

3.5 Supplementary section

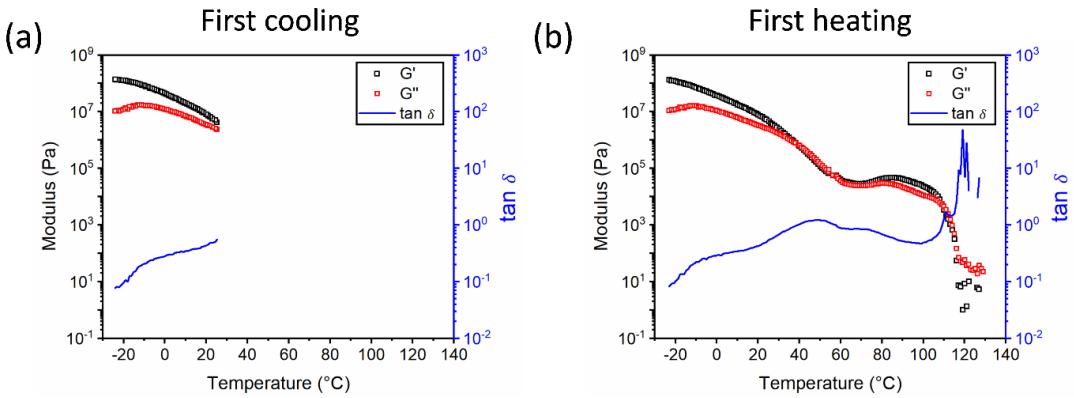

Figure 3.6 Dynamic mechanical analysis (DMA) of *cis* PAzo/UCNP. G': storage modulus; G'': loss modulus; tan $\delta = G''/G'$: loss tangent. (a) *Cis* PAzo/UCNP was cooled from room temperature to -20 °C. T_g was -11 °C. (b) After cooled to -20 °C, *cis* PAzo/UCNP was heated from -20 °C to 130 °C. The *cis* content of azobenzene groups in *cis* PAzo/UCNP was 88%.

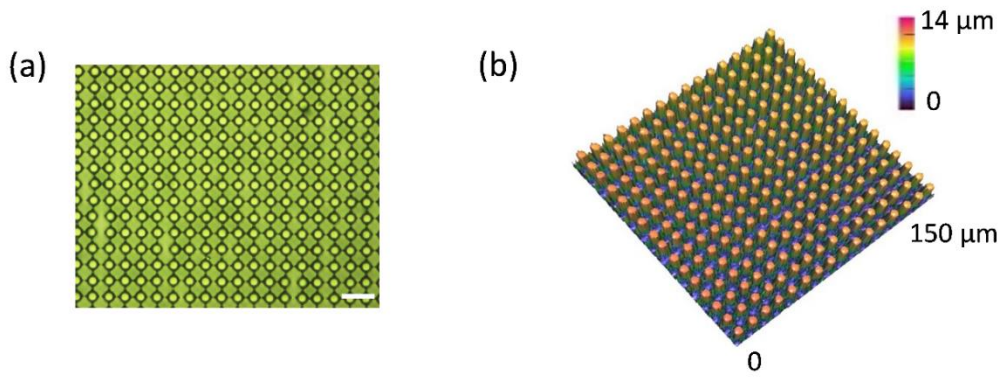

Figure 3.7 (a) Optical microscopy image of an SU-8 mold. The diameter of the pillars is 5 µm and the distance between two adjacent centers is 10 µm. Scale bar, 20 µm. (b) Confocal microscopy image of an SU-8 mold. The height of the pillars is 10 µm.

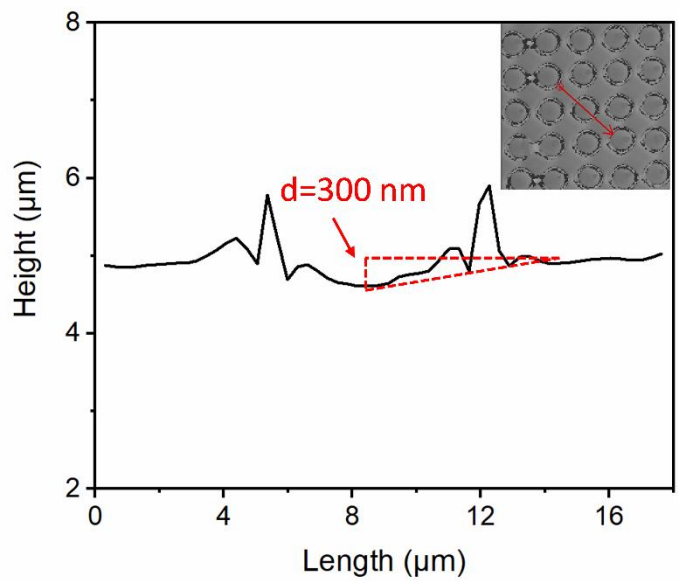

Figure 3.8 The height profile of an imprinted structure on a PAzo/UCNP film along the red line. Inset: confocal microscopy image of the imprinted PAzo/UCNP film.

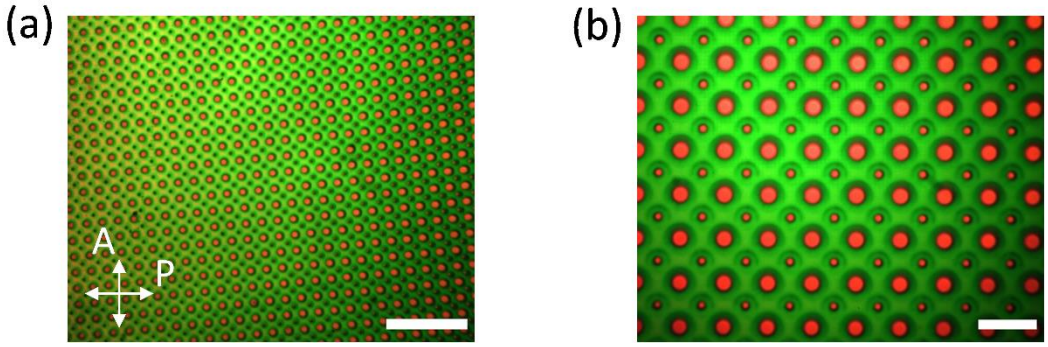

Figure 3.9 POM images of a PAzo/UCNP film. First, the whole film was irradiated by UV and polarized blue light. Then, the film was irradiated by UV and polarized blue light through a photomask. The pixel size is <10 μm. (a) Scale bar, 200 μm. (b) Scale bar, 100 μm.

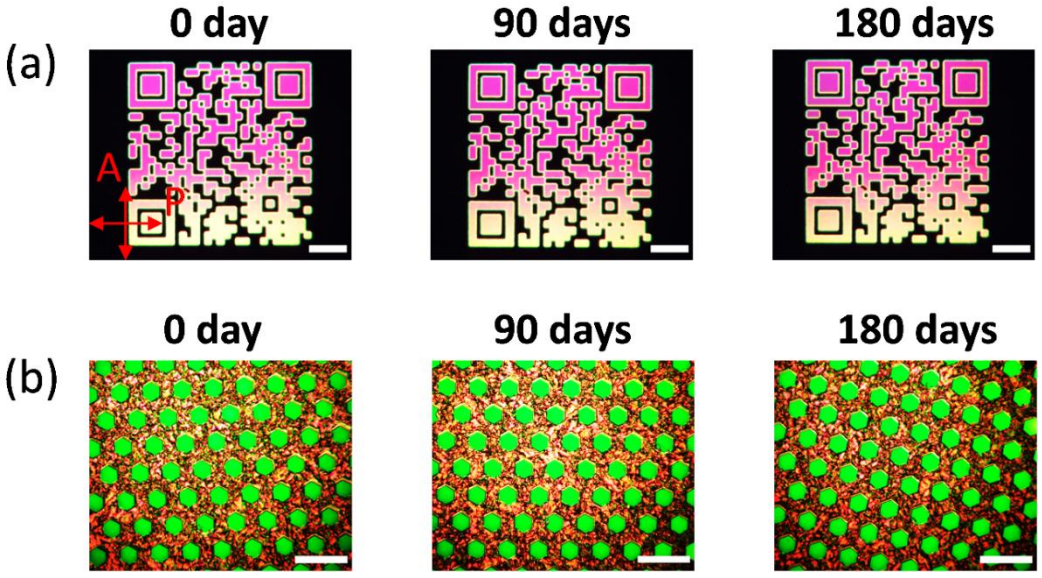

Figure 3.10 The patterns can be stored for more than 180 days in an office under natural light and room temperature. (a) POM images of a QR code on PAzo/UCNP nanocomposite film after UV (365 nm, 68 mW cm^{-2}, 10 min) and linearly polarized blue light (470 nm, 29 mW cm^{-2}, 30 min) irradiation through a photomask. Scale bars, 200 μm. (b) POM images of a PAzo/UCNP nanocomposite film after UV (365 nm, 68 mW cm^{-2}, 10 min) and linearly polarized blue light (470 nm, 29 mW cm^{-2}, 30 min) irradiation through a TEM grid. Scale bars, 100 μm.

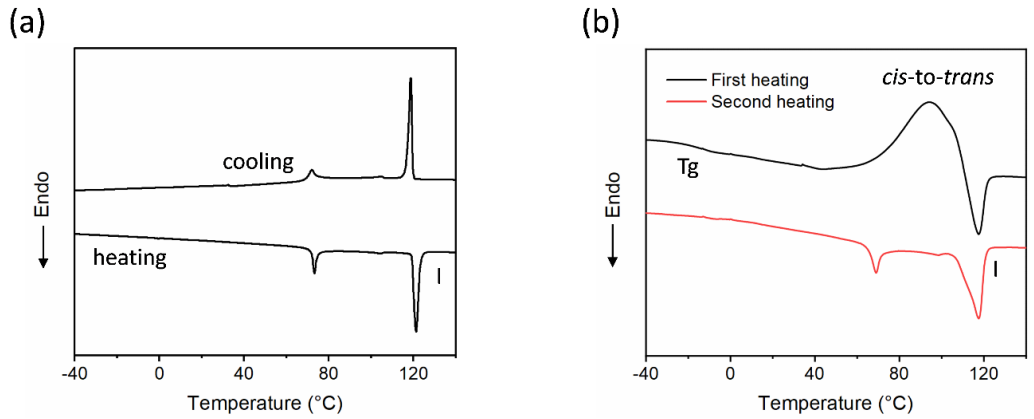

Figure 3.11 (a) Second heating and second cooling DSC curves of *trans* PAzo/UCNP. (b) First heating and second cooling DSC curves of *cis* PAzo/UCNP. The *cis* content of azobenzene groups in *cis* PAzo was 88%. *Trans* PAzo/UCNP showed two phase transitions at 73 ℃ and 122 ℃, respectively (**Figure S10a**). *Cis* PAzo/UCNP had a T_g at −10 °C and a broad exothermic band at ~95 °C due to the thermal *cis-trans* isomerization in the first heating curve (**Figure S10b**). The second heating DSC curve of *cis* state was the same as that of *trans* PAzo/UCNP, showing that *cis* PAzo/UCNPs was thermally converted to *trans* state in the first heating process. Polarized optical microscopy (POM) images showed the mesophases of PAzo/UCNP at different temperatures (**Figure S11**).

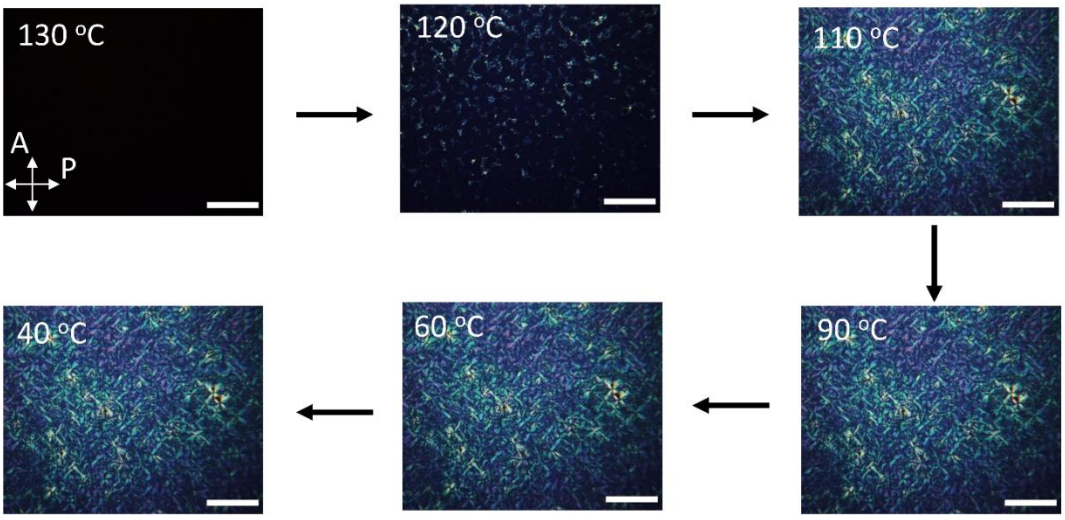

Figure 3.12 POM images of PAzo/UCNP at different temperatures. First, PAzo/UCNP was annealed at 130 °C for 2 h. Then, it was cooled down to the experimental temperatures at a cooling rate of 1 °C/min.

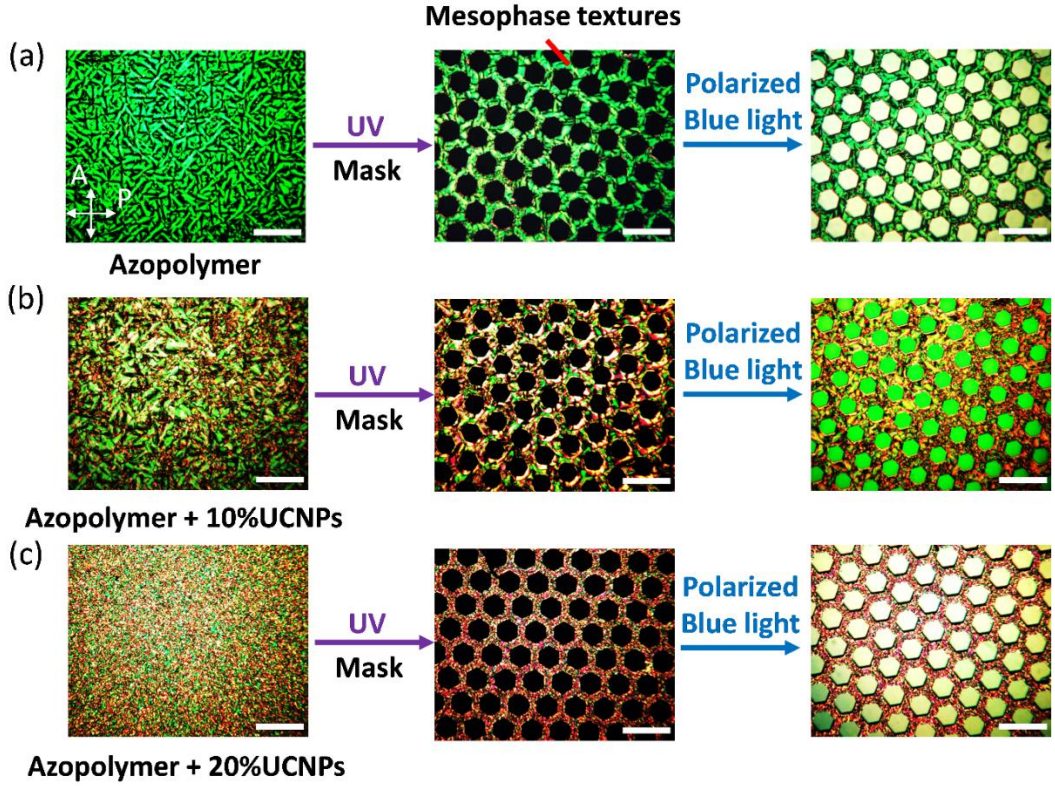

Figure 3.13 POM images of (a) pure PAzo, PAzo/UCNP nanocomposites with (b) 10 wt% and (c) 20 wt% UCNPs films before irradiation and after UV (365 nm, 67 mW

cm^{-2}, 10 min) and subsequent linearly polarized blue light irradiation (470 nm, 29 mW cm^{-2}, 30 min) through a photomask. Scale bars, 100 μm. Before irradiation, these samples were annealed at 130 °C for 2 h. Then, they were cooled down to room temperature at a cooling rate of 1 °C/min. Large crystalline grains were formed in the pure PAzo; doping UCNPs into PAzo increased defects in mesophase structures, which resulted in smaller crystalline grains. In the POM images, the mesophase textures of the samples with different contents of UCNPs are different. The mesophase textures were used as finger-print-like structures for anti-counterfeiting.

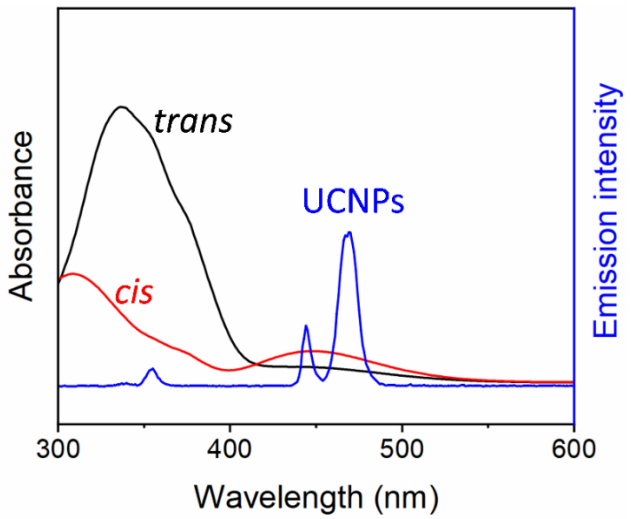

Figure 3.14 Absorption spectra of *trans* (black line) and *cis* (red line) PAzo and emission spectrum of UCNPs (blue line) under excitation by 979 nm light (4.6 W cm^{-2}). The blue emission of UCNPs overlapped with n-π* band of the *cis* isomer. Thus, the upconverted blue light was absorbed by the *cis* isomer.

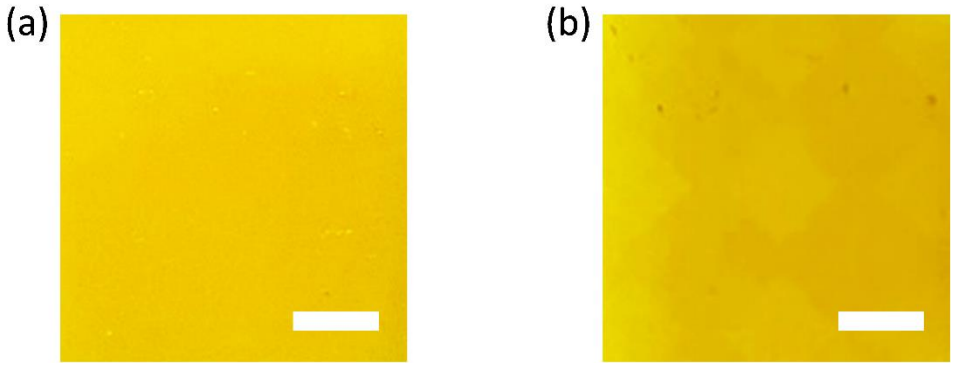

Figure 3.15 Photographs of a polarization-dependent pattern on a thick PAzo/UCNP film under natural light (a) and monitor screen light (b). Scale bars, 5 mm. The thickness of this PAzo/UCNP nanocomposite film was 20 μm, which was much thicker than the films in Figure 3. A weak polarization-dependent pattern was fabricated on such a film. In contrast, upconversion luminescence was very sensitive to read out such a weak polarization-dependent pattern (Figure 4e).

Chapter 4: Three-dimensional photon upconversion direct lithography of photoalignment nanocomposite

4.1 Introduction

In the digital age, information storage has become an indispensable part of our lives. From personal data to vast amounts of knowledge, how we store and manage information has evolved remarkably. [112-114] Photolithography has emerged as a vital and transformative technology in information storage. [115-117] Photolithography is essential in fabricating integrated circuits and memory devices central to information storage and processing systems. [118, 119] In photolithography, photochromic compounds, including azobenzene, [120-122] spiropyran, [123-125] diarylethene, [126-128] coumarin, [129-131] and so on, were proposed for optical recording. These compounds exhibit reversible and controllable changes in properties upon exposure to ultraviolet (UV) or visible light. However, using UV or visible light to record three-dimensional (3D) patterns is challenging because of the poor penetration capacity. To increase information density, simultaneous two-photon absorption was used to record 3D patterns on photochromic compounds within the same recording volume to increase information density. [132-135] The advantage of two-photon absorption is that it provides 3D high spatial resolution. However, two-photon absorption has two bottlenecks: low efficiency and high costs of femtosecond lasers. [126, 137] It is well known that most photosensitive materials have small two-photon absorption cross-sections. Although creating extremely small feature sizes is attractive, it is no efficiency for most patterns (incredibly bulky patterns with a few fine features). These bottlenecks hinder the fast development of 3D information storage. Hence, developing high-efficiency and low-cost 3D photolithography techniques is highly desirable to overcome the bottlenecks.

Photon upconversion provides a transformative solution to these problems. Recently, lanthanide-doped UCNPs were developed to convert NIR to UV/visible light efficiently. [138-140] Therefore, photosensitive materials are mixed with UCNPs. UCNPs convert NIR light to UV or visible light, which triggers photoreactions of photosensitive compounds.[141] This process is referred to as UCNP-assisted photochemistry. Compared with two-photon absorption, UCNP-assisted photochemistry is much more efficient and does not require expensive ultrafast lasers. The light intensity required for

UCNP-assisted photochemistry is several orders of magnitude lower than that for two-photon absorption. A cheap CW laser diode can efficiently trigger upconversion. UCNP-assisted photochemistry is also a general approach for conventional photosensitive compounds. UCNP-assisted photochemistry of various photosensitive compounds, such as photochromic compounds, [142] photocurable resins, [143] and photodegradable polymers, [144] have been reported. Among them, azobenzene, one of the extensively studied photoresponsive compounds, exhibits a property of photoinduced orientation. This characteristic enables the formation of polarization-dependent patterns by selectively exposing the layer to polarized light, as previously demonstrated in our research. [145] Utilizing a mask-less approach in photolithography provides several advantages, including enhanced pattern resolution and increased flexibility in reconfiguring pattern designs through programmable laser or sample stage movements. Therefore, photolithography is a powerful technique for generating high-resolution spatial patterns in various functional optical materials. Besides, previous studies have reported the ability of NIR light to induce photoisomerization of azobenzene in the presence of UCNPs. Consequently, azobenzene proves to be a suitable candidate for 3D photolithography applications.

Herein, we develop a novel 3D PUDL system (**Figure 4.1**). In this system, we used an objective to focus the beam from a low-cost CW NIR laser. The focal position is fixed while the 3D motorized sample stage is moved, facilitating the creation of 3D patterns on the optical recording layers. The optical recording material we used here is a photoresponsive nanocomposite composed of a photoresponsive azopolymer and UCNPs. Before exposure, the nanocomposite film underwent pretreatment to establish alignment under UV and polarized blue light. Upon exposure to NIR light, the upconverted UV and blue light emitted from the UCNPs led to continuous *trans-cis-trans* isomerization of the azobenzene molecules. This continuous isomerization disrupted the initial molecular alignment, causing the azobenzene molecules to adopt random orientations. Consequently, patterns exhibiting diverse orientations were generated, which could be observed by polarized optical microscope and the reflection mode of confocal microscope. Our work would open a new avenue for optical recording and advance the 3D photolithography field.

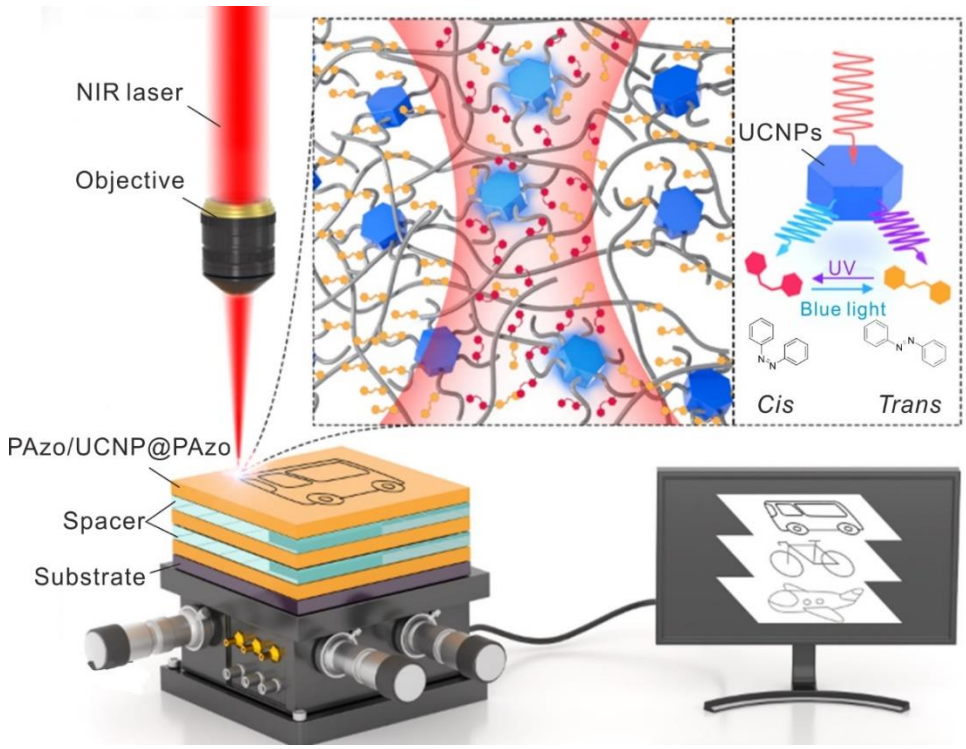

Figure 4.1 Schematic, illustrating 3D Photon Upconversion Direct Lithography (PUDL). The focused NIR is fixed. The sample is scanned by a 3D motorized stage. The movements of the stage are controlled by a computer with three-dimensional coordinates of patterns as input The optical recording material consisted of a multilayer thin film (~600 nm) composed of azobenzene containing polymer (azopolymer) incorporated with UCNPs, interposed with a cover slip spacer (100 µm). This three-layer superimposed patterns can be read out by confocal microscopy without crosstalk. By modulating the direction of the polarized light during the pretreatment stage, it was possible to obtain three-layer films with distinct orientations. Under NIR irradiation, continuous *trans-cis-trans* photoisomerization of azobenzene molecules takes place within the focus region with the assistance of UCNPs. Thus, the initial alignment of azobenzene molecules is disrupted, leading to the adoption of random orientations by the molecules.

4.2 Results and discussions

4.2.1 Photoresponsive nanocomposite for photolithography

The schematic for fabricating 3D optical patterns through the 3D PUDL process is depicted in Figure 1. The output power of the diode laser was quantified using an optical power meter. In the PUDL process, the sample consisted of a multilayered stack where thin recording layers were separated by a thin cover slip. The first thin photoalignment layer of the optical recording nanocomposite was spin-coated onto a silicon wafer.

To create the desired optical recording nanocomposites, we synthesized azopolymer PAzo and β-phase $NaYF_4$:TmYb@$NaYF_4$ UCNPs (core = $NaYF_4$: 0.5 mol% Tm^{3+}/30 mol% Yb^{3+}; shell = $NaYF_4$) (**Figure 4.2a**). The chemical structure and reversible photoisomerization of PAzo are presented in **Figure 4.2b**. Gel permeation chromatography was employed to measure the M_n and PDI of PAzo, yielding values of 3.0×10^4 g mol^{-1} and 1.13, respectively (Figure S3). To achieve a more uniform dispersion of nanoparticles within the PAzo polymer matrix, we developed azopolymer-capped UCNPs (UCNPs@PAzo) through ligand exchange, resulting in noticeable shell structures compared to the UCNPs (**Figure 4.2c**). TEM analysis revealed average particle diameters of 47 nm for UCNPs and 50 nm for UCNPs@PAzo. Then PAzo and UCNP@PAzo were mixed in an organic solvent, and thin PAzo/UCNP@PAzo films were prepared by spin-coating. SEM images of the cross-section of the nanocomposite film demonstrated the homogeneity of the material (**Figure 4.2d**). TGA indicated that the purified UCNP@PAzo and PAzo/UCNP@PAzo contained 30 wt% and 80 wt% of PAzo, respectively. Moreover, it is postulated that the doping rate of UCNP@PAzo should be carefully controlled to avoid excessive aggregation (**Figure 4.6**). The absorption spectrum of *trans* PAzo (red line), *cis* PAzo (black line), and upconversion luminescence emission spectra of UCNPs (blue line) in tetrahydrofuran (THF) solution upon 980 nm excitation are shown in **Figure 4.2e**. The specific emission bands of the UCNPs exhibited significant overlap with the absorption band of both *trans* and *cis* PAzo. The power-dependent fluorescence spectra of UCNPs in THF solution at different 980 nm light intensities is shown in **Figure 4.2f**. A comparison with UCNPs revealed the disappearance of UV and blue region emissions

in the PAzo/UCNP@PAzo, indicating efficient absorption of UV and blue photons by *trans* and *cis* PAzo, respectively (**Figure 4.2g**).

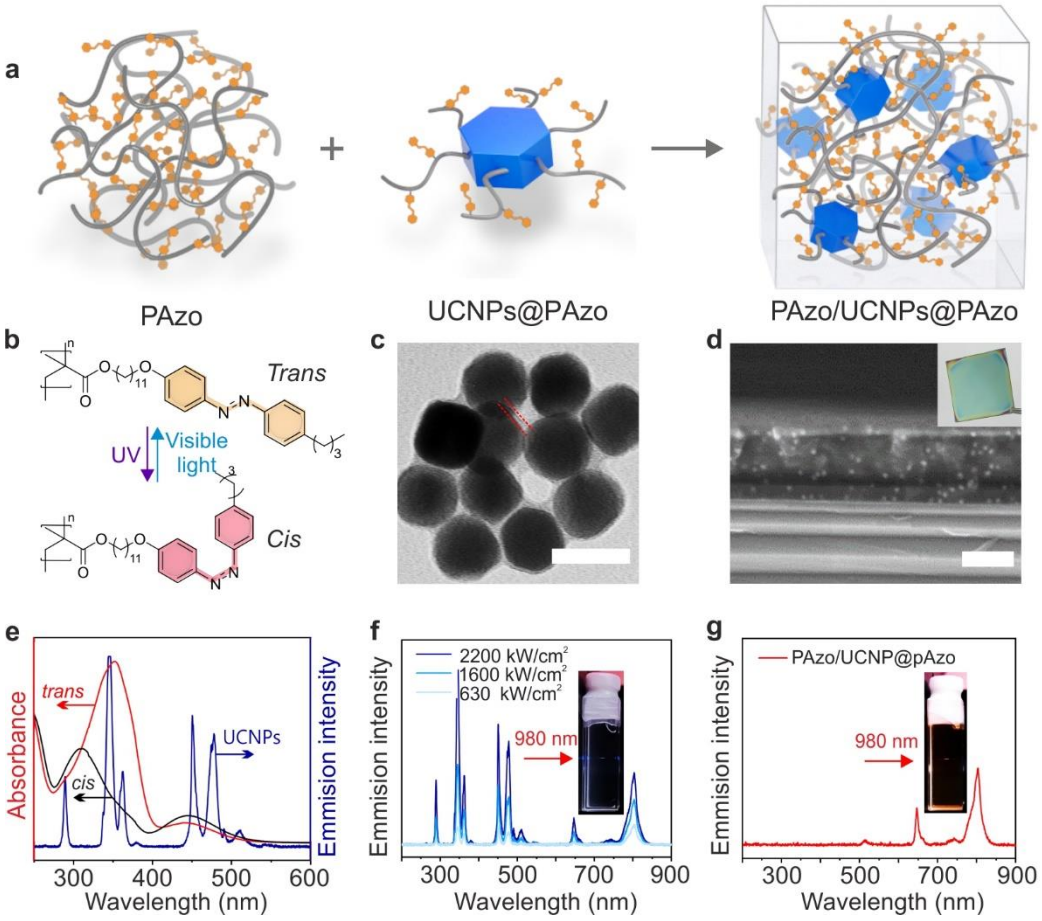

Figure 4.2 a. Schematic illustration of the fabrication of PAzo/UCNP@PAzo. UCNP@PAzo was fabricated by grafting PAzo to UCNPs via ligand exchange. b. Chemical structure and reversible photoisomerization of PAzo. c. Transmission electron microscopy (TEM) images of UCNPs@PAzo. Scale bar, 50 nm. d. Cross-sectional SEM image of a PAzo/UCNP@PAzo nanocomposite film. Scale bar: 200 nm. Inset: a photograph of a spin-coated PAzo/UCNP@PAzo nanocomposite film on the silicon wafer. e. The absorption spectrum of *trans* PAzo (red line), *cis* PAzo (black line), and upconversion luminescence emission spectra of UCNPs (blue line) in tetrahydrofuran (THF) solution upon 980 nm excitation. f. Upconversion luminescence emission spectrum of UCNPs excited with NIR light at the excitation intensity at 630, 1600, and 2100 kW cm^{-2}. Insets: fluorescent voxel in a 10 mm ×10 mm cuvette containing UCNPs (left) in hexane produced by a focused CW 980 nm laser beam (intensity at the focal plane: 500 kW cm^{-2}). g. Upconversion luminescence emission

spectrum of PAzo/UCNPs@PAzo dispersion in THF upon NIR light excitation (500 kW cm^{-2}). Insets: fluorescent voxel in a 10 mm ×10 mm cuvette containing PAzo/UCNPs@PAzo (right) in THF produced by a focused CW 980 nm laser beam (intensity at the focal plane: 500 kW cm^{-2}).

4.2.2 Tunable feature size

The fabrication of dot arrays was successfully achieved using the PULD process on a spin-coated PAzo/UCNPs@PAzo photoalignment layer (**Figure 4.3a**). Upon UV irradiation, *trans*-to-*cis* isomerization was induced. Subsequently, the *cis* nanocomposite film was irradiated with polarized blue light, resulting in the alignment of the azobenzene chromophores. This alignment was confirmed through polarized Raman spectroscopy (**Figure 4.3b**) and polarized absorption spectroscopy (**Figure 4.7**).

To quantify the degree of alignment, the orientation parameter, also known as the pseudo-order parameter, was calculated. The order parameter for the aligned azobenzene chromophores was determined to be 0.76, based on the polarized Raman intensities of the 1146 cm^{-2} peak (**Figure 4.8**). No differences in Raman intensity were observed under different polarizations in the amorphous PAzo/UCNPs@PAzo film before alignment (**Figure 4.9**). This phenomenon is referred to as photoinduced orientation, which occurs when azobenzene chromophores in an azopolymer film align perpendicular to the polarization direction of incident linearly polarized light irradiation.

Subsequently, the PULD process was employed to create dot arrays on the alignment nanocomposite film. Under NIR light exposure, the upconverted UV and blue light induced continuous *trans-cis-trans* isomerization of the azobenzene molecules. This continuous isomerization disrupted the initial molecular alignment, resulting in random orientations of the azobenzene molecules. Consequently, patterns with diverse orientations were generated, which could be observed using a polarized optical microscope and the reflection mode of a confocal microscope. The Raman spectra of the dots under different exposure times are presented in **Figure 4.3c**. The Raman intensity decreased as the detection polarization angle increased to 90° and increased as it decreased to 0° with increasing exposure time. The order parameter also decreased with increasing exposure time (**Figure 4.3d**). These results indicate that the NIR light disrupted the original orientation, leading to the creation of the pattern.

To demonstrate the indispensable of UCNPs, pure PAzo films were fabricated and irradiated with NIR light for 10 minutes. Compared to the PAzo/UCNPs@PAzo film, no dots were observed on the pure PAzo film (**Figure 4.10**). AFM results show the surface morphology of these dots created by the PUDL process (**Figure 4.11**). The observed increase in the height of the exposed area can be attributed to the transition of the orientation of azobenzene molecules from an in-plane arrangement to a random distribution. This phenomenon suggests that the manipulation of azobenzene molecules through the PUDL process induces significant structural changes at the nanoscale level, thereby influencing the surface morphology of the generated dots.

Figure 4.3e illustrates the simulated intensity and profile of the NIR Gaussian laser spot at the focal point. The theoretical spot size at the focus was approximately 1.4 μm. The entrance pupil diameter is assumed to be filled by a Gaussian input beam profile truncated at the $1/e^2$ diameter. **Figure 4.3f** displays the POM image of the dot arrays created at different NIR laser powers. The POM image was processed using Matlab to extract the coordinates and gray values, which were then plotted on a graph to obtain the cross-section of the gray values. The pixel size was defined using the half-peak width (**Figure 4.12**). **Figure 4.3g** shows the pixel size as a function of exposure time at different CW laser powers. Thus, the smallest pixel size on PAzo/UCNPs@PAzo film that could be printed using the PULD process was approximately 1.15 μm.

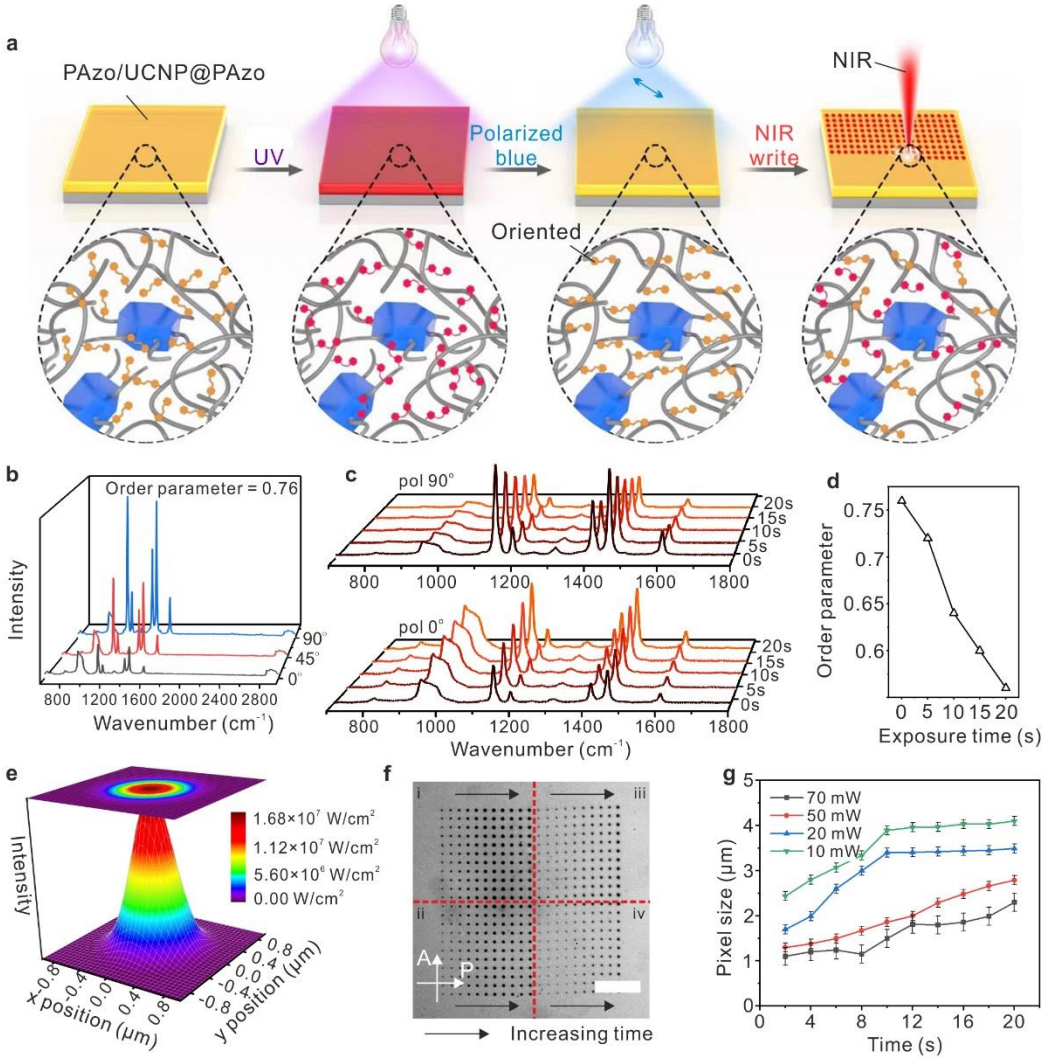

Figure 4.3 a. Schematic illustration of the photoalignment recording layer and polarization-dependent dots array fabrication process. b. Polarized Raman spectra of a nanocomposite film after UV (365 nm, 67 mW cm^{-2}, 5 min) and linearly polarized blue light (470 nm, 29 mW cm^{-2}, 15 min) irradiations. c. Polarized Raman spectra of these dots were created by different exposure times. Pol 0^o (pol 90^o) means the long axis of the azobenzene molecules in the oriented background is parallel (perpendicular) with the propagation direction of the incident and scattered light in Raman micro-spectrometry. d. The order parameter as a function of exposure time. e. Simulated intensity and profile of the NIR Gaussian laser spot at the focus.f. POM image of the dot arrays created by the PUDL process (black and white mode). i, 70 mW. ii, 50mW. iii, 20 mW. iv, 10 mW. Scale bar: 100 μm. g. Pixel size as a function of exposure time at different CW laser powers.

4.2.3 2D patterns fabricated on photoalignment layers

The successful fabrication of arbitrary erasable and rewritable 2D patterns using the PUDL process on a spin-coated PAzo/UCNPs@PAzo photoalignment layer (**Figure 4.4a**). The oriented photoalignment layer was obtained through pre-treatment involving UV and polarized blue light irradiation. By precisely controlling the movement of a motorized stage, the desired 2D pattern was directly written onto this layer. The pattern exhibited an amorphous orientation of azobenzene molecules, while the background remained oriented. The orientation of the azobenzene molecules within the pattern could be erased by UV light, rendering the pattern erasable, and subsequently rewritable using the PULD process. **Figure 4.4b** displays the POM images of the film during the PULD process, confirming the successful fabrication of erasable and rewritable patterns. Furthermore, by manipulating the sample's rotation under POM (**Figure 4.13**), these patterns could be selectively hidden or made visible. Moreover, we could also fabricate complicated QR codes by the PUDL process (**Figure 4.14**), which demonstrates the great potential of anticounterfeiting of the PUDL process. Our previous work demonstrated the fabrication of polarization-dependent patterns using photomasks. However, the PULD process eliminates the need for masks, providing a mask-less strategy that enhances the flexibility of pattern reconfiguration by enabling precise control of the sample stage movements. Additionally, by combining polarization-dependent patterns created by photomasks with patterns generated via the PULD process, we successfully fabricated erasable and rewritable amorphous patterns on polarization-dependent backgrounds (**Figure 4.4c**). The complete pattern became visible only when the sample was rotated in a specific direction. The ability to write randomly amorphous patterns on polarization-dependent backgrounds holds potential for applications in random encryption and anti-counterfeiting. Moreover, by adjusting the excitation power or exposure time, the line widths and contrasts of the patterns can be modified (**Figure 4.4d and e**). Polarized Raman mapping of the pattern, considering different angles between the long axis of the azobenzene molecules in the oriented background and the incident/scattered light's propagation direction, also reveals the internal orientation changes within the pattern (**Figure 4.4g**). Furthermore, these patterns fabricated via the PULD process exhibited remarkable stability, remaining intact for over 150 days in an office environment exposed to natural light and room temperature conditions (Figure S17).

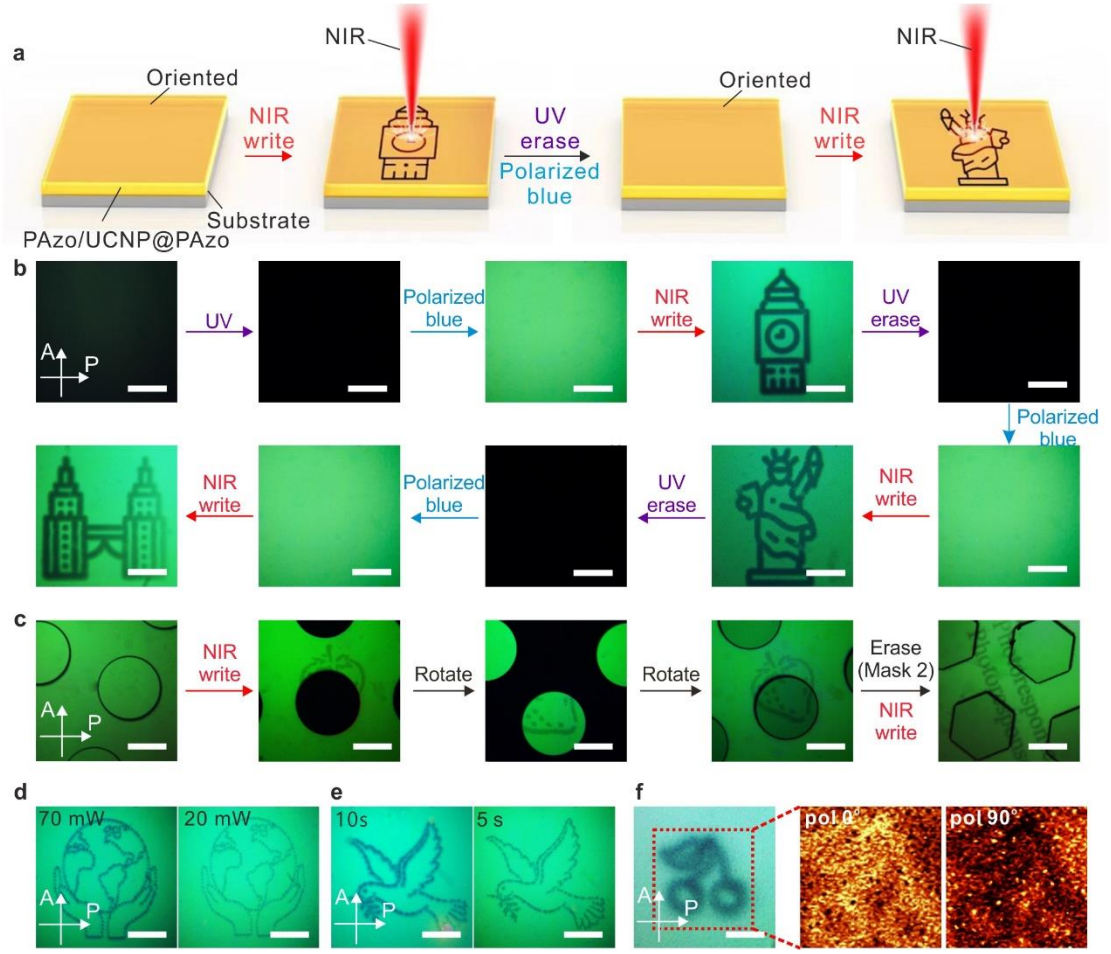

Figure 4.4 a. Schematic illustration of the fabrication of photoalignment recording layer and erasable/rewritable polarization-dependent nonaligned pattern on photoalignment background by PUDL process. b. POM images of photoalignment background and erasable/rewritable polarization-dependent nonaligned patterns. Scale bars: 200 μm. c. POM images of the erasable/rewritable pattern written by NIR laser on PAzo/UCNP@PAzo film with the differently oriented background. Scale bars: 200 μm. d. POM images of the patterns written by different excitation powers with the same exposure time (10s per pixel). Scale bars: 200 μm. e. POM images of the patterns written by the same excitation power (70 mW) with different exposure times. Scale bars: 200 μm. f. Left: POM image of a pattern created by NIR laser. Scale bar: 20 μm. Right: Polarized Raman mapping of the pattern with different angles between the long axis of the azobenzene molecules in the oriented background and the propagation direction of the incident and scattered light in Raman microspectrometry.

4.2.4 3D patterns on three layers

The motorized stage was precisely controlled in the z-axis direction, enabling the successful fabrication of 3D patterns on a three-layer PAzo/UCNP@PAzo film using the PUDL process (**Figure 4.5a**). The patterned images were generated in three layers, with a layer spacing of 100 μm. Pre-treatment of the three-layer film was conducted using blue light with three different polarization directions, resulting in each layer possessing distinct orientations. By rotating the scan field during the observation of the 3D pattern, varying contrast changes in each pattern could be observed (**Figure 4.5b**).

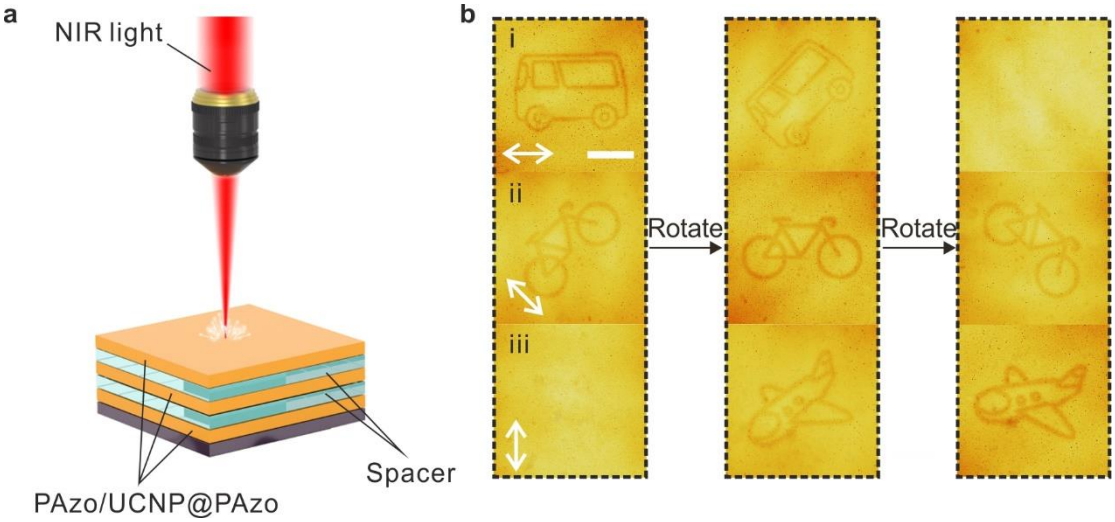

Figure 4.5 a. Schematic illustration of 3D patterns fabricated bt PUDL process. b. Confocal images show the 3D patterns on a three-layer film composed of PAzo/UCNP@PAzo, captured under the reflection mode while changing the direction of incident polarized light.

4.3 Conclusion

In conclusion, we developed an innovative system known as 3D PUDL. The optical recording material utilized in our study consists of a photoresponsive nanocomposite comprising an azopolymer and UCNPs. Leveraging the continuous photoisomerization facilitated by UCNPs, we successfully fabricated 3D patterns on reoriented layers. By incorporating a fluorescent molecule and employing polarization-dependent patterns as a background, we demonstrated the fabrication of diverse types of 3D patterns. Compared to the two-photon process, our PUDL process exhibits high efficiency, low cost, and a versatile approach for photosensitive compounds. Moreover, by employing appropriate UCNPs and photoresponsive molecules, the application of the PUDL process can be easily extended. Consequently, the outcomes of our research not only introduce new possibilities for optical recording but also signify a significant advancement in 3D photolithography.

4.4 Supplementary section

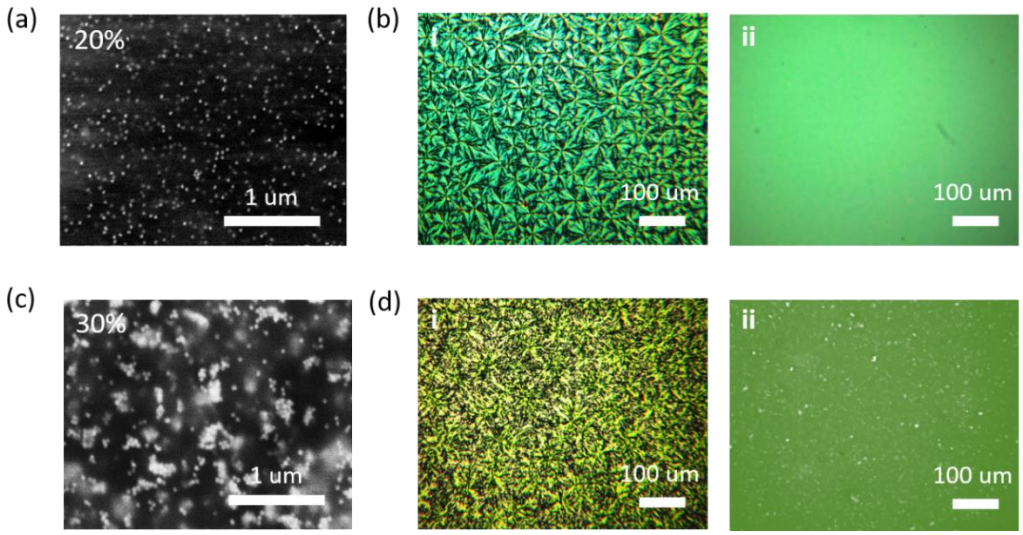

Figure 4.6 SEM images of PAzo/UCNPs@PAzo film spin-coated on Si substrate with 20% (a) and 30% (c) doping ratio of UCNPs@PAzo. (b) POM images of PAzo/UCNPs@PAzo film with 20% doping ratio of UCNPs@PAzo in the initial state (i) and after UV (365 nm, 68 mW cm^{-2}, 10 min) and linearly polarized blue light (470

nm, 29 mW cm^{-2}, 30 min) irradiation (ii). (d) POM images of PAzo/UCNPs@PAzo film with 30% doping ratio of UCNPs@PAzo in the initial state (i) and after UV (365 nm, 68 mW cm^{-2}, 10 min) and linearly polarized blue light (470 nm, 29 mW cm^{-2}, 30 min) irradiation (ii).

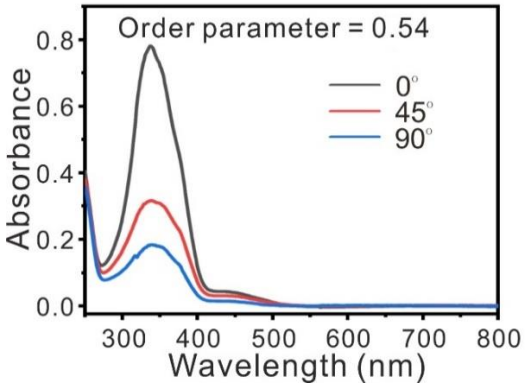

Figure 4.7 Polarized absorption spectra of a nanocomposite film after UV (365 nm, 67 mW cm^{-2}, 5 min) and linearly polarized blue light (470 nm, 29 mW cm^{-2}, 15 min) irradiations.

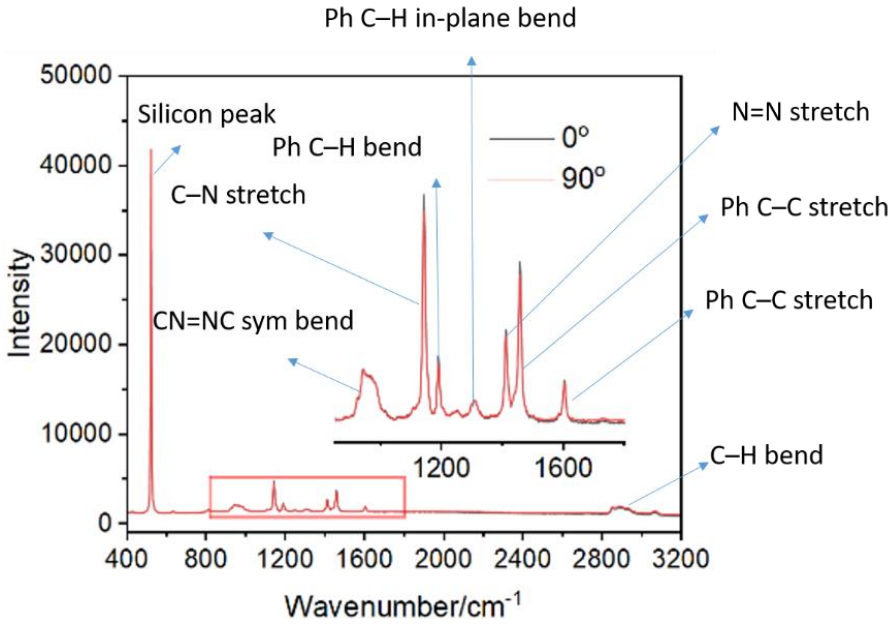

Figure 4.8 Raman spectra of a PAzo film spin-coated on silicon wafer. The peak at 948 cm^{-1} the CN=NC symmetric in-plane bend. The peak at 1146^{-1} is C–N stretching and ring breathing components. The band at 1190 cm^{-1} corresponds to the H–C–H bending group. The Raman peak at 1310 cm^{-1} is the H–C–H bending mode of the phenyl group.

The peak at 1415 cm^{-1} is predominately an N=N stretching mode of the *trans* state with minor contributions from the in-plane ring bending mode of the benzene group and the H–C–H bending mode of the alkyl group. The bands at 1465 cm^{-1} and 1600 cm^{-1} are C=C stretching mode. The bands from 2842 cm^{-1} to 3000 cm^{-1} are H–C–H bending mode of the alkyl group. [148, 149]

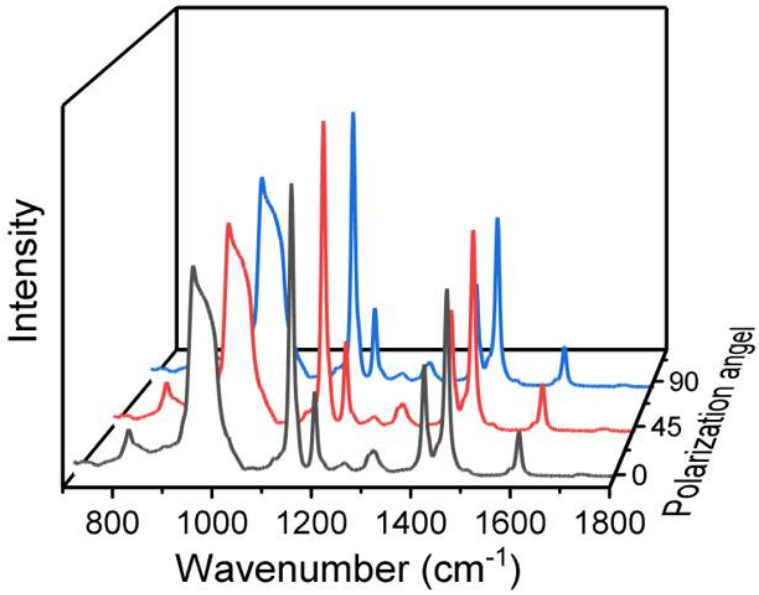

Figure 4.9 Polarized Raman spectra of amorphous PAzo/UCNPs@PAzo film spin-coated on silicon wafer.

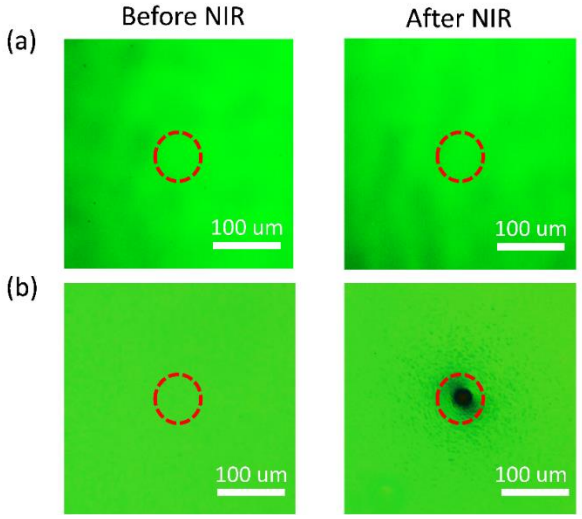

Figure 4.10 POM images of PAzo film (a) and PAzo/UCNPs@PAzo film (b) before and after NIR laser irradiation (75 mW, 10 min).

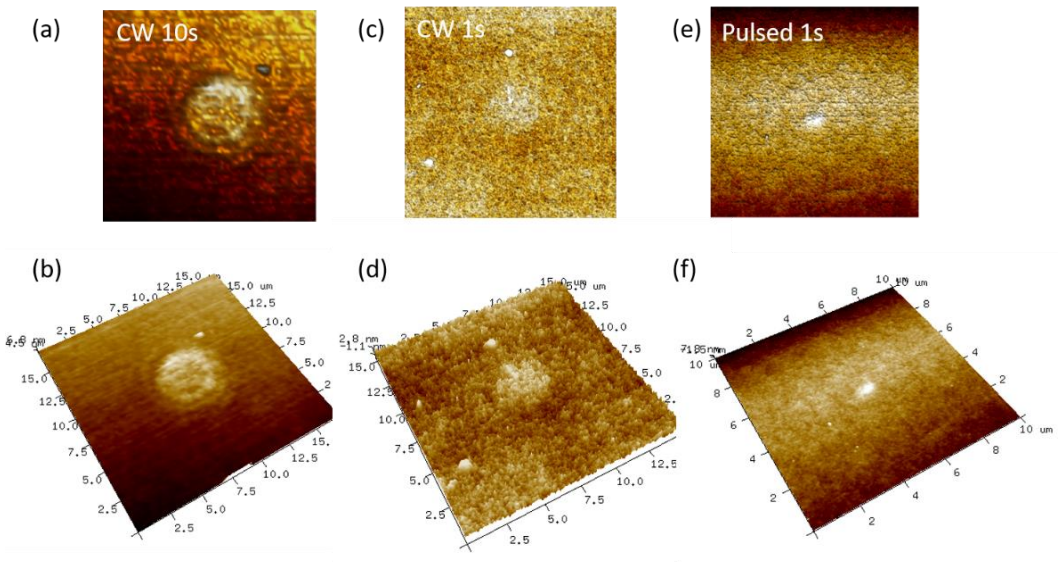

Figure 4.11 (a) 2D and (b) 3D AFM images of dots created by CW laser (70 mW, 10s). (c) 2D and (d) 3D AFM images of dots created by CW laser (70 mW, 1s). (e) 2D and (f) 3D AFM images of dots created by Pulsed laser (70 mW, 1s).

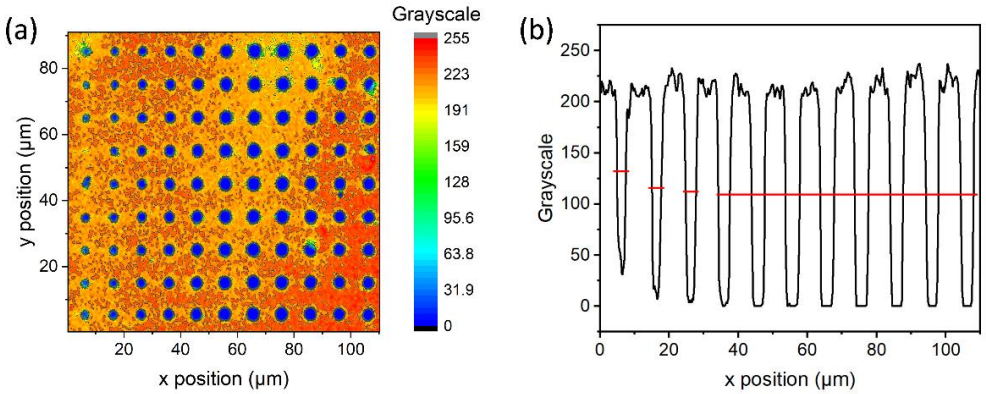

Figure 4.12 (a) The grayscale image processed using Matlab by mapping the position and corresponding gray values to generate the desired picture. (b) The cross-section profile of grayscale image.

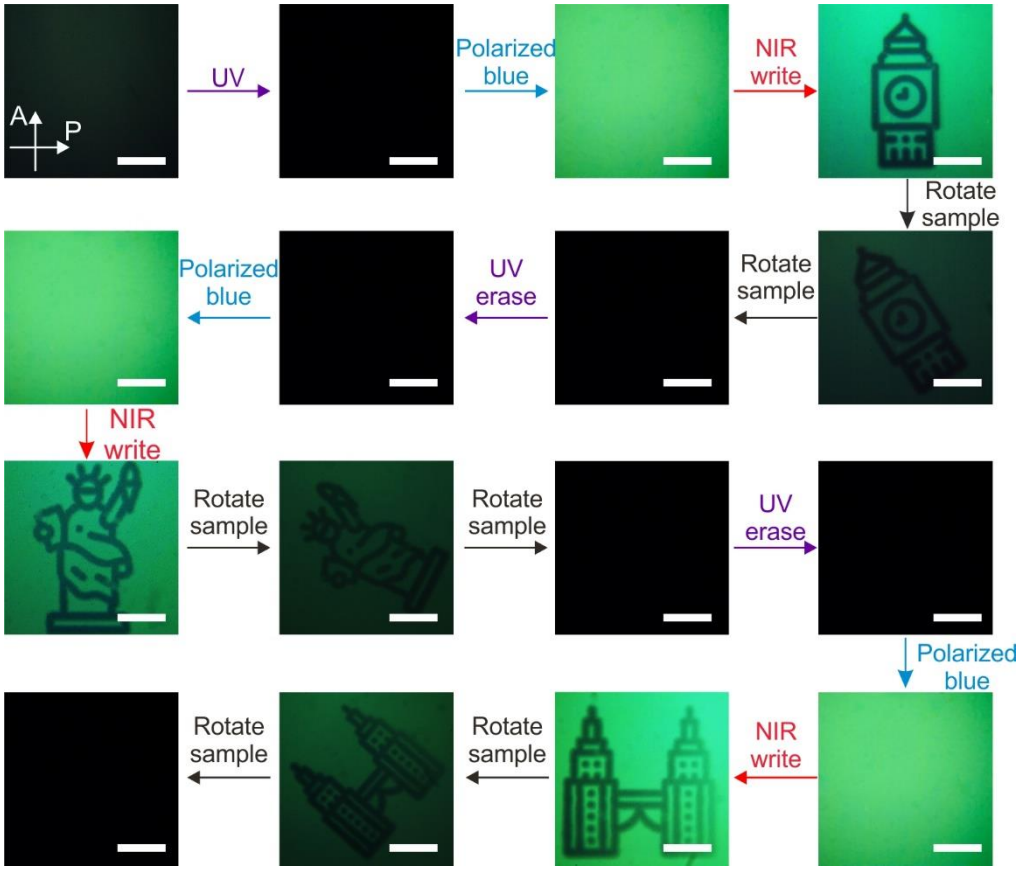

Figure 4.13 POM images of 2D patterns created using the PUDL process. These patterns can be revealed or concealed by rotating the sample under POM, allowing for both hidden and visible features to be observed.

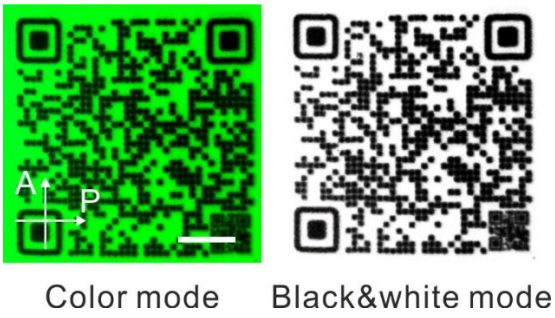

Figure 4.14 Color mode and black&white mode POM images of quick response (QR codes) on nanocomposite films fabricated by PUDL process. Scale bar: 200 μm.

Figure 4.15 POM images of a peace dove pattern on PAzo/UCNP@PAzo film fabricated by PUDL process. The pattern can be store for more than 150 days in an office with natural light at room temperature.

Chapter 5: Summary and outlook

5.1 Summary

This thesis focuses on the synthesis of a photoresponsive azopolymer and UCNPs, and subsequently fabricating nanocomposites using these components. By combining the unique properties of the azopolymer and UCNPs, the resulting nanocomposites exhibited a synergistic behavior. Based on these properties, we successfully fabricated 2D and 3D photopatterns using the synthesized nanocomposites. Furthermore, we investigated various applications enabled by these photopatterns, aiming to explore their potential in diverse fields.

Azopolymers exhibit a reversible *cis-trans* photoisomerization process, which gives rise to photochromism, photoswitchable T_g values, and photoinduced orientations. These inherent photoresponsive properties provide a foundation for the development of diverse anticounterfeiting features on the nanocomposite, including color-changing structures, photonic structures, and polarization-dependent structures. Additionally, the incorporation of UCNPs adds an extra dimension to functionality. UCNPs possess the ability to convert NIR light to visible light, leading to the generation of high-contrast color, structural modifications, and polarization-dependent upconversion luminescence within the nanocomposite. The integration of the azopolymer and UCNPs establishes the nanocomposite as an advanced material with significant potential for anticounterfeiting applications.

Upon the successful fabrication of 2D patterns, the second part of the work aims to harness the potential of a nanocomposite material for laser direct writing, enabling precise photopatterning. To this end, a novel 3D PUDL system has been developed. Prior to exposure, the nanocomposite films undergo a pretreatment process to establish molecular alignment in response to UV and polarized blue light. When subjected to NIR light, the upconverted UV and blue light facilitate a continuous *trans-cis-trans* isomerization of the azobenzene molecules. This sustained isomerization disrupts the initial molecular alignment, leading to the adoption of random orientations by the azobenzene molecules. The outcomes of this research introduce a promising approach to optical recording and signify a notable advancement in 3D photolithography.

5.2 Outlook

Although we successfully fabricated different photopatterns using photoresponsive nanocomposites comprising azopolymer and UCNPs, there are still certain drawbacks associated with both materials. One limitation of this azopolymer is the metastability of its *cis* form, which results in some photopatterns being relatively unstable. Therefore, a promising future direction would be to explore more stable photoresponsive azopolymers. As for the UCNPs, it would be advantageous to identify UCNPs with enhanced nonlinearity at the intensity level utilized in PUDL process. This would help overcome the issue of saturation in the upconversion process and then improve resolution. Possible strategies include adjusting the doping ratio of lanthanide ions in the UCNPs or employing pulsed laser excitation to modulate the saturated power intensity of UCNPs and enhanced nonlinearity. Furthermore, the utilization of UCNP-assisted photochemistry presents a versatile approach applicable to a wide range of photosensitive compounds. For instance, this setup could be extended to UCNP-assisted photolysis and photopolymerization, enabling the creation of more versatile structures and 3D printing. Overall, while UCNPs-assisted photoisomerization still requires further improvement, exploring other types of UCNPs-assisted photoreactions holds great potential for various application fields.

References

[1] S. Kawata and Kawata Y., Chem Rev, 2000. 100(5): p. 1777.

[2] J. Jensen, Dyer A. L., Shen D. E., Krebs F. C. and Reynolds J. R., Advanced Functional Materials, 2013. 23(30): p. 3728.

[3] W.-C. Xu, Liu C., Liang S., Zhang D., Liu Y. and Wu S., Advanced Materials, 2022. 34(31): p. 2202150.

[4] P. Zijlstra, Chon J. W. M. and Gu M., Nature, 2009. 459(7245): p. 410.

[5] A. Royon, Bourhis K., Bellec M., Papon G., Bousquet B., Deshayes Y., Cardinal T. and Canioni L., Advanced Materials, 2010. 22(46): p. 5282.

[6] W. Ren, Lin G., Clarke C., Zhou J. and Jin D., Advanced Materials, 2020. 32(18): p. 1901430.

[7] Z. Li, Liu X., Wang G., Li B., Chen H., Li H. and Zhao Y., Nature Communications, 2021. 12(1): p. 1363.

[8] L. Yang, Hu H., Scholz A., Feist F., Cadilha Marques G., Kraus S., Bojanowski N. M., Blasco E., Barner-Kowollik C., Aghassi-Hagmann J., and Wegener M., Nature Communications, 2023. 14(1): p. 1103.

[9] D. Gräfe, Walden S. L., Blinco J., Wegener M., Blasco E. and Barner-Kowollik C., Angewandte Chemie International Edition, 2020. 59(16): p. 6330.

[10] H. Roghani-Mamaqani and Tajmoradi Z. 2022. p. 53.

[11] Y. Wang, Dang A., Zhang Z., Yin R., Gao Y., Feng L. and Yang S., Advanced Materials, 2020. 32(46): p. 2004270.

[12] R. Klajn, Wesson P. J., Bishop K. J. M. and Grzybowski B. A., Angewandte Chemie International Edition, 2009. 48(38): p. 7035.

[13] H. Zhou, Xue C., Weis P., Suzuki Y., Huang S., Koynov K., Auernhammer G. K., Berger R., Butt H.-J. and Wu S., Nature Chemistry, 2017. 9(2): p. 145.

[14] W. Wang, Zhou Y., Yang L., Yang X., Yao Y., Meng Y. and Tang B., Advanced Functional Materials, 2022. 32(40): p. 2204744.

[15] K. M. Lee, Reshetnyak V. Y., Ambulo C. P., Marsh Z. M., McConney M. E. and Godman N. P., Materials Advances, 2023. 4(11): p. 2418.

[16] A. Centeno, Terrades O., Lladós J. and Cañero C., Identity Document and banknote security forensics: a survey. 2019.

[17] W. Huang, Xu M., Liu J., Wang J., Zhu Y., Liu J., Rong H. and Zhang J., Advanced Functional Materials, 2019. 29(17): p. 1808762.

[18] S. Gandla, Moon C., Baek S., Park H. and Kim S., Advanced Functional Materials, 2023. 33(17): p. 2211762.

[19] H. R. Stapert, del Valle S., Verstegen E. J. K., van der Zande B. M. I., Lub J. and Stallinga S., Advanced Functional Materials, 2003. 13(9): p. 732.

[20] R. Narayan and Popham R., Nature, 1993. 362(6423): p. 820.

[21] A. Miura, Bartel C. J., Goto Y., Mizuguchi Y., Moriyoshi C., Kuroiwa Y., Wang Y., Yaguchi T., Shirai M., Nagao M., Rosero-Navarro N. C., Tadanaga K., Ceder G., and Sun W., Advanced Materials, 2021. 33(24): p. 2100312.

[22] C. H. Lee, Sutrisno A., Hofmann T., Helbig T., Liu Y., Ang Y. S., Ang L. K., Zhang X., Greiter M. and Thomale R., Nature Communications, 2020. 11(1): p. 4385.

[23] P. H. Jacobse, Kimouche A., Gebraad T., Ervasti M. M., Thijssen J. M., Liljeroth P. and Swart I., Nature Communications, 2017. 8(1): p. 119.

[24] C. Wickleder, Angewandte Chemie International Edition, 2011. 50(4): p. 806.

[25] N. Liu, Chen Z., Dunphy D. R., Jiang Y.-B., Assink R. A. and Brinker C. J., Angewandte Chemie International Edition, 2003. 42(15): p. 1731.

[26] P. R. Anusuyadevi, Shanker R., Cui Y., Riazanova A. V., Järn M., Jonsson M. P. and Svagan A. J., Advanced Materials, 2021. 33(36): p. 2101519.

[27] A. Gupta, Patel D. K., Lee S. Y., Rigosi A. F., Elmquist R. E., Adusumalli V. N. K. B., Liang C.-T. and Park Y. I., Advanced Functional Materials, 2022. 32(44): p. 2206496.

[28] F. A. Jerca, Jerca V. V. and Hoogenboom R., Chem, 2017. 3(4): p. 533.

[29] J. Pang, Liu C., Huang Y., Wu M., Jiang F., Yuan D., Hu F., Su K., Liu G. and Hong M., Angewandte Chemie International Edition, 2016. 55(26): p. 7478.

[30] X. Laloyaux, Fautré E., Blin T., Purohit V., Leprince J., Jouenne T., Jonas A. M. and Glinel K., Advanced Materials, 2010. 22(44): p. 5024.

[31] S. Nowag and Haag R., Angewandte Chemie International Edition, 2014. 53(1): p. 49.

[32] T. Mena-Barragán, Narita A., Matias D., Tiscornia G., Nanba E., Ohno K., Suzuki Y., Higaki K., Garcia Fernández J. M. and Ortiz Mellet C., Angewandte Chemie International Edition, 2015. 54(40): p. 11696.

[33] M. Wang and Yin Y., Journal of the American Chemical Society, 2016. 138(20): p. 6315.

[34] Y. Hu, Ma H., Wu M., Lin T., Yao H., Liu F., Cheng H. and Qu L., Nature Communications, 2022. 13(1): p. 4335.

[35] Y. Ahn, Kim E., Hyon J., Kang C. and Kang Y., Advanced Materials, 2012. 24(23): p. OP127.

[36] Z.-F. Huang, Song J., Pan L., Zhang X., Wang L. and Zou J.-J., Advanced Materials, 2015. 27(36): p. 5309.

[37] A. Brotchie, Nature Reviews Materials, 2017. 2(4): p. 17022.

[38] G. Sinawang, Osaki M., Takashima Y., Yamaguchi H. and Harada A., Polymer Journal, 2020. 52(8): p. 839.

[39] W. C. Xu, Sun S. and Wu S., Angewandte Chemie International Edition, 2019. 58(29): p. 9712.

[40] R. Klajn, Chem Soc Rev, 2014. 43(1): p. 148.

[41] T. Satoh, Sumaru K., Takagi T. and Kanamori T., Soft Matter, 2011. 7(18): p. 8030.

[42] C. Li, Iscen A., Palmer L. C., Schatz G. C. and Stupp S. I., Journal of the American Chemical Society, 2020. 142(18): p. 8447.

[43] W. Francis, Dunne A., Delaney C., Florea L. and Diamond D., Sensors and Actuators B: Chemical, 2017. 250: p. 608.

[44] S. Panja and Adams D. J., Chem Soc Rev, 2021.

[45] Y. Gu, Alt E. A., Wang H., Li X., Willard A. P. and Johnson J. A., Nature, 2018. 560: p. 65.

[46] L. Li, Scheiger J. M. and Levkin P. A., Adv. Mater., 2019. 31: p. 1807333.

[47] E. R. Ruskowitz and DeForest C. A., Nature Reviews Materials, 2018. 3(2): p. 1.

[48] J. A. Shadish, Benuska G. M. and DeForest C. A., Nat Mater, 2019. 18(9): p. 1005.

[49] C. A. DeForest and Anseth K. S., Nat Chem, 2011. 3(12): p. 925.

[50] P. Weis, Wang D. and Wu S., Macromolecules, 2016. 49(17): p. 6368.

[51] J. Liu, Xie C., Kretzschmann A., Koynov K., Butt H.-J. and Wu S., Advanced Materials, 2020. 32(14): p. 1908324.

[52] S. He, Krippes K., Ritz S., Chen Z., Best A., Butt H.-J., Mailänder V. and Wu S., Chemical Communications, 2015. 51(2): p. 431.

[53] Z. Chen, He S., Butt H.-J. and Wu S., Advanced Materials, 2015. 27(13): p. 2203.

[54] B. H. Cumpston, Ananthavel S. P., Barlow S., Dyer D. L., Ehrlich J. E., Erskine L. L., Heikal A. A., Kuebler S. M., Lee I. Y. S., McCord-Maughon D., Qin J., Röckel H., Rumi M., Wu X.-L., Marder S. R., and Perry J. W., Nature, 1999. 398(6722): p. 51.

[55] D. Day, Gu M. and Smallridge A., Advanced Materials, 2001. 13(12-13): p. 1005.

[56] C. E. Olson, Previte M. J. R. and Fourkas J. T., Nature Materials, 2002. 1(4): p. 225.

[57] F. Helmchen and Denk W., Nature Methods, 2005. 2(12): p. 932.

[58] S. C. Laza, Polo M., Neves A. A. R., Cingolani R., Camposeo A. and Pisignano D., Advanced Materials, 2012. 24(10): p. 1304.

[59] M. Pawlicki, Collins H. A., Denning R. G. and Anderson H. L., Angewandte Chemie International Edition, 2009. 48(18): p. 3244.

[60] D. Kim, Kang J., Wang T., Ryu H. G., Zuidema J. M., Joo J., Kim M., Huh Y., Jung J., Ahn K. H., Kim K. H., and Sailor M. J., Advanced Materials, 2017. 29(39): p. 1703309.

[61] Z. Sun, Zhang L.-P., Wu F. and Zhao Y., Advanced Functional Materials, 2017. 27(48): p. 1704079.

[62] J. Lott, Ryan C., Valle B., Johnson III J. R., Schiraldi D. A., Shan J., Singer K. D. and Weder C., Advanced Materials, 2011. 23(21): p. 2425.

[63] B. Jia, Buso D., van Embden J., Li J. and Gu M., Advanced Materials, 2010. 22(22): p. 2463.

[64] J.-M. Jung, Yoo H.-W., Stellacci F. and Jung H.-T., Advanced Materials, 2010. 22(23): p. 2542.

[65] J. C. Culver, Hoffmann J. C., Poché R. A., Slater J. H., West J. L. and Dickinson M. E., Advanced Materials, 2012. 24(17): p. 2344.

[66] Y. Shi, Salter P. S., Li M., Taylor R. A., Elston S. J., Morris S. M. and Bradley D. D. C., Advanced Functional Materials, 2021. 31(7): p. 2007493.

[67] F. Han, Gu S., Klimas A., Zhao N., Zhao Y. and Chen S.-C., Science, 2022. 378(6626): p. 1325.

[68] H. M. D. Bandara and Burdette S. C., Chemical Society Reviews, 2012. 41(5): p. 1809.

[69] G. S. Hartley, Nature, 1937. 140(3537): p. 281.

[70] J. Henzl, Mehlhorn M., Gawronski H., Rieder K.-H. and Morgenstern K., Angewandte Chemie International Edition, 2006. 45(4): p. 603.

[71] J. L. Magee, Shand Jr W. and Eyring H., Journal of the American Chemical Society, 1941. 63(3): p. 677.

[72] T. Fujino, Arzhantsev S. Y. and Tahara T., The Journal of Physical Chemistry A, 2001. 105(35): p. 8123.

[73] Nature, 1946. 158(4007): p. 222.

[74] Y. Zhou, Chen M., Ban Q., Zhang Z., Shuang S., Koynov K., Butt H.-J., Kong J. and Wu S., ACS Macro Letters, 2019. 8(8): p. 968.

[75] M. Chen, Yao B., Kappl M., Liu S., Yuan J., Berger R., Zhang F., Butt H.-J., Liu Y. and Wu S., Advanced Functional Materials, 2020. 30(4): p. 1906752.

[76] W.-C. Xu, Sun S. and Wu S., Angewandte Chemie International Edition, 2019. 58(29): p. 9712.

[77] S. Wu and Butt H.-J., Advanced Materials, 2016. 28(6): p. 1208.

[78] A. Terenzi and Salassa L., J.P. Prieto and M.G. Béjar, Editors. 2019, Elsevier. p. 43.

[79] K. Malhotra, Hrovat D., Kumar B., Qu G., Houten J. V., Ahmed R., Piunno P. A. E., Gunning P. T. and Krull U. J., ACS Applied Materials & Interfaces, 2023. 15(2): p. 2499.

[80] W. Wu, Yao L., Yang T., Yin R., Li F. and Yu Y., Journal of the American Chemical Society, 2011. 133(40): p. 15810.

[81] J. Liu, Bu W., Pan L. and Shi J., Angewandte Chemie International Edition, 2013. 52(16): p. 4375.

[82] M. Yamada, Kondo M., Mamiya J.-i., Yu Y., Kinoshita M., Barrett C. J. and Ikeda T., Angewandte Chemie International Edition, 2008. 47(27): p. 4986.

[83] E. L. Prime, D. H. Solomon, *Angew. Chem. Int. Ed.* **2010**, 49, 3726.

[84] R. Arppe, T. J. Sørensen, *Nat. Rev. Chem.* **2017**, 1, 0031.

[85] H. Rekola, A. Berdin, C. Fedele, M. Virkki, A. Priimagi, *Sci. Rep.* **2020**, 10, 19642.

[86] G. Babakhanova, T. Turiv, Y. Guo, M. Hendrikx, Q.-H. Wei, A. P. H. J. Schenning, D. J. Broer, O. D. Lavrentovich, *Nat. Commun.* **2018**, 9, 456.

[87] A. J. J. Kragt, D. C. Hoekstra, S. Stallinga, D. J. Broer, A. P. H. J. Schenning, *Adv. Mater.* **2019**, 31, 1903120.

[88] P. Zhang, G. Zhou, L. T. Haan, A. P. H. J. Schenning, *Adv. Funct. Mater.* **2020**, 31, 1900789.

[89] L. Qin, X. Liu, K. He, G. Yu, H. Yuan, M. Xu, F. Li, Y. Yu, *Nat. Commun.* **2021**, 12, 699.

[90] A. Priimagi, A. Shevchenko, *J. Polym. Sci. B: Polym. Phys.* **2014**, 52, 163.

[91] J. Feng, F. Yang, X. Wang, F. Lyu, Z. Li, Y. Yin, *Adv. Mater.* **2019**, 31, 1900789.

[91] X. Zhou, L. Wang, Z. Wei, G. Weng, J. He, *Adv. Funct. Mater.* **2019**, 29, 1903543.

[92] Z. Shi, P. Peng, D. Strohecker, Y. Liao, *J. Am. Chem. Soc.* **2011**, 133, 14699.

[93] M. Cheng, Q. Liu, G. Ju, Y. Zhang, L. Jiang, F. Shi, *Adv. Mater.* **2014**, 26, 306.

[94] Y. Zheng, M. K. Liong Han, Q. Jiang, B. Li, J. Feng, A. del Campo, *Mater. Horiz.* **2020**, 7, 111.

[95] H. Zeng, P. Wasylczyk, D. S. Wiersma, A. Priimagi, *Adv. Mater.* **2018**, 30, 1703554.

[96] L. Huang, W. Wu, Y. Li, K. Huang, L. Zeng, W. Lin, G. Han, *J. Am. Chem. Soc.* **2020**, 142, 18460.

[97] M. Dietrich, G. Delaittre, J. P. Blinco, A. J. Inglis, M. Bruns, C. Barner-Kowollik, *Adv. Funct. Mater.* **2012**, 22, 304.

[98] B. Hardwick, W. Jackson, G. Wilson, A. W. H. Mau, *Adv. Mater.* **2001**, 13, 980.

[99] Y. Zheng, C. Jiang, S. H. Ng, Y. Lu, F. Han, U. Bach, J. J. Gooding, *Adv. Mater.* **2016**, 28, 2330.

[100] W.-C. Xu, S. Sun, S. Wu, *Angew. Chem. Int. Ed.* **2019**, 58, 9712.

[101] X. Tong, M. Pelletier, A. Lasia, Y. Zhao, *Angew. Chem. Int. Ed.* **2008**, 47, 3596.

[102] Z. Mahimwalla, K. G. Yager, J.-I. Mamiya, A. Shishido, A. Priimagi, C. J. Barrett, *Polym. Bull.* **2012**, 69, 967.

[103] G. S. Kumar, D. Neckers, *Chem. Rev.* **1989**, 89, 1915.

[104] H. Zhou, C. Xue, P. Weis, Y. Suzuki, S. Huang, K. Koynov, G. K. Auernhammer, R. Berger, H.-J. Butt, S. Wu, *Nat. Chem.* **2017**, 9, 145.

[105] Y. Wu, T. Ikeda, Q. Zhang, *Adv. Mater.* **1999**, 11, 300.

[106] J.-a. Lv, Y. Liu, J. Wei, E. Chen, L. Qin, Y. Yu, *Nature* **2016**, 537, 179.

[107] B. Yan, J.-C. Boyer, N. R. Branda, Y. Zhao, *J. Am. Chem. Soc.* **2011**, 133, 19714.

[108] W. M. Gibbons, T. Kosa, P. Palffy-Muhoray, P. J. Shannon, S. T. Sun, *Nature* **1995**, 377, 43.

[109] A. Natansohn, P. Rochon, *Chem. Rev.* **2002**, 102, 4139.

[110] S. He, K. Krippes, S. Ritz, Z. Chen, A. Best, H. J. Butt, V. Mailander, S. Wu, *Chem. Commun.* **2015**, 51, 431.

[111] Z. Chen, S. He, H. J. Butt, S. Wu, *Adv. Mater.* **2015**, 27, 2203.

[112] J. Heber, *Nature Materials*, **2007**, 6, 11, 807.

[113] J. Maddox, *Nature*, **1987**, 327, 6118, 97.

[114] C. Bancroft, T. Bowler, B. Bloom, C.T. Clelland, *Science*, **2001**, 293, 5536, 1763.

[115] M. Striccoli, *Science*, **2017**, 357, 6349, 353.

[116] A.A. Eliseev, N.A. Sapoletova, I. Snigireva, A. Snigirev, K. Napolskii, *Angew. Chem. Int. Ed.* **2012**, 51, 46, 11602.

[117] T.F. Scott, B.A. Kowalski, A.C. Sullivan, C.N. Bowman, R.R. Mcleod, *Science*, **2009**, 324, 5929, 913.

[118] U.A. Gurkan, R.E. Assal, S.E. Yildiz, Y. Sung, A.J. Trachtenberg, W.P. Kuo, U. Demirci, *Adv. Mater.* **2013**. 25(8): p. 1192.

[119] Y. Yao, T. Sano, H. Kobayashi, H. Yamashita, *J. Am. Chem. Soc.* **2018**. 140(22): p. 698.

[120] G.S. Hartley, *Nature*, **1937**. 140(3537): p. 281.

[121] H. Zhou, C. Xue, P. Weis, Y. Suzuki, S. Huang, K. Koynov, G.K. Auernhammer, R. Berger, H.-J. Butt, S. Wu, *Nature Chemistry*, **2017**. 9(2): p. 145.

[122] W.-C. Xu, C. Liu, S. Liang, D. Zhang, Y. Liu, S. Wu, *Adv. Mater.* **2022**. 34(31): p. 2202150.

[123] J. Kohl-Landgraf, M. Braun, C. Ö zcoban, D.P.N. Goncalves, A. Heckel, J. Wachtveitl, *J. Am. Chem. Soc.* **2012**. 134(34): p. 14070.

[124] J. Andersson, S. Li, P. Lincoln, J. Andreasson, *J. Am. Chem. Soc.* **2008**. 130(36): p. 11836.

[125] M. Inouye, M. Ueno, T. Kitao, K. Tsuchiya, *J. Am. Chem. Soc.* **1990**. 112(24): p. 8977.

[126] T. Yamaguchi, K. Uchida, M. Irie, *J. Am. Chem. Soc.* **1997**. 119(26): p. 6066.

[127] D. Kitagawa, H. Nishi, S. Kobatake, *Angew. Chem. Int. Ed.* **2013**. 52(35): p. 9320.

[128] Herder, M., et al., *J. Am. Chem. Soc.* **2015**. 137(7): p. 2738.

[129] R.S. Shah, S.L. Bafna, *Nature*, **1965**. 208(5005): p. 76.

[130] C.N. Zhu, Y.L. Chen, H. Wang, W. Hong, F. Huang, Q. Zheng, Z.L. Wu, *Adv. Mater.* **2021**. 33(18): p. 2008057.

[131] L.J. Audus, J.H. Quastel, *Nature*, **1947**. 159(4036): p. 320.

[132] S.C. Laza, M. Polo, A. Neves, R. Cingolani, A. Camposeo, D. Pisignano, *Adv. Mater.* **2012**. 24(10): p. 1304.

[133] D. Schwärzle, X. Hou, O. Prucker, J. Rühe, *Adv. Mater.* **2017**. 29(39): p. 1703469.

[134] D. Kim, D. Lee, W. Lee, Y. Kim, J.I. Han, K. Cho, *Adv. Mater.* **2017**. 29(39): p. 1703309.

[135] A.S. Dvornikov, E.P. Walker, P.M. Rentzepis, *J. Phy. Chem. A*, **2009**. 113(49): p. 13633.

[136] T. Furuta, S.-H. Wang, J.L. Dantzker, R.Y. Tsien, *Proc. Natl. Acad. Sci.* **1999**. 96(4): p. 1193.

[137] M. Álvarez, A. Best, A. Unger, J.M. Alonso, A. Campo, M. Schmelzeisen, L. Koynov, M. Kreiter, *Adv. Funct. Mater*. **2010**, 20(24): p. 4265.

[138] F. Wang, X. Liu, *Chem. Soc. Rev.*, **2009**. 38(4): p. 976.

[139] M. Haase, H. Schäfer, *Angew. Chem. Int. Ed.* **2011**. 50(26): p. 5808-5829.

[140] S. Wu, H.-J. Butt, *Adv. Mater.* **2016**. 28(6): p. 1208.

[141] C.-J. Carling, J.-C. Boyer, N.R. Branda, *J. Am. Chem. Soc.* **2009**. 131(31): p. 10838.

[142] J. Liu, W. Bu, J. Shi, *Angew. Chem. Int. Ed.* **2013**. 125(16): p. 4471.

[143] S. Beyazit, S. Ambrosini, N. Marchyk, E. Palo, V. Kale, T. Soukka, B.T. Bui, K. Haupt, *Angew. Chem. Int. Ed.* **2014**. 53(34): p. 8919.

[144] C. Yao, P. Wang, X. Li, J. Hou, L. Wang, F. Zhang, *Adv. Mater.* **2016**. 28(42): p. 9341.

[145] Y. Liu, S. Liang, C. Yuan, A. Best, M. Kappl, K. Koynov, H.-J. Butt, S. Wu, *Adv. Funct. Mater*. **2021**. 31(37): p. 2103908.

[146] S. He, K. Krippes, S. Ritz, Z. Chen, A. Best, H.-J. Butt, V. Mailänder, S. Wu, *Chem. Comm.* **2015**. 51(2): p. 431.

[147] Z. Chen, S. He, H.-J. Butt, S. Wu, *Adv. Mater.* **2015**. 27(13): p. 2203.

[148] L. Sun, *J. Raman Spectro.* **2020**. 51(5): p. 756.

[149] F. Anariba, U. Viswanathan, D.F. Bocian, R.L. McCreery, *Anal. Chem.* **2006**. 78(9): p. 3104.

Abbreviations

Azopolymer	Azobenzene-containing polymer
AFM	Atom force microscope
AIBN	2,2′-azobisisobutyronitrile
CCD	Charge-coupled device
CPDB	Cyanoisopropyl dithiobenzoate
CW	Continuous wavelength
DDS	Drug delivery system
DLS	Dynamic light scattering
DMA	Dynamic mechanical analysis
DOX	Doxorubincin
F8BT	Liquid crystalline conjugated polymer
G	Storage modulus
G″	Loss modulus
GPC	Gel permeation chromatography
HPLC	High-performance liquid chromatography
LED	Light-emitting diode
mAzo	Ortho-methoxy-substituted azobenzene
M_n	Number-average molecular weight
NIR	Near-infrared
NMR	Nuclear magnetic resonance
PAzo	Azobenzene-containing polymer
PAzo/UCNP	Nanocomposites consisting of azobenzene-containing polymer and upconverting nanoparticles
PAzo/UCNP@PAzo	Nanocomposites consisting of azobenzene-containing polymer and azobenzene-containing polymer capped upconverting nanoparticles
PDI	Polydispersity index
PEG	Polyethylene glycol
PET	Polyethylene terephthalate
POM	Polarized optical microscopy
PUCL	Photon upconversion lithography

PUDL	Photon upconversion direct lithography
QR	Quick response
RAFT	Reversible addition-fragmentation chain-transfer polymerisation
SCP	Polyelectrolyte
SD1	Sulphonic dye
SEM	Scanning electron microscopy
tan δ	Loss tangent
TEM	Transmission electron microscopy
T_g	Glass transition temperatures
TGA	Thermogravimetric analysis
TPA	Two photon absorption
TTA	Triplet-triplet annihilation
UCNPs	Upconverting nanoparticles
UCNPs@PAzo	Azobenzene-containing polymer capped upconverting nanoparticles
UV	Ultraviolet
2D/3D	Two/three-dimensional

Publications

1. **Yazhi Liu**, Shuofeng Liang, Chenrui Yuan, Andreas Best, Michael Kappl, Kaloian Koynov, Hans-Jürgen Butt, Si Wu. Anticounterfeiting Nanocomposites with Multiple Security Features via Integration of a Photoresponsive Polymer and Upconverting Nanoparticles. *Adv. Funct. Mater. 2021, 31, 2103908.*

2. **Yazhi Liu**, Shaodong Sun and Si Wu. Moving Polymers via Photoisomerization. *Chin. J. Chem., 2020, 38: 1019-1022.*

3. **Yazhi Liu**, Jingning Cao, Andreas Best, Kaloian Koynov, Hans-Jürgen Butt and Si Wu. Three-dimensional Photon Upconversion Direct Lithography of a Photoalignment Nanocomposite. *In preparation.*

4. Chengwei Liu, Ann-Kathrin Steppert, **Yazhi Liu**, Philipp Weis, Jianyu Hu, Chen Nie, Wen-Cong Xu, Alexander J. C. Kuehne and Si Wu. A Photopatternable Conjugated Polymer with Thermal-Annealing-Promoted Interchain Stacking for Highly Stable Anti-Counterfeiting Materials. *Adv. Mater.* 2023, *2303120.*

5. Zhenlin Zhang, Mingsen Chen, Igor Schneider, **Yazhi Liu**, Shuofeng Liang, Shijie Sun, Kaloian Koynov, Hans-Jürgen Butt and Si Wu. Long Alkyl Side Chains Simultaneously Improve Mechanical Robustness and Healing Ability of a Photoswitchable Polymer. *Macromolecules 2020 53 (19), 8562-8569.*

6. Wen-Cong Xu, Chengwei Liu, Shuofeng Liang, Dachuan Zhang, **Yazhi Liu** and Si Wu. Designing Rewritable Dual-Mode Patterns using a Stretchable Photoresponsive Polymer via Orthogonal Photopatterning. *Adv. Mater. 2022, 34, 2202150.*

‘

Acknowledgment

This thesis is the result of a long effort, which I could never have endured without the help and support of many, whom I would like to thank presently. First and foremost, I am deeply grateful to my supervisors, Prof. Dr. Hans-Jürgen Butt and Prof. Dr. Si Wu, who gave me this incredible opportunity. Prof. Dr. Hans-Jürgen Butt has consistently displayed kindness, helpfulness, and patience, providing me with unwavering support, encouragement, and scientific guidance. His constant support and positivity have been instrumental in boosting my confidence. I consider myself extremely fortunate to have been a part of AK Butt group. Prof. Dr. Si Wu has played a crucial role as my supervisor, providing invaluable guidance and mentoring. Despite facing the challenges posed by the COVID-19 pandemic, including his return to China these few years, Prof. Dr. Si Wu maintained regular contact and remained available to help me overcome various problems. I greatly benefited from his vast knowledge and expertise.

I would like to extend a special thanks to Dr. Kaloian Koynov, who went above and beyond to help me with my work. Although he may not hold the official title of my supervisor, his support and guidance towards me are akin to that of my supervisor. In my heart, he holds a significant supervisor role. Without his invaluable help and understanding, I would have been unable to accomplish my project successfully.

I am immensely grateful to my colleagues who support me during this period. Andreas Best has been instrumental in assisting me with all the optical setups. I must sincerely acknowledge that my work would not have been completed without his help. I am also grateful to Gabriele Schaefer. Not only did she assist me with my experiments, but she also took the time to teach me swimming skills. I also want to express my gratitude to Gunnar Kircher for his help with daily lab work.

I would also like to thank my friends and all the group members. I would like to say thanks to Yunqi Gong, Dr. Jiahui Zhou, Dr. Xiaoqian Wang, Yue Ma, Dr. Rui Guo, Dr. Philipp Weis, Dr. Mingjia Chen, Dr. Mingsen Chen, Dr. Jiahui Liu, Dr. Jianxiong Han, Dr. Xiaolong Zeng, Dr. Meijia Yang, Dr. Yaolei Xiang, Dr. Shuai Li, Yun Dong, Xiaotang Shi, Yuwen Ji, Jingning Cao and all of the AK Butt members. I will never forget the happy time we experienced together. Thank you for bring me a lot of joy and encouraging me during the past years.

Finally, I would like to express my deepest gratitude to my parents and my younger brother for their love and support throughout this journey. I am also thankful to everyone I have had the pleasure of meeting. The memories we shared in Mainz will always hold a special place in my heart, and I will genuinely miss each and every one of you. Thank you for the wonderful times we had together.